SAMSO-TR-68-4

8525-3-Q

Copy ____

THE UNIVERSITY OF MICHIGAN

COLLEGE OF ENGINEERING

DEPARTMENT OF ELECTRICAL ENGINEERING

Radiation Laboratory

8525-3-Q = RL-2182

Investigation of Re-Entry Vehicle Surface Fields (U)

Quarterly Report No. 3
18 June - 18 September 1967

By
R. F. GOODRICH, B. A. HARRISON, J. J. BOWMAN, E. F. KNOTT, T. B. A. SENIOR, T. M. SMITH, H. WEIL and V. H. WESTON

October 1967

Contract F 04694-67-C-0055

Contract With: Hq. Space and Missile Systems Organization
Air Force Systems Command
Norton Air Force Base, California 92409

Administered through: OFFICE OF RESEARCH ADMINISTRATION · ANN ARBOR

SECRET

THE UNIVERSITY OF MICHIGAN
8525-3-Q

SAMSO-TR-68-4

Investigation of Re-entry Vehicle Surface Fields (U)

Quarterly Report No. 3
18 June - 18 September 1967

F 04694 67 C 0055

By

R. F. Goodrich, B. A. Harrison, J. J Bowman, E. F. Knott
T. B. A. Senior, T. M. Smith, H. Weil, and V. H. Weston

October 1967

Prepared for

HQ, SPACE AND MISSILE SYSTEMS ORGANIZATION
AIR FORCE SYSTEMS COMMAND
NORTON AFB, CALIFORNIA

SECRET

FOREWORD

(U) This report, SAMSO-TR-68-4, was prepared by the Radiation Laboratory of the Department of Electrical Engineering of The University of Michigan under the direction of Dr. Raymond F. Goodrich, Principal Investigator and Burton A. Harrison, Contract Manager. The work was performed under Contract F 04694-67-C-0055, "Investigation of Re-entry Vehicle Surface Fields SURF." The work was administered under the direction of the Air Force Headquarters, Space and Missile Systems Orgainzation, Norton Air Force Base, California 92409, by Capt. J. Wheatley, SMYSP, and was monitored by Mr. H.J. Katzman of the Aerospace Corporation.

(U) The studies presented herein cover the period 18 June 1967 through 18 September 1967.

(U) In addition to security requirements which must be met, this document is subject to special export controls and each transmittal to foreign governments or foreign nationals may be made only with prior approval of SAMSO, SMSD, Air Force Station, Los Angeles, CA 90045.

(U) Information in this report is embargoed under the Department of State International Traffic in Arms Regulations. This report may be released to Foreign governments by departments or agencies of the U.S. Government subject to approval of Hq. Space and Missile Systems Organization (SMSD), Air Force Station, Los Angeles, Calif., 90045 or higher authority within the Department of the Air Force. Private individuals or firms require a Department of State lincense.

(U) The publication of this report does not constitute Air Force Approval of the report's findings or conclusions. It is published only for the exchange of stimulation of ideas.

SAMSO Approving Authority
William J. Schlerf BSYDR
Contracting Officer

ABSTRACT

(S) This is the Third Quarterly Report on Contract F 04694-67-C-0055 and covers the period 18 June to 18 September 1967. The report discusses work in progress on Project SURF and on a related short pulse investigation. Project SURF is a continuing investigation of the radar cross section of metallic cone-sphere shaped re-entry bodies and the effect on radar cross section of absorber and ablative coatings, antenna and rocket nozzle perturbation, changing the shape of the rear spherical termination, and of the plasma re-entry environment. The objective of the short pulse study is the determination of methods of modifying the short pulse signature of cone-sphere shaped re-entry bodies and of decoys. SURF investigations make use of experimental measurements in surface field and backscatter ranges to aid in the analytical formulation of mathematical expressions for the computation of radar cross section. A computer program for determining the radar cross section of any rotationally symmetric metallic body is being developed.

TABLE OF CONTENTS

Table of Contents (Cont'd)

I

INTRODUCTION

(S) This is the Third Quarterly Report on Contract F 04694-67-C-0055, "Investigation of Re-entry Vehicle Surface Fields (Backscatter)(SURF)". It covers the period 18 June to 18 September 1967. Work under this program includes an investigation of methods to compute the radar cross section of cone-sphere shaped re-entry vehicles both in and out of the atmosphere and a method for changing the short pulse discrimination characteristics of such re-entry vehicles and their decoys. These studies are monitored by Capt. J. Wheatley for the Space and Missile Systems Organization and by Mr. H. J. Katzman for the Aerospace Corporation.

(S) The approach adopted in the SURF investigation makes use of experimental measurements of the surface fields induced on various scale models of re-entry bodies and related shapes to aid in the construction of a theory to explain radar scattering behavior and in the formulation of mathematical expressions for the computation of radar cross section. In addition to the surface field measurements, backscatter measurements are relied on to furnish substantiation of the theory being developed or to guide the investigation in areas wherein surface field measurements alone do not provide adequate data. A digital computer program is being developed to aid in the study of cases of oblique incidence on the target and to provide supplementary data in cases where the very low backscatter from the target is difficult to measure accurately.

(S) The SURF program is a comprehensive attempt to provide radar cross section formulas for such practical situations as may be expected to arise. They include formulas for the following:

(a) The metallic cone-sphere and the cone with non-spherical modifications to the cap.

(b) Modifications of the cone-sphere due to the addition of antennas and rocket nozzles.

(c) The addition of absorbing materials to the cone-sphere surface.

(d) The effect of the re-entry plasma environment.

(S) Short pulse discrimination methods permit one to distinguish between a warhead and accompaning decoys by a simple numerical count of the pulses returned by each body. The short pulse investigation has been undertaken to determine methods for countering this discrimination method and to recommend penetration aids to accomplish this. The investigation in its early stages was principally mathematical so that the basic theory of short pulse scattering can be set forth. Its application to re-entry shapes now follows. Experimental data is available at Lincoln Laboratory to be used as part of this analysis should it prove desirable.

II

TASK 2: EXPERIMENTAL INVESTIGATIONS

2.1 Introduction

(U) The experimental work for this Quarter was concerned with three main subjects. It was carried out to furnish experimental data for the study of (a) the effect on radar cross section of exposing the flush mounted antennas which had hitherto, in studies up to this period, been covered by absorber material; (b) the effect on radar cross section of perturbations to the cap of the conical re-entry vehicle, including the effect of rounding the cone-sphere join; and (c) the effect on radar cross section of the cone-sphere in the plasma re-entry environment.

(U) The work on Item (a) originated in Agreement No. 2 at the Technical Discussion Meeting held at the Radiation Laboratory on 3 August 1967. It was requested that work be done "to perform surface current measurements of a cone-sphere model when the coated material does not cover the antenna perturbations and to compare these results when the coated material covers the antenna perturbations of same model." The surface field measurements were completed. The comparison will be made during the next reporting period.

2.2 Surface Field Measurements of Coated Perturbed Re-entry Shapes (Tasks 2.1.1 and 2.1.2).

(U) In previous surface field measurements, dielectric spacers were used to study the effect of placing flush mounted antennas near the tip or near the join of the cone-sphere re-entry vehicles. The model with the spacer near the tip is designated LSP and that with the spacer near the join is designated LSH in the discussions which follow. These studies showed that the effect of the dielectric spacers were strongly suppressed when the model was covered with absorber. Based upon the surface field data alone, it was often difficult to tell which model was underneath the coating, the metallic unperturbed cone-

sphere, model LSP or model LSH. The study was thereafter extended to determine the effect of exposing portions of the underlying body through annular slots cut in the coating.

(U) Since the spacers are simulators of possible antennas, and since an absorber coating would reduce the radiation efficiency of such antennas, one would like to slice away the coating directly over the antenna to permit more rf to be radiated. Slicing away the coating, however, exposes the underlying structure to the incident EM wave and there is a strong possibility that large local perturbations may be imparted to the surface field intensity. The series of measurements described below thus represent a natural course of surface field studies.

(U) No new models were constructed for the measurements and instead several combinations of existing models and coatings were relied upon to obtain the modifications shown in Fig. 2-1. There are four configurations for each of two spacer locations, one near the tip and one near the join. The models of Fig. 2-1a and 2-1b are simply conducting cone spheres having an annular slot cut in the coating at a point corresponding to that of model LSP; the slot is filled respectively with air or Lucite. The next two models, shown in 2-1c and 2-1d, have the same coating configurations as those in 2-1a and 2-1b, except that the model inside the absorber sheath is model LSP and not a plain cone-sphere. The same treatment is given to the models shown in 2-1e and 2-1h except that the slot in the coating appears near the join instead of the tip; the basic model for 2-1e and 2-1f is a plain cone-sphere while for 2-1g and 2-1h, we have model LSH.

(U) In general, the measured surface fields behave as might have been predicted; exposing the surface of the model beneath the absorber by means of an annular slot in the coating produces a stronger field perturbation than when

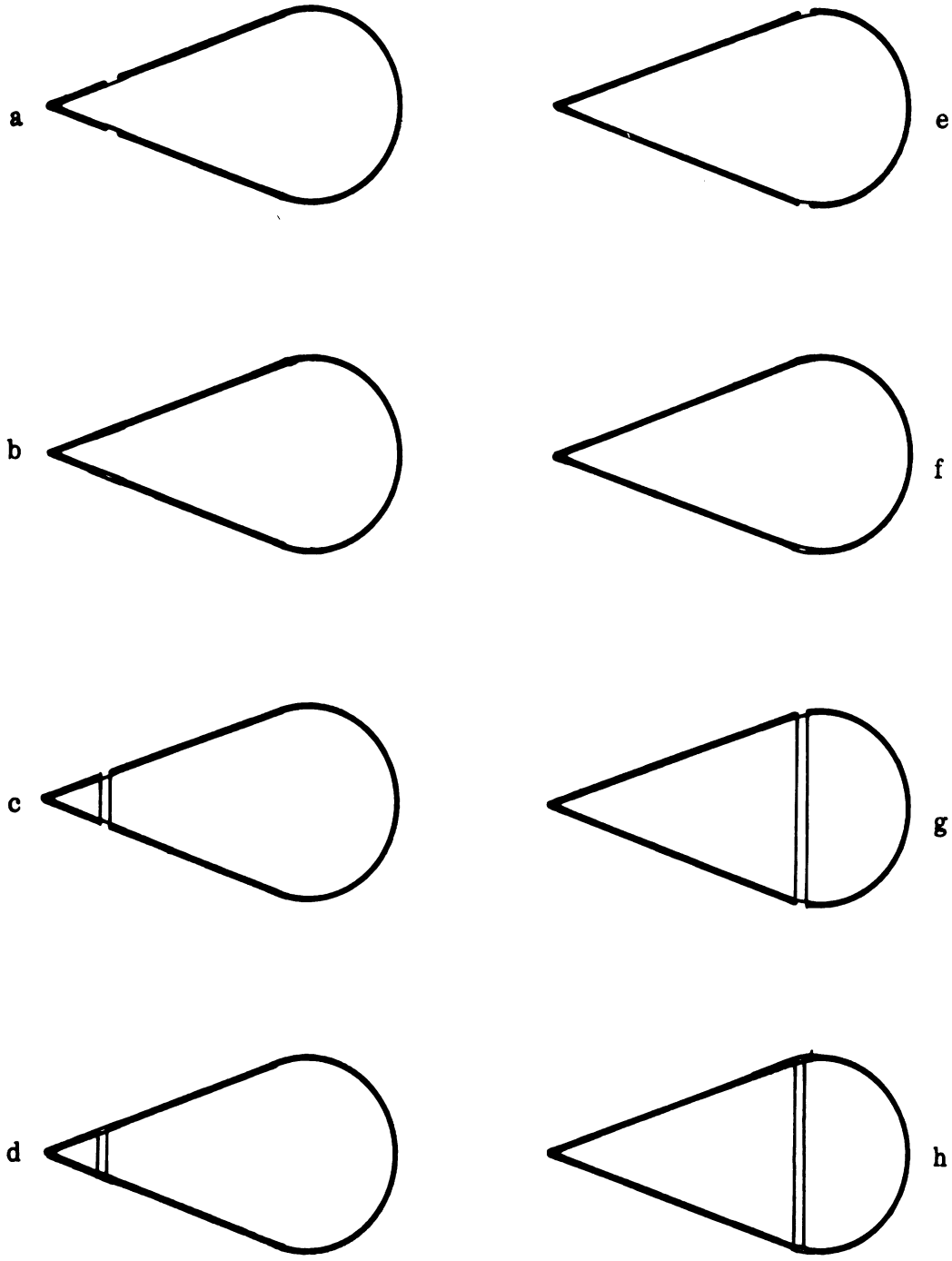

FIG. 2-1: EIGHT CONFIGURATIONS WERE EMPLOYED IN STUDYING THE EFFECTS OF AN ANNULAR SLOT IN THE COATING.

the coating is intact. The slot in the coating has less effect on the fields when the spacer is near the join (model LSH) than when the spacer is near the tip (model LSP). The effect is also weaker when the underlying model is a plain cone-sphere and usually (but not always) the slot has a stronger effect when it is packed with Lucite than when simply air-filled. Finally, as might be expected, the effects are stronger for higher ka then lower ka, usually independently of the model inside the coating. Each of the models of Fig. 2-1 was measured for nose-on incidence at the following values of ka: 1.1, 3.0, 5.0 and 8.0. The results thus form a set of 32 patterns, but we shall present only a selection of typical data.

(U) In Fig. 2-2 one can see the effect of the kind of model that has been exposed by an annular slot cut in the lossy sheath. The models used for this comparison were five wavelengths in circumference and the slot in the coating lay just aft of the join. The slot was filled with a Lucite ring whose width matched that of the coating (so that the outer surfaces of both ring and coating were a continuous profile and whose thickness matched that of the spacer used in model LSH 1/4 inch). The dashed curve shows the surface field behavior when the model under the coating is a plain cone-sphere and, although the fields are small near the spacer because of the presence of the absorber on the conical part of the model, there is a decided jump near the slot. When the model is the LSH model, having a dielectric spacer electrically separating the front and rear parts of the model, one also sees a jump in the fields near the slot, except that it has a slightly different character than before (the solid trace). The field intensity along the conical portion of the model show perturbations that were nearly totally absent for a plain cone-sphere, suggesting that the depth of the spacer used for model LSH has some influence. Whether the underlying model is a solid one or one with a spacer also dictates the character of the fields around the spherical portion of the body, as evidenced by the differences shown in Fig. 2-2.

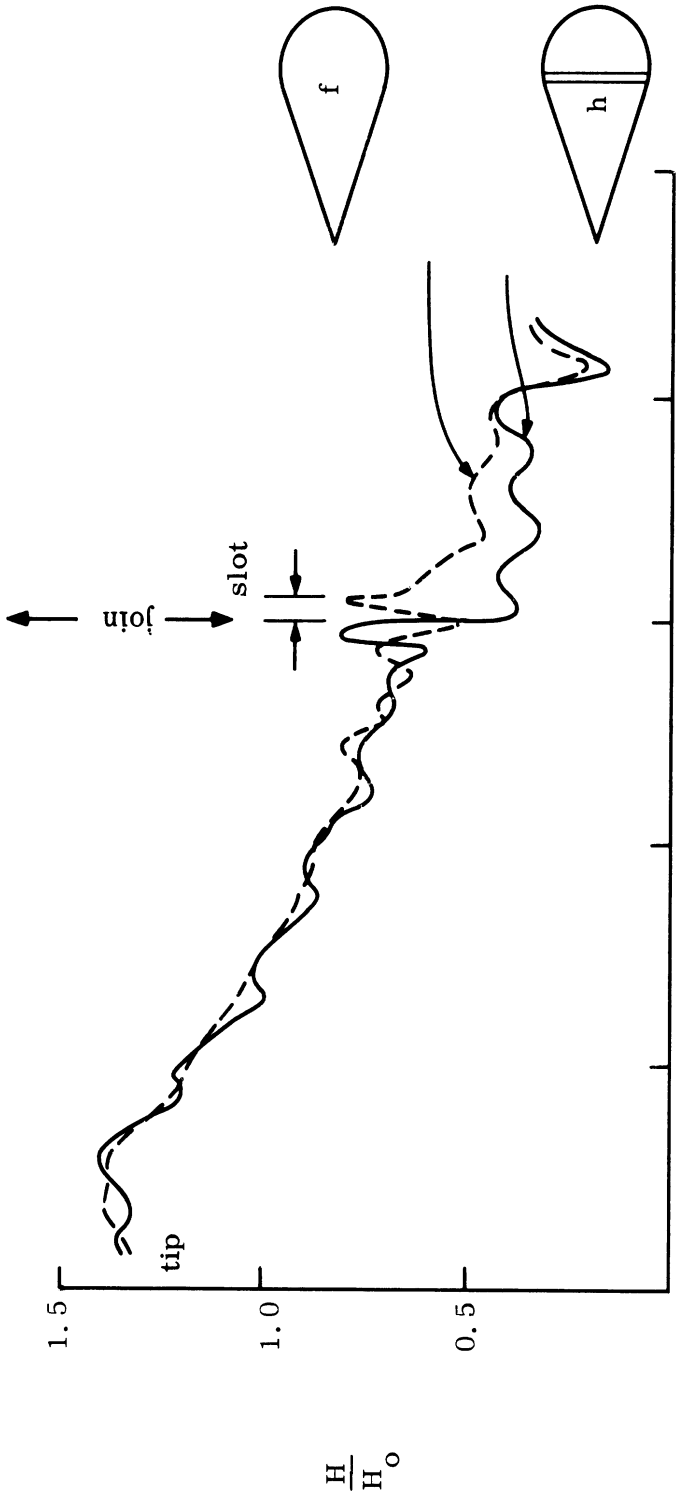

FIG. 2-2: A SLOT IN THE ABSORBER COATING HAS DIFFERENT EFFECTS DEPENDING UPON THE MODEL UNDERNEATH THE COATING - COMPARISON OF MODELS f AND h (SEE FIG. 2-1) AT ka OF 5.0.

(U) In Fig. 2-3 we present the same kind of comparison as in Fig. 2-2, except that the ka is lower. The dashed trace shows the field when the model inside the coating is a plain cone-sphere and the solid curve corresponds to model LSH being coated. The slot cut in the coating near the join gives rise to perturbations in both cases, but they are stronger with model LSH. Note that, in addition to an enhancement of the periodic wobbles on the cone, the fields around the back have been suppressed. The effects are apparently magnified versions of those seen in Fig. 2-2.

(U) In Fig. 2-4 we see the effect of frequency on the surface fields of the coated LSP model. This object, it will be recalled, has an isolated tip antenna simulated by a 1/4" spacer near the tip. The data presented in Fig. 2-3 are for ka = 5.0 and 1.1; the solid trace corresponds to the higher ka. Note that aft of the slot cut in the coating the fields behave much as they might on a solid cone-sphere coated with absorber. Forward of the slot we see a strong perturbation for ka = 5, but the perturbation is nothing more than a ripple for ka = 1.1. Thus the annular slot has a very small effect at low frequencies, and can have a large effect at high frequencies, if the slot is situated near the tip.

(U) One can also assess the relative effects of exposing the LSP and LSH spacers by comparing the solid traces of Figs. 2-2 and 2-3. These traces are for the same frequency (ka = 5.0) and it can be seen that the LSH model exhibits less perturbation effects than the LSP one. This should come as no surprize, for, it will be recalled, without lossy coatings the same relative, qualitative effects were noted in the Second Quarterly Report (Goodrich et al, 1967b).

(U) In addition to the studies described above, the effects of coating indented base models was also investigated. It was difficult to fasten the absorber coating to the complicated, doubly curved surfaces around the bases of

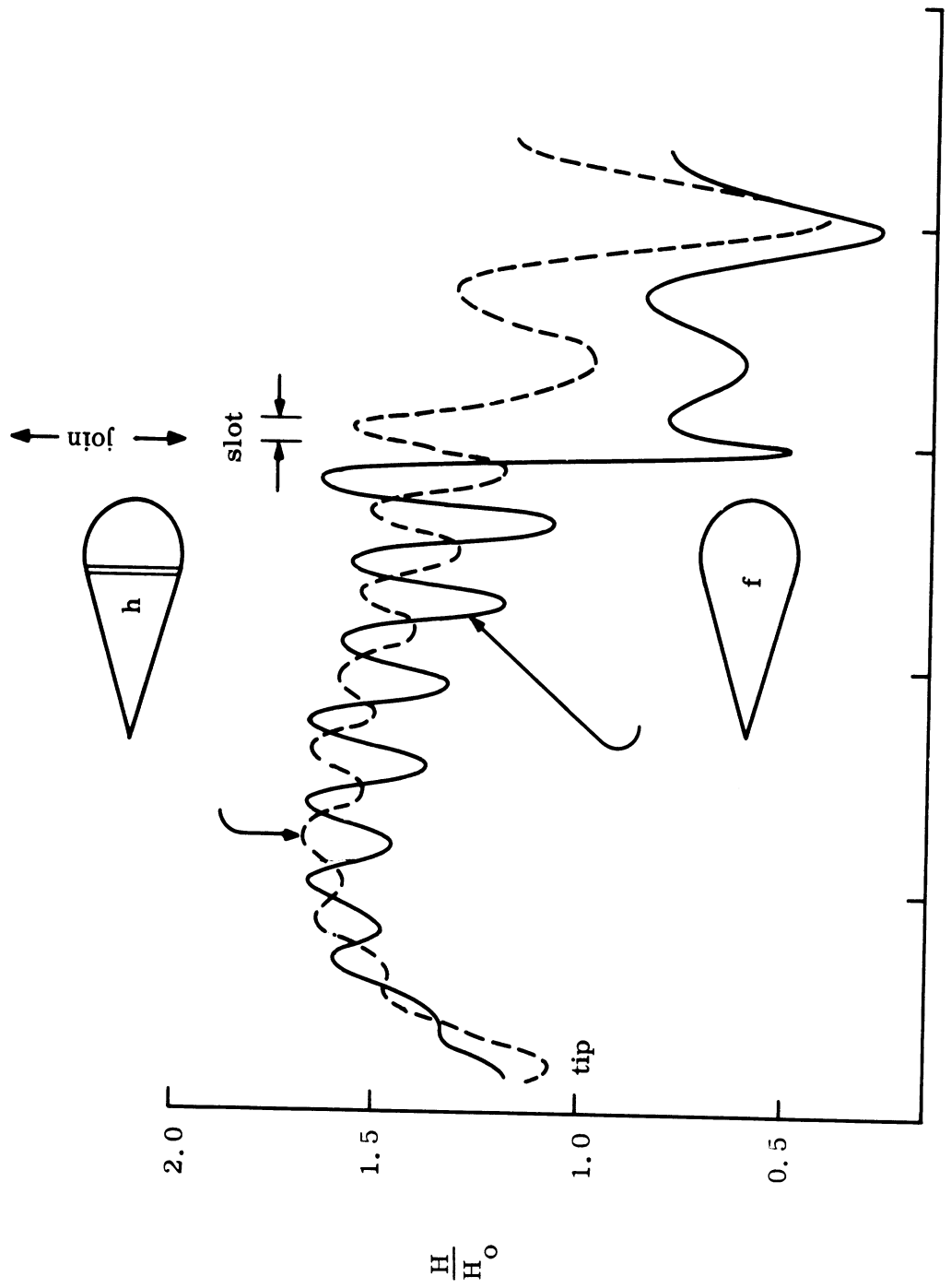

FIG. 2-3: A SLOT IN THE ABSORBER NEAR THE JOIN HAS GREATER EFFECT WHEN MODEL LSH IS INSIDE THE COATING - COMPARISON OF MODELS f AND h (SEE FIG. 2-1) AT ka OF 3.0.

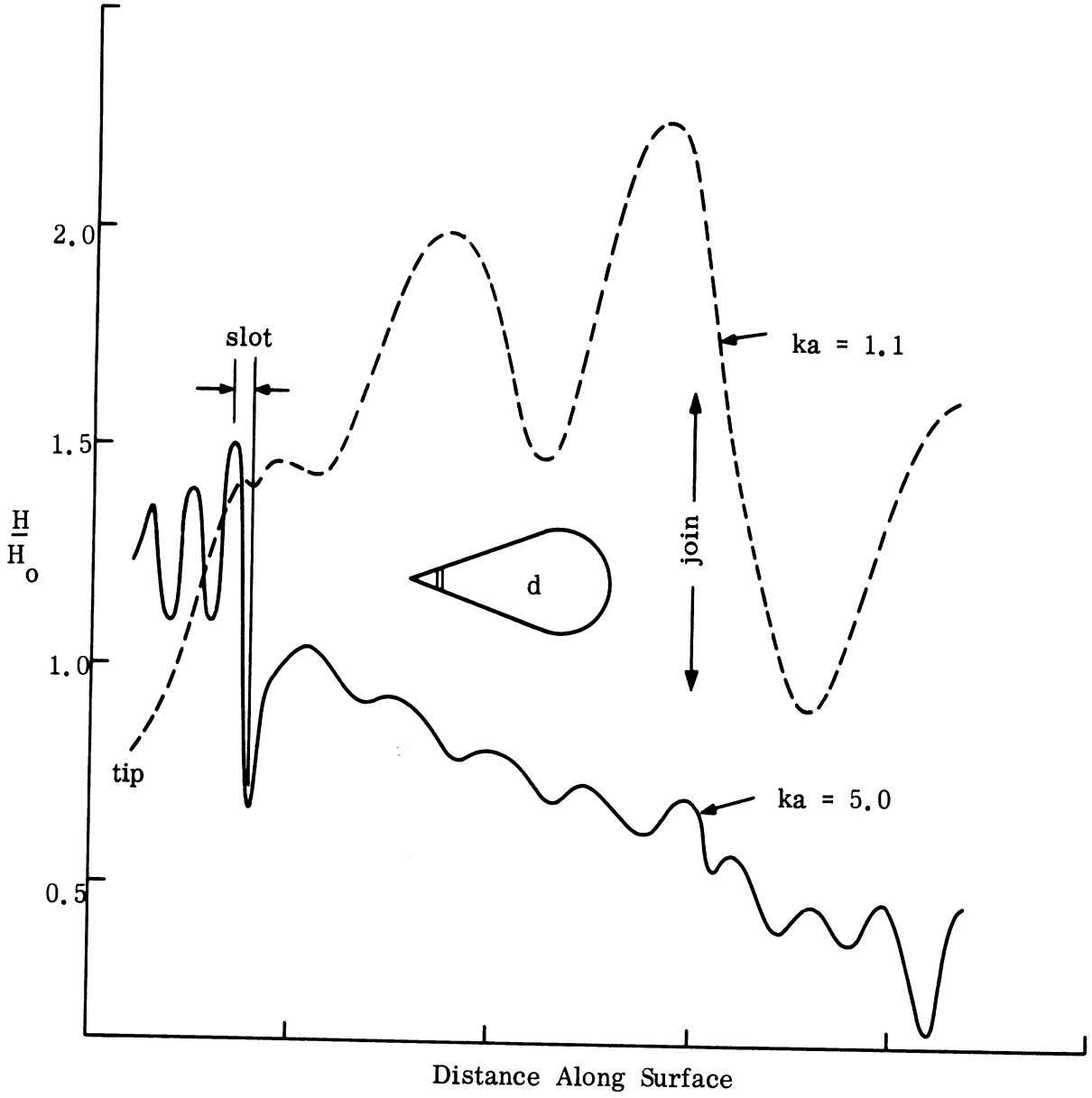

FIG. 2-4: THE SLOT HAS A LARGER EFFECT FOR HIGHER FREQUENCY THAN LOWER FREQUENCY WHEN LSP MODEL d (SEE FIG. 2-1) IS EXPOSED BY AN ANNULAR SLOT IN THE COATING.

these models, so we simply stretched the coating across the back of the models, as shown in Fig. 2-5. Three indented-base models were available (ID-1, ID-2 and ID-3) from earlier studies and each was coated and measured at four frequencies, corresponding to ka = 1.1, 3.0, 5.0 and 8.0. The measurements were obtained for nose-on incidence only.

(U) The resulting data (12 patterns) showed such marked independence on the depth of indentation that we present results for ka = 5.0 as typical of all four frequencies. In Fig. 2-6 we have superposed the surface field data for the three models and since the data are substantially the same for each, we make no attempt to differentiate one from the other. The fields along the coated cone decay as expected (based on measurements of coated cone-spheres) with slight periodic wiggles that betray a possible reflection emanating from near the join. The intensity builds up slightly near the tip, attaining a maximum value of about 1.4, then falls off to a value of about 0.6 at the join. Around the rear of the model we see the greatest differences and amount to about 2.5 db.

(U) We thus conclude that it matters little how deep the base is indented if the model is absorber-coated, and would guess that a coated flat-backed model would behave precisely the same as the indented base models if the first radius of curvature would be made the same.

2.3 Backscatter Measurements of Perturbed Shapes (Tasks 2.1.3 and 2.1.4)

(U) In addition to measurements of surface fields during this quarter, considerable time has been expended in far field measurements of both "clean" and perturbed shapes. We hasten to point out that no measurements of coated, perturbed shapes were made. The subjects of the backscatter measurements were a plain 15-degree (total angle) cone-sphere, model LSP (a 15-degree cone-sphere with a simulated tip antenna), and a series of four flat-backed cones having varying radii of curvature connecting the cones with bases. The flat backed models are sketched in Fig. 2-7.

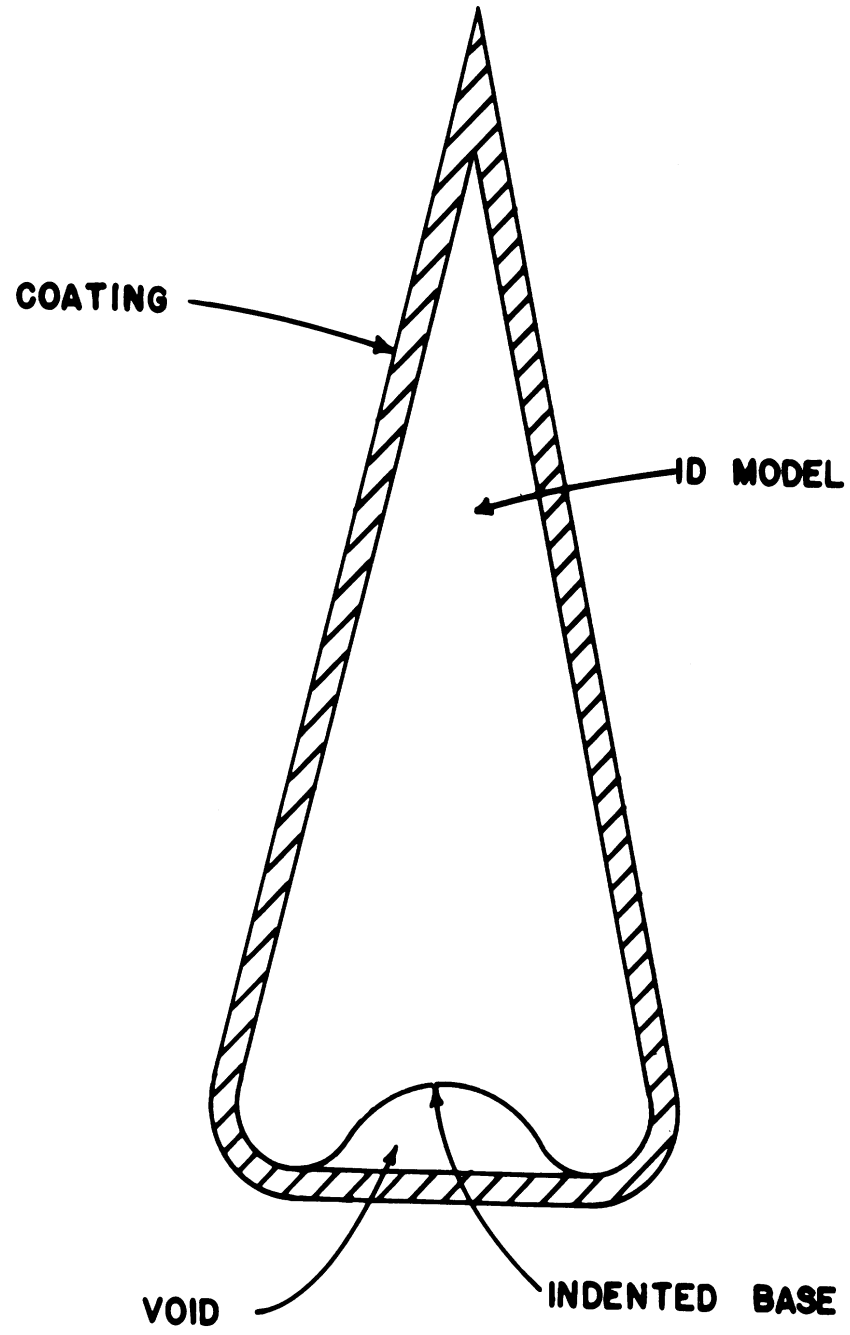

FIG. 2-5: THE COATING WAS SIMPLY STRETCHED ACROSS THE BACK OF THE ID MODELS.

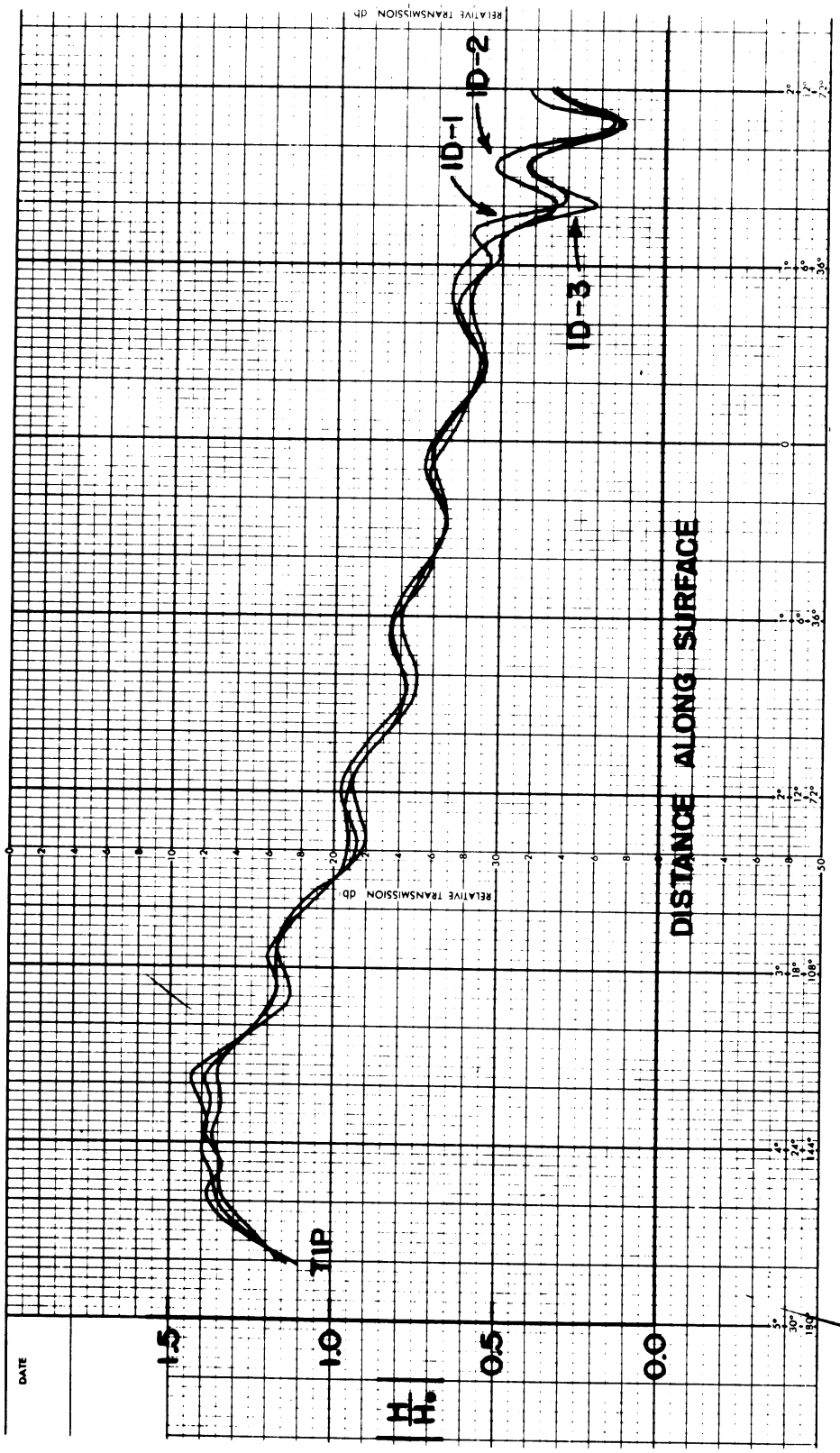

FIG. 2-6: BEHAVIOR OF ALL THREE COATED ID MODELS IS ABOUT THE SAME: THIS PLOT IS FOR ka = 5.0.

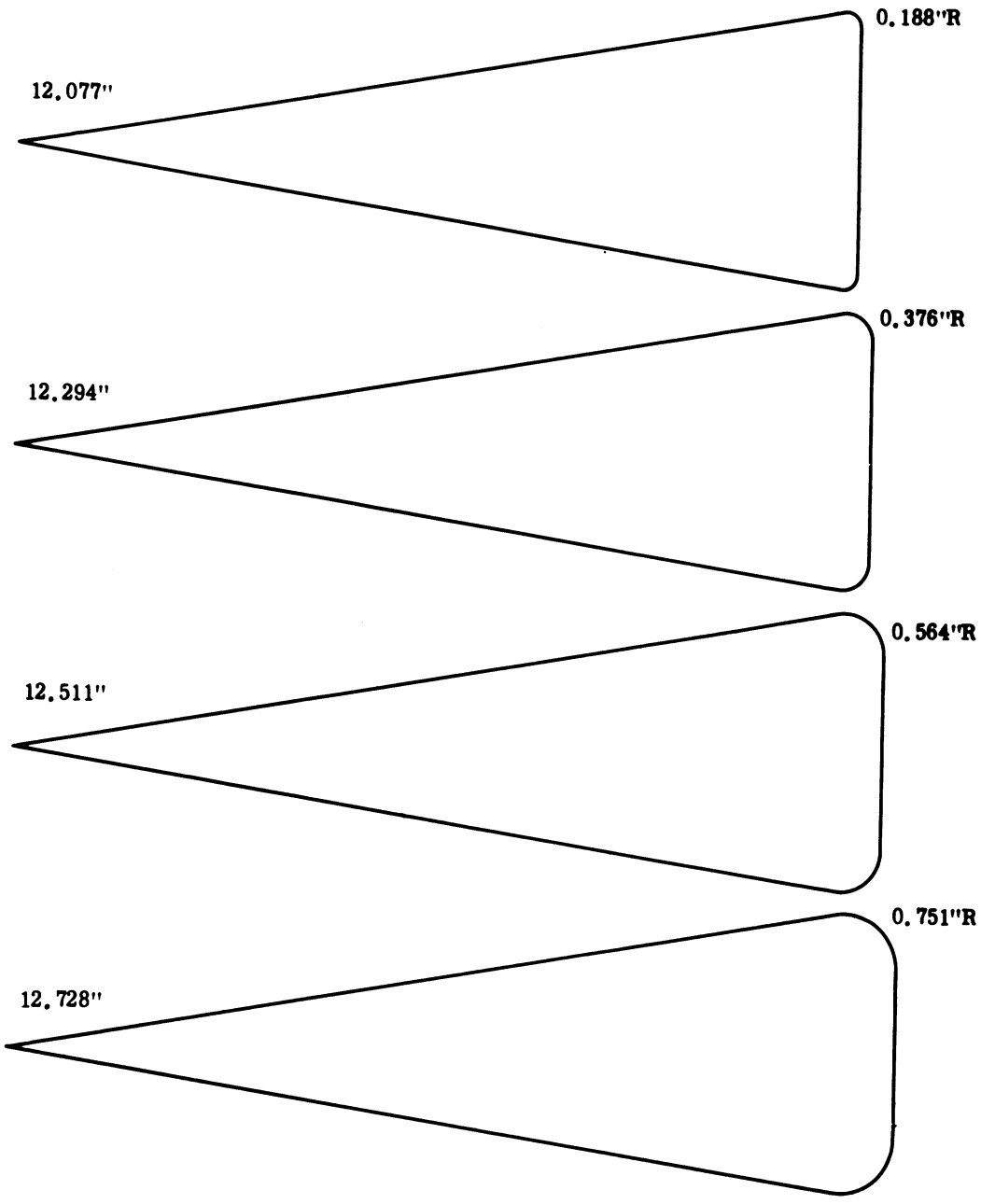

FIG. 2-7: THE FINAL APPEARANCE OF THE MODELS IS SHOWN IN THE SKETCHES. Beside each is the total model length, assuming a perfect tip (a point) and perfect tolerance. Cone base diameter at point of tangency = 3.765" total cone angle = 18^{o}.

(U) The radar cross section of each of the six models was measured as a function of aspect angle for a host of frequencies. In all, a total of 286 patterns were recorded in order to obtain the close frequency spacing that was desired. The nose-on, tail-on, and specular returns were read from each pattern and then plotted as functions of ka; as will be shown in a later portion of this report, the close frequency spacing was of considerable value in analyzing backscattering behavior. We mention in passing that the return of model LSP had been measured once before, but for only four widely separated frequencies, and that the present data is of much more value than the earlier data.

(U) In Fig. 2-8 we have plotted the behavior of a metallic cone-sphere for purposes of reference. Observe that the specular glint remains more or less a steady 15 db above the tail-on return, and both increase with increasing ka. The nose-on return shows the familiar oscillatory pattern as the join echo goes in and out of phase with the contribution of the creeping wave. Note that $2.5 \leq ka \leq 6.8$ for this figure.

(U) We have plotted the returns of model LSP in Fig. 2-9 and for the sake of clarity have displaced the nose-on behavior downward by 25 db. Note that the specular glint is much the same as for a cone-sphere in spite of the presence of the insulating wafer between the tip and the main part of the object. The tail-on return is severely perturbed for ka between about 4 and 7 due to a wave that is launched toward the tip from the shadow boundary. The nose-on return in this region is markedly enhanced over that of a plain cone-sphere but there are no strong oscillations like those in the tail-on behavior. The enhancement amounts to 10 db or more and is analyzed in a later portion of this report.

(U) In Figs. 2-10 through 2-13 we present the backscattering behavior of the four flat-backed models sketched in Fig. 2-7. In all four of these figures the three returns have been displaced from each other for clarity and the

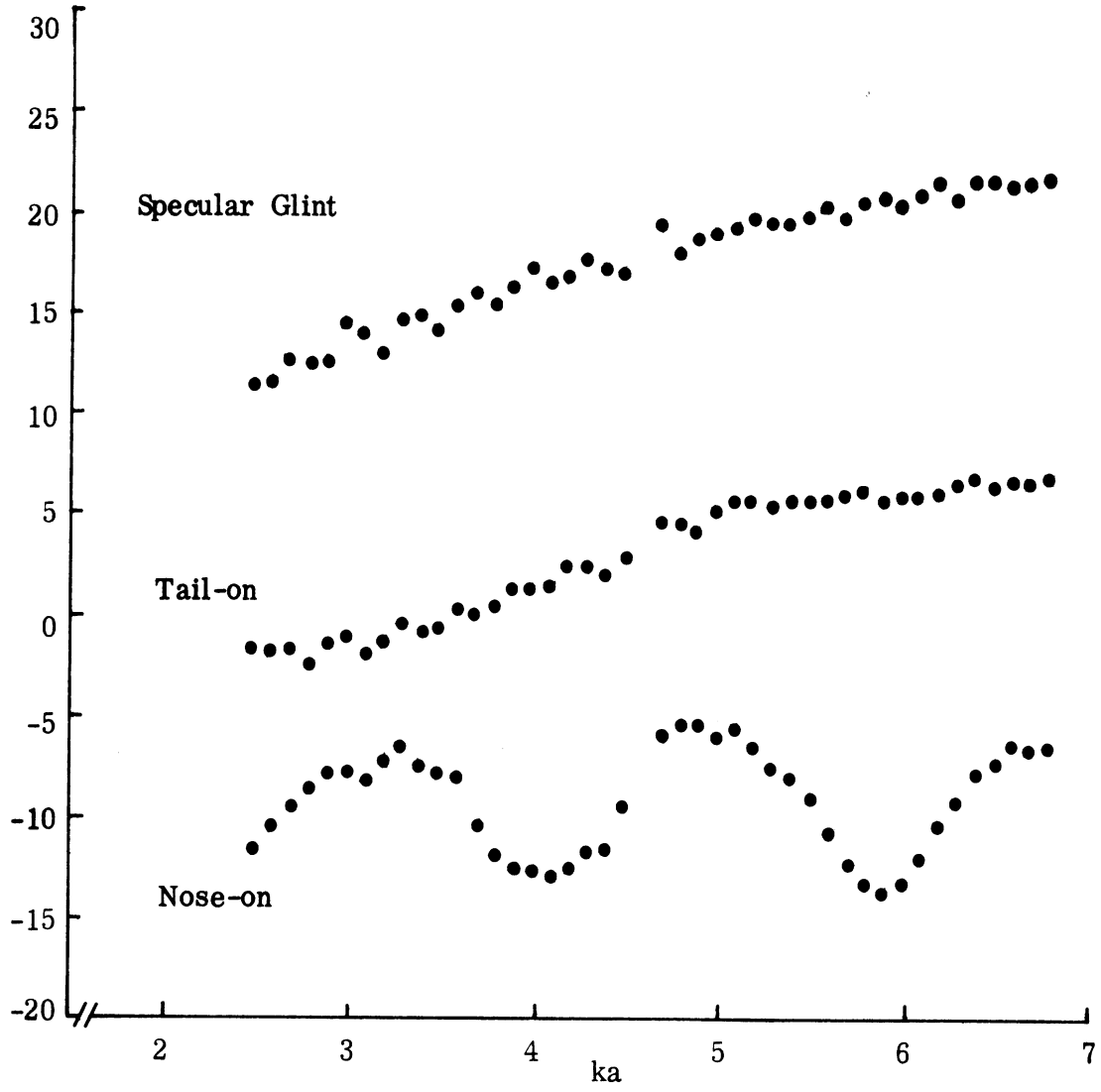

FIG. 2-8: BEHAVIOR OF 15^{o} CONE-SPHERE CROSS SECTIONS.

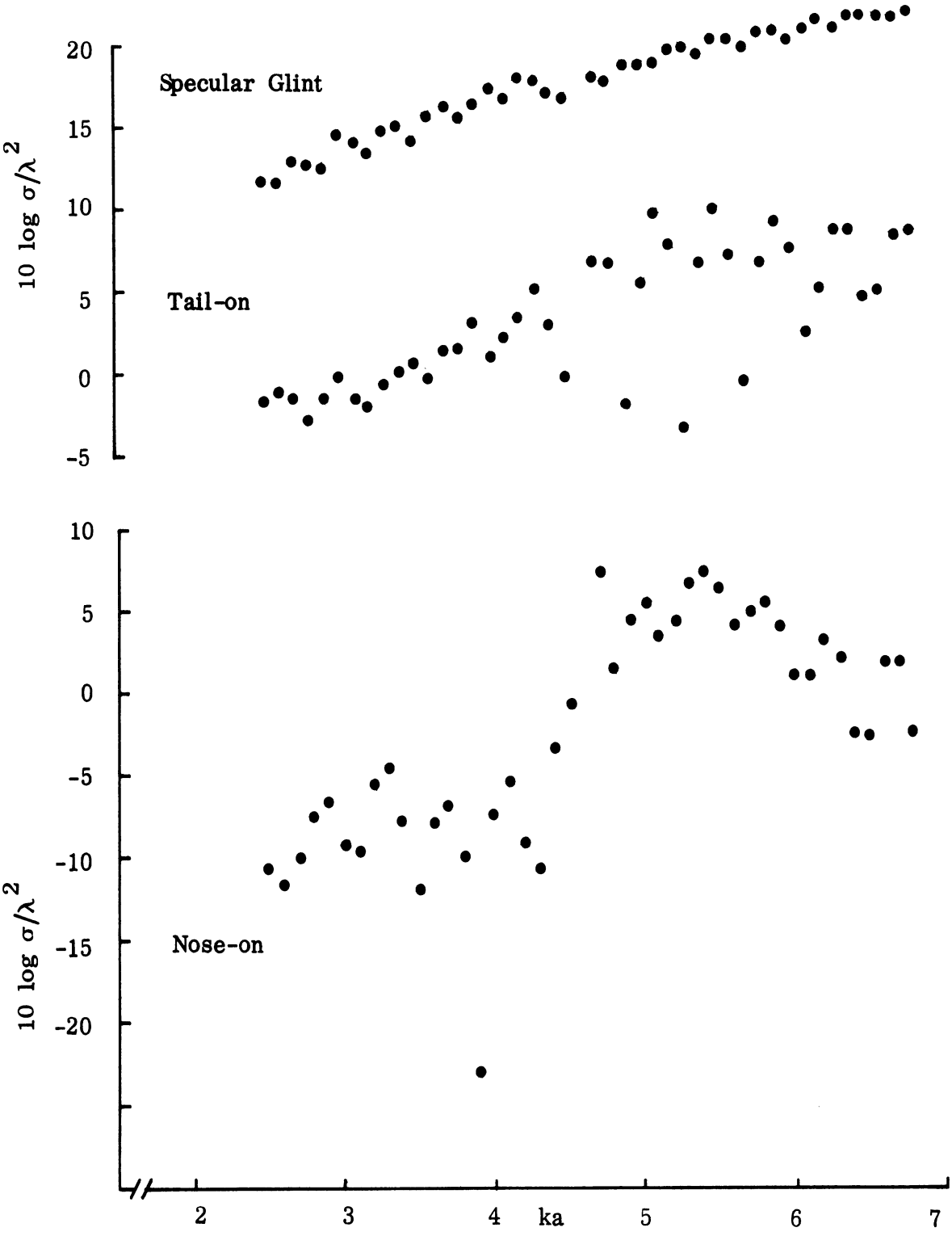

FIG. 2-9: THE NOSE-ON RETURN FOR THE LSP MODEL HAVE BEEN DISPLACED FROM THE OTHER RETURNS FOR CLARITY.

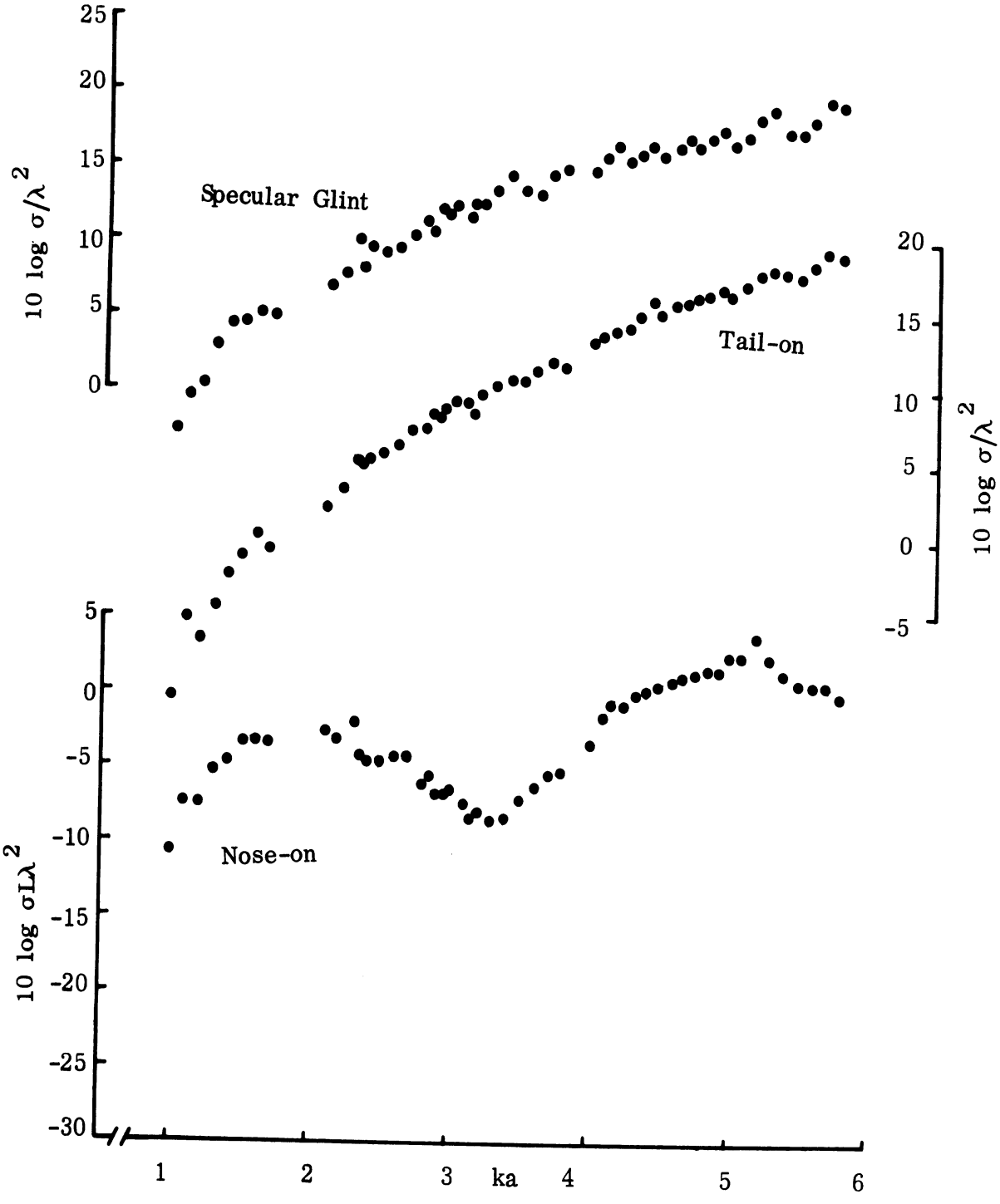

FIG. 2-10: RADAR CROSS SECTIONS OF MODEL FB-1.

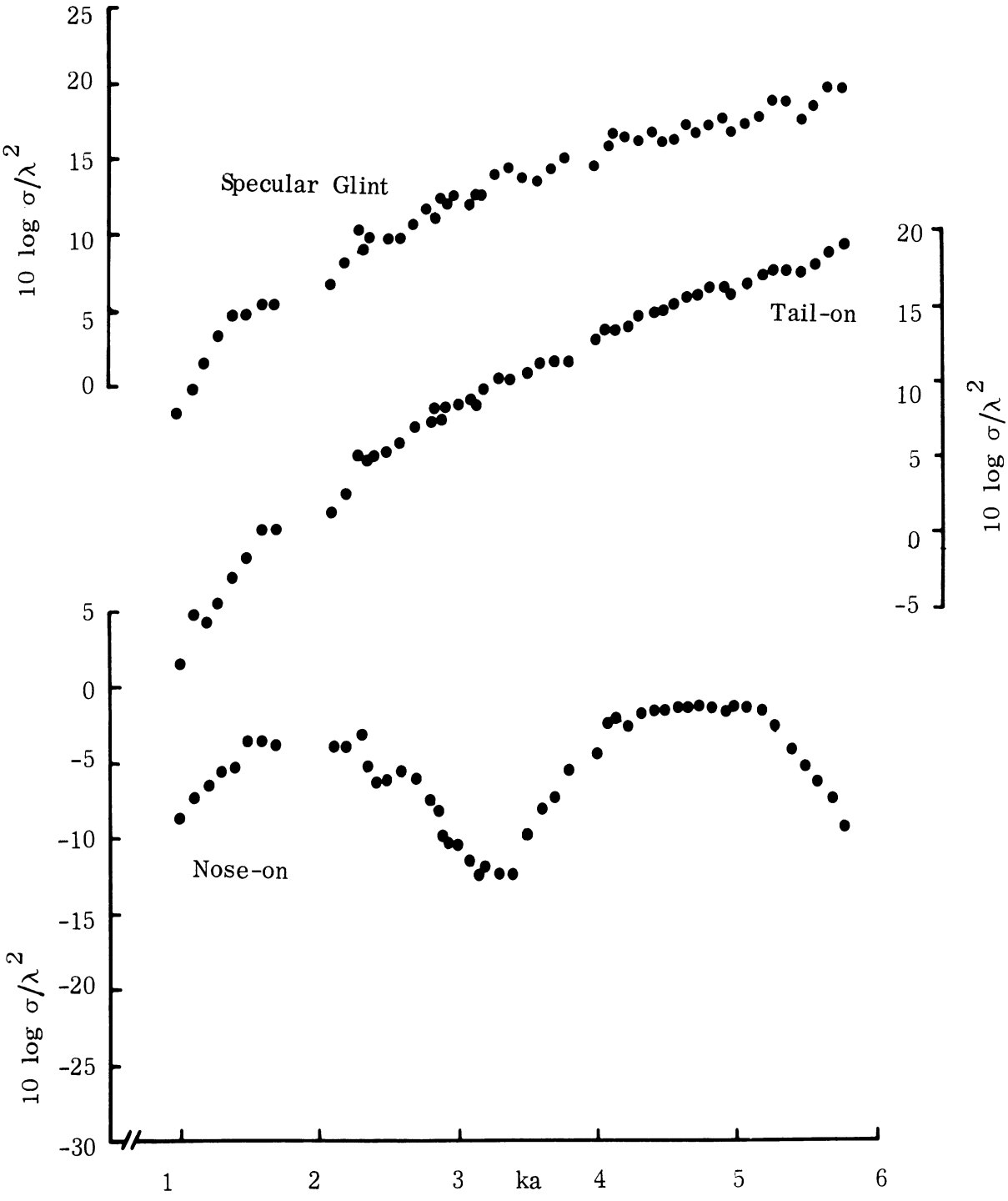

FIG. 2-11: RADAR CROSS SECTIONS OF MODEL FB-2.

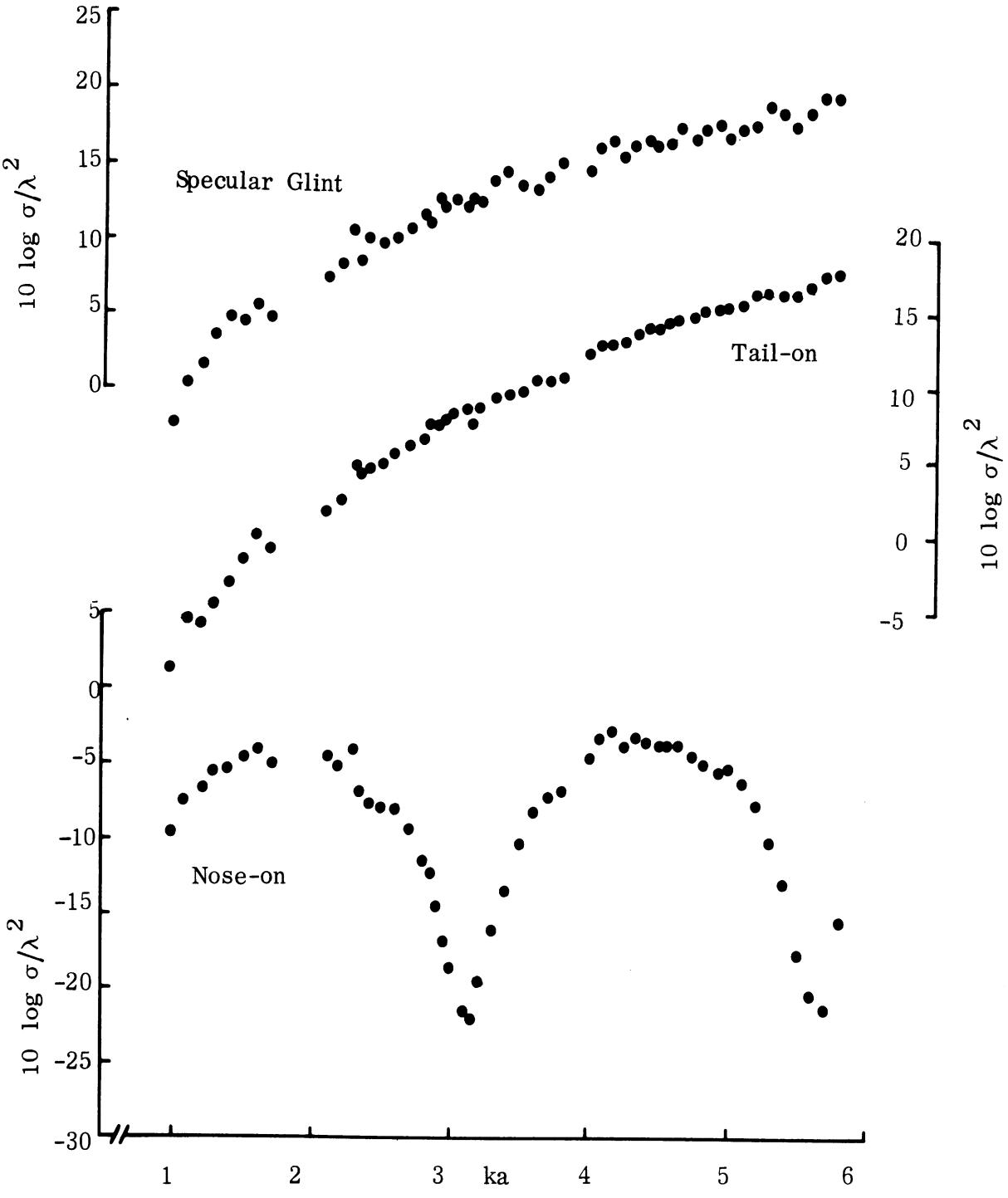

FIG. 2-12: RADAR CROSS SECTIONS OF MODEL FB-3.

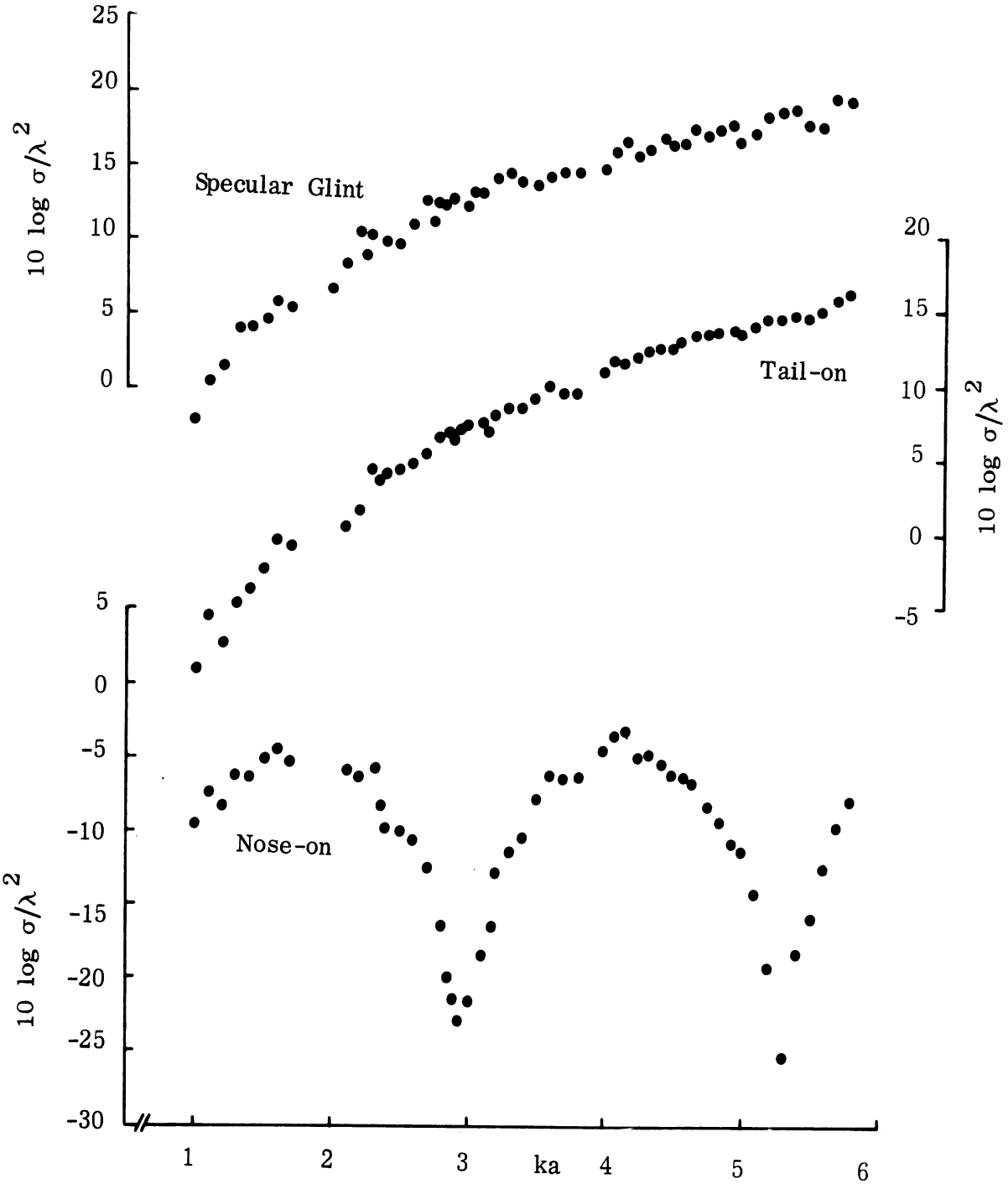

FIG. 2-13: RADAR CROSS SECTIONS OF MODEL FB-4.

reader is cautioned to inspect the appropriate scales before attempting to read off any values from the plots. A cursory comparison of all four figures shows the specular glints and tail-on responses to be nearly the same for the four models but small differences persist due to the curvature near the join. It is the nose-on cross sections that change from model to model.

(U) In Fig. 2-10 we see an oscillatory pattern in the character of the nose-on return of model FB-1. A null appears near ka = 3.3 and the radar cross section there is about -9 dbλ^2. This model has the sharpest radius of curvature of the flat-backed cones. In Fig. 2-11, the null has drifted to about ka = 3.2 and the return is about -12 dbλ^2. In Fig. 2-12, the null is becoming pronounced and has moved to about ka = 3.1, reaching a depth of about -22 dbλ^2. Finally in Fig. 2-13 the null appears slightly below ka = 3.0 with value of -23 dbλ^2. In these last two figures we can see another null forming, near ka = 5.6 in Fig. 2-12 and near ka = 5.3 in Fig. 2-13; this second null appears to be sharper than the first one. This phenomena could not be immediately explained by theory. A more detailed discussion is given in Section 3.2.

2.4 Effects of Radius of Curvature on Surface Fields (Task 2.1.4)

(U) During this quarter a series of surface field measurements were obtained for the FB models. Again, the ka values used were 1.1, 3.0, 5.0 and 8.0 and the models were illuminated nose-on. The results of the measurements for ka = 5.0 are shown in Figs. 2-14 and 2-15 and are typical.

(U) The effect of the radius of curvature near the join is clearly shown in these figures. For model FB-1, the shape with the sharpest curvature, we observe the strongest interference pattern in the field structure. The magnitude of the perturbation steadily decreases as we examine the responses on models FB-2, 3, and 4, the fields on the last being perturbed least of all. We

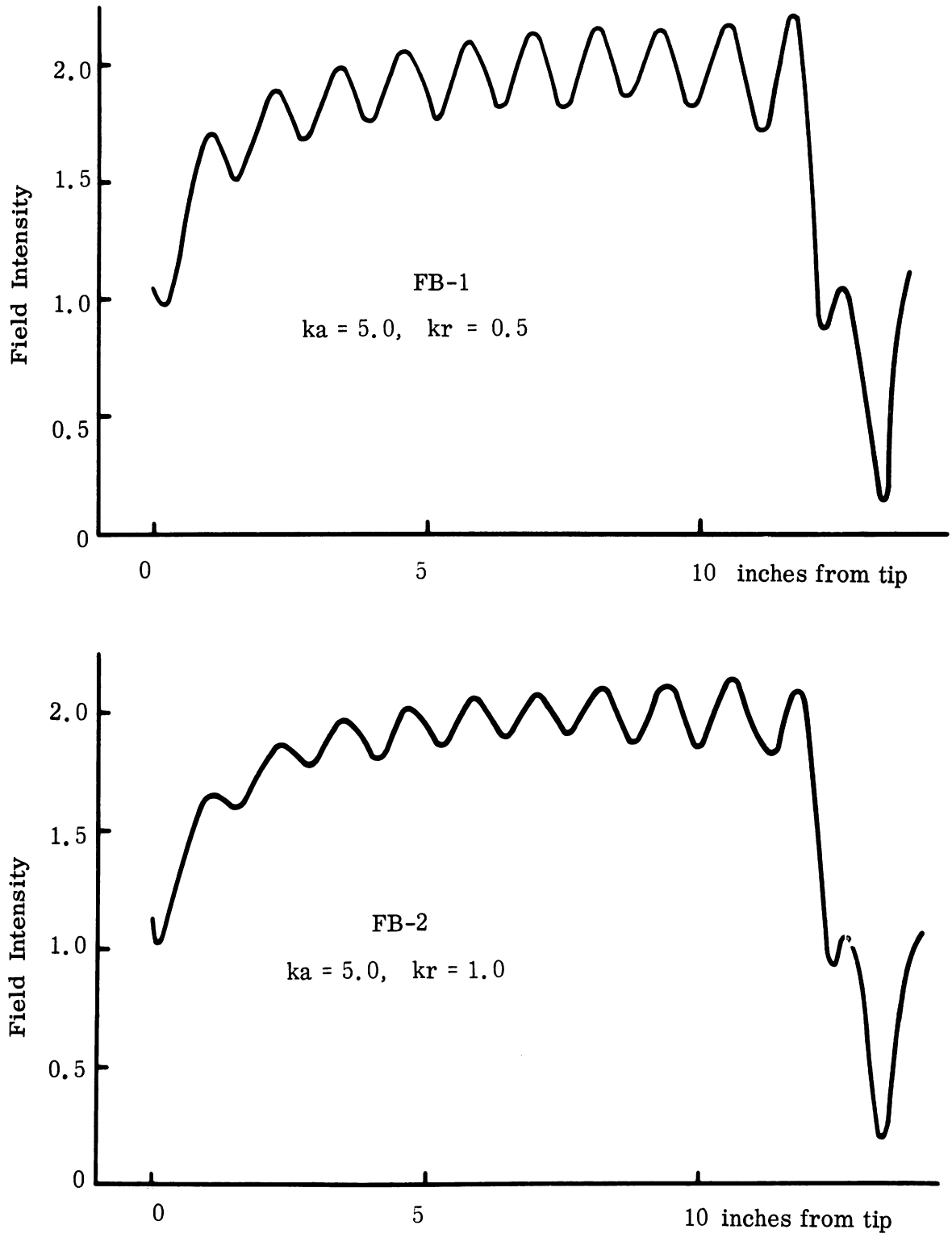

FIG. 2-14: SURFACE FIELDS ON BARE FLAT-BACKED MODELS FB-1 AND FB-2.

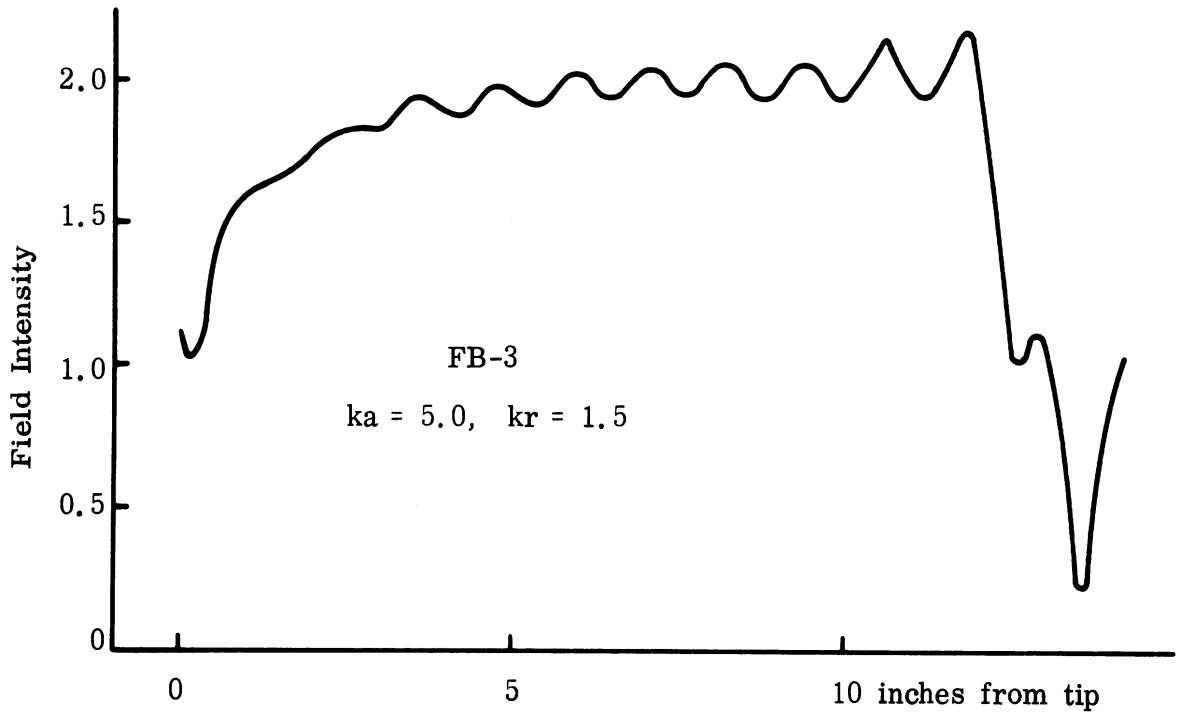

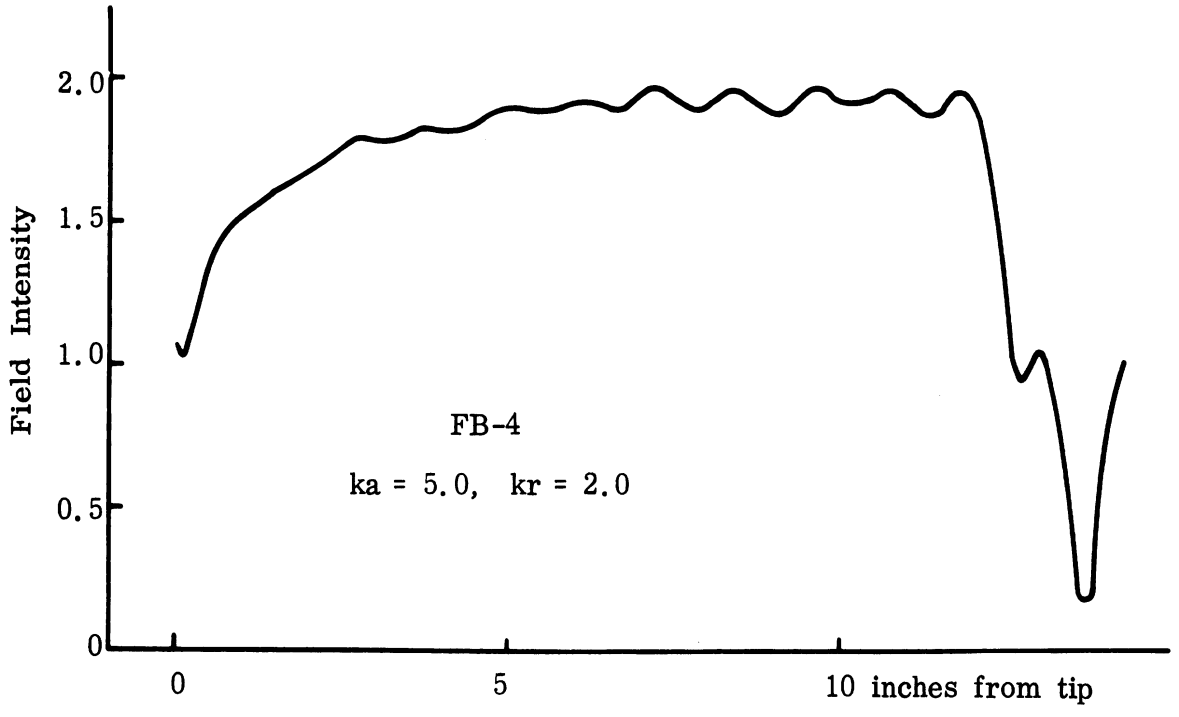

FIG. 2-15: SURFACE FIELDS ON BARE FLAT-BACKED MODELS FB-3 AND FB-4.

conclude that the radar return arising near the join should become progressively lower as that radius increases. Indeed, inspection of Figs. 2-10 through 2-13 show that the average nose-on return falls approximately 6 db from the first (Fig. 2-10) to the last (Fig. 2-13). The reader is cautioned to strike these averages carefully, for the scales are logarithmic and the return cannot be "averaged" when expressed in decibels.

2.5 Re-entry Plasma Experiments (Task 2.1.5)

2.5.1 Introduction

(U) During the Third Quarter radar cross section measurements were made on a flat-back cone covered with a wire grid (simulated plasma with no loss) at S-band (2.1 to 3.0 GHz). Separate tests were performed on the uncoated cone for reference and calabration purposes. The test results on the perfectly conducting cone check out well with theory for nose-on, broadside and end-on, but no theoretical explanations have been developed for the behavior of a cone when it is covered with a wire grid. Typically the return from the coated cone is reduced 5 to 13 db at nose-on whereas the return from the lobes away from nose-on is substantially increased compared to that for the perfectly conducting cone. Examples of experimental results are presented and analyzed for the tests made on the conical geometry.

(U) Additional work has been done on the flat plate covered with a wire grid, a problem which was discussed in the last Quarterly Report (Goodrich et al, 1967b). This Quarter, surface field measurements were made at angles of incidence where the extraordinary lobe peaks and nulls appeared in the scattering patterns for the coated flat plate. These measurements verified that there were correspondingly large and small surface fields present in the lobe peak and null regions. Further studies were made to determine if complex of leaky wave modes could be supported by this geometry. For the lossless

current sheath approximate calculations show that the complex poles of the composit reflection coefficient are located in the vacancy of the extraordinary lobe peaks. Work is continuing on the formulation of the leaky wave model to fit our problem. Since this work is incomplete at the present time, it will be presented in the final report.

2.5.2 Backscatter Cone Measurements

(U) A number of measurements were made on the conical geometry shown in Fig. 2-16 at 2.1, 2.5 and 3.0 GHz and for VV and HH polarization. During the tests the cone is mounted on a foam pedestal with its cone axis normal to the axis of rotation. The distance between the target and transmit-receive antenna was 25' which is L^2/λ (L is the slant length of the cone) instead of the usual far field range $2L^2/\lambda$. This slight reduction in the far field range did not cause any noticable effects in the scattering patterns.

(U) Referring once again to Fig. 2-16, it is seen that the test model consists of an aluminum flat-backed cone with half angle $\alpha_c = 12.2^o$, slant length L = 36 3/8" and radius a = 7 5/8" which is covered by an open-base wire grid cone with $\alpha_g = 14.5^o$, L = 36 1/2" and a = 9 1/4". The wire grid structure is supported by four foam rings which also act as spacers. The grid is easily removed for making tests on the aluminum cone alone.

(U) Number 38 gauge copper wire was glued to a thin plastic sheet in the form of 0.3" square inch grid to form the conical grid. When the half angle cone of the grid is 14.5^o, it is easy to fabricate. The surface impedance Z_s of thin wire grid (neglecting curvature effect) is purely inductive, $Z_s = jX_s$, and has the values 0.17 at 2.1 GHz, 0.2 at 2.5 GHz, and 0.24 at 3.0 GHz. These values are normalized with respect to the impedance of free space ($Z_o = 377\ \Omega$).

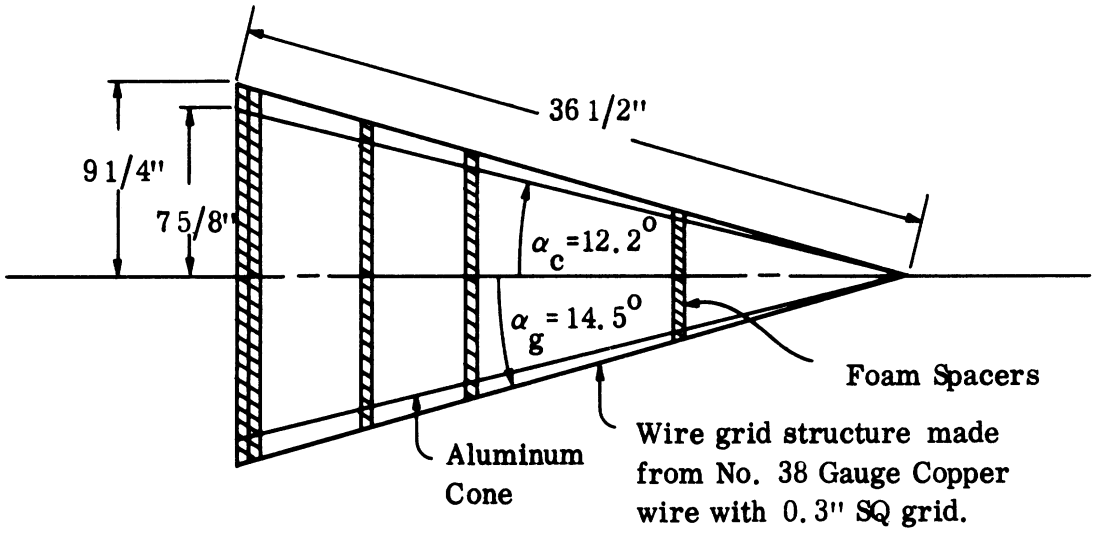

FIG. 2-16: THE COATED CONE GEOMETRY.

(U) Figures 2-17 through 2-22 represent the experimental results obtained for monostatic radar cross section tests made on the conical model. In these six figures the upper pattern (a) is for the cone with the wire grid present and (b) is with the grid removed (bare aluminum cone). It should be noted that when the wire grid is present it only extends from the cone tip along the slant-length to the base; the flat-back is exposed with no grid covering it. Thus the return at $\theta = 180^{\circ}$ is about the same for the coated and uncoated cases and serves as a secondary reference. In addition there is a calabration reference mark on each pattern which is a thin, flat circular disc whose diameter is 15 1/4". The patterns are arranged according to frequency and polarization as indicated in the captions.

(U) Special attention is called to Figs. 2-18, 2-19, 2-21 and 2-22 where additional raised plots also have been included in cases where the return went off the low end of the recorder. The term "Regular RCS" means the unaltered

(a)

(b)

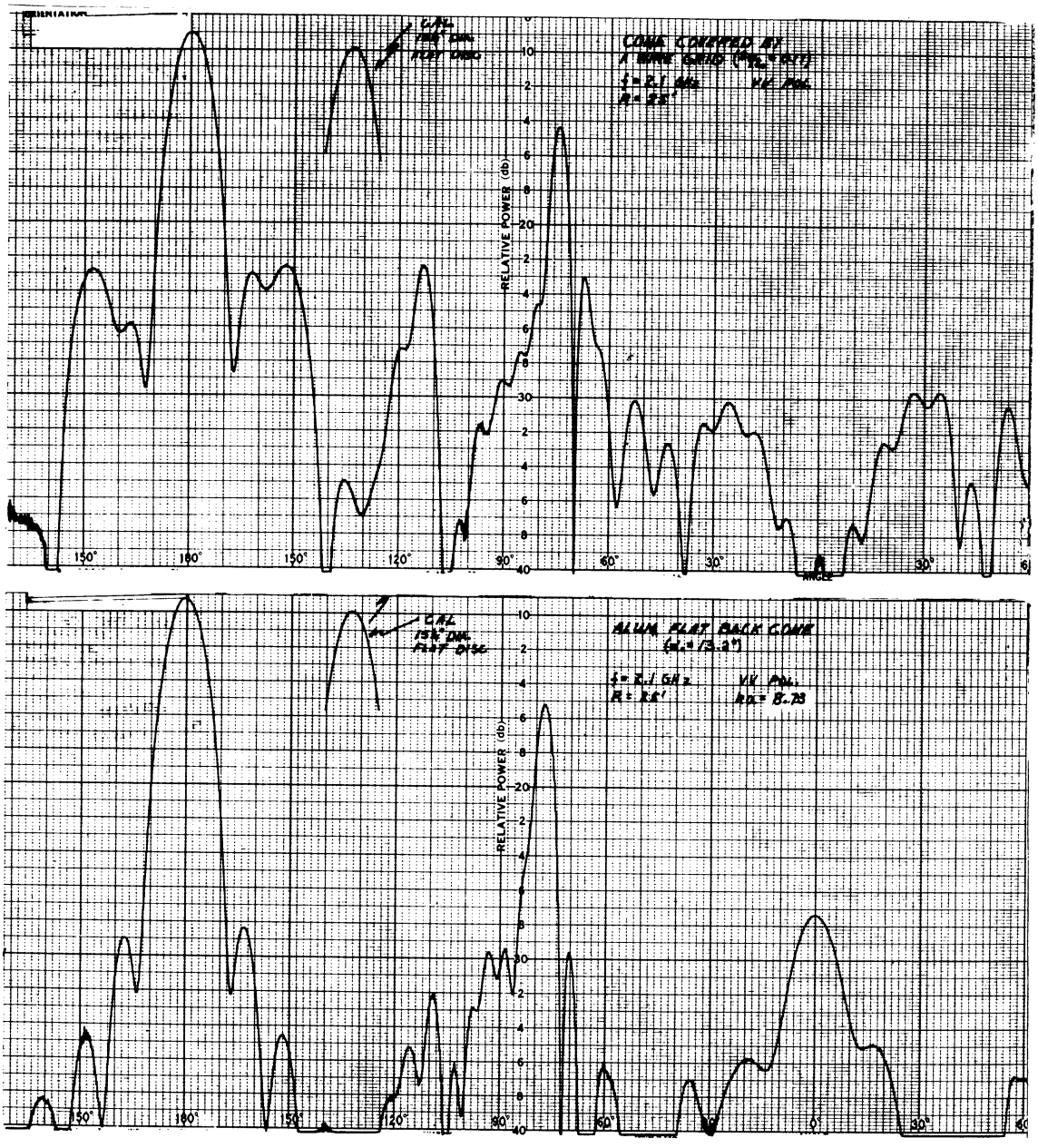

FIG. 2-17: RCS PATTERNS FOR FLAT-BACK CONE (a) WITH WIRE GRID (b) WITHOUT WIRE GRID, f = 2.1 GHz, VV POLARIZATION.

(a)

(b)

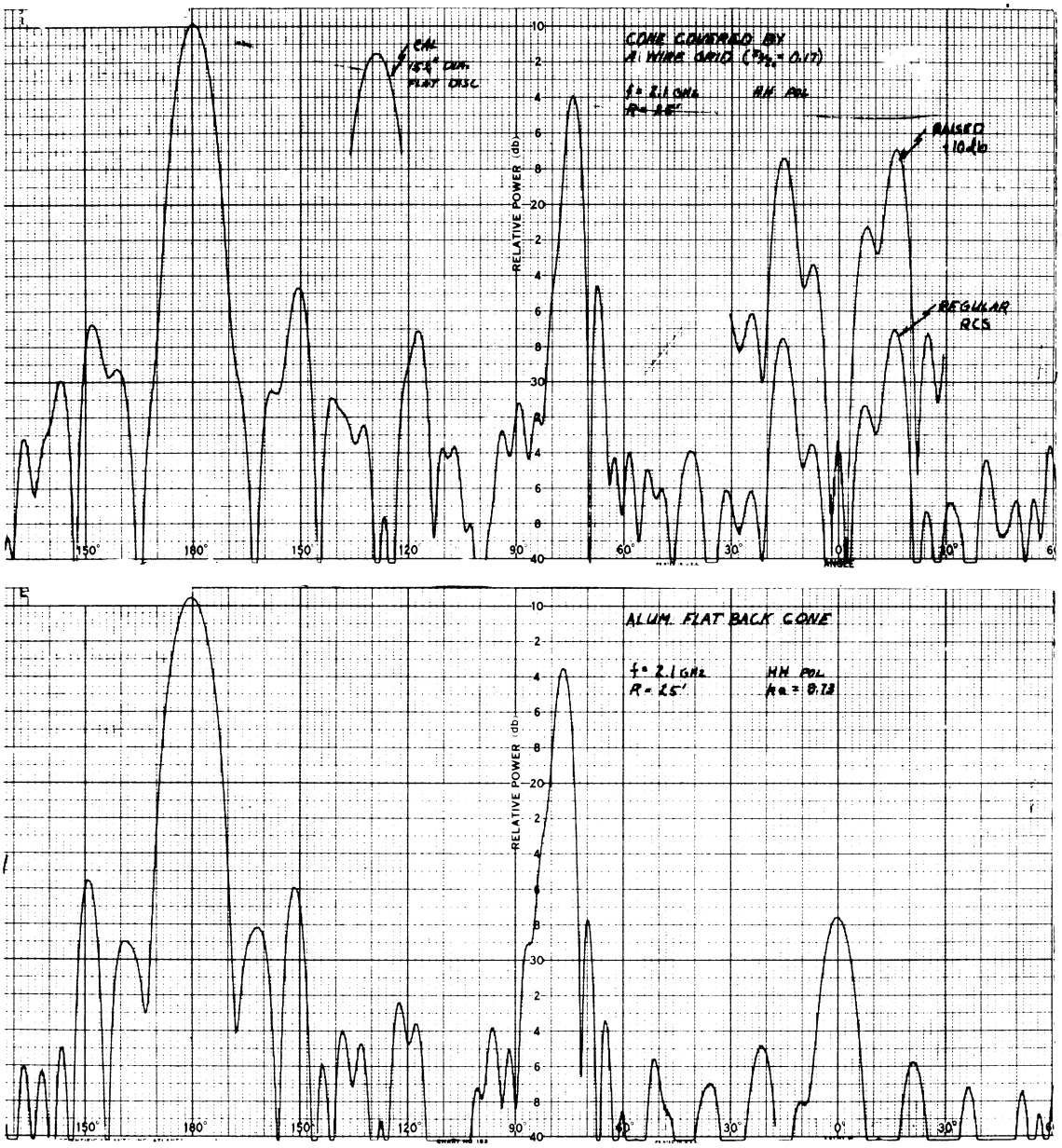

FIG. 2-18: RSC PATTERNS FOR FLAT-BACK CONE (a) WITH WIRE GRID (b) WITHOUT GRID, f = 2.1 GHz, HH POLARIZATION.

(a)

(b)

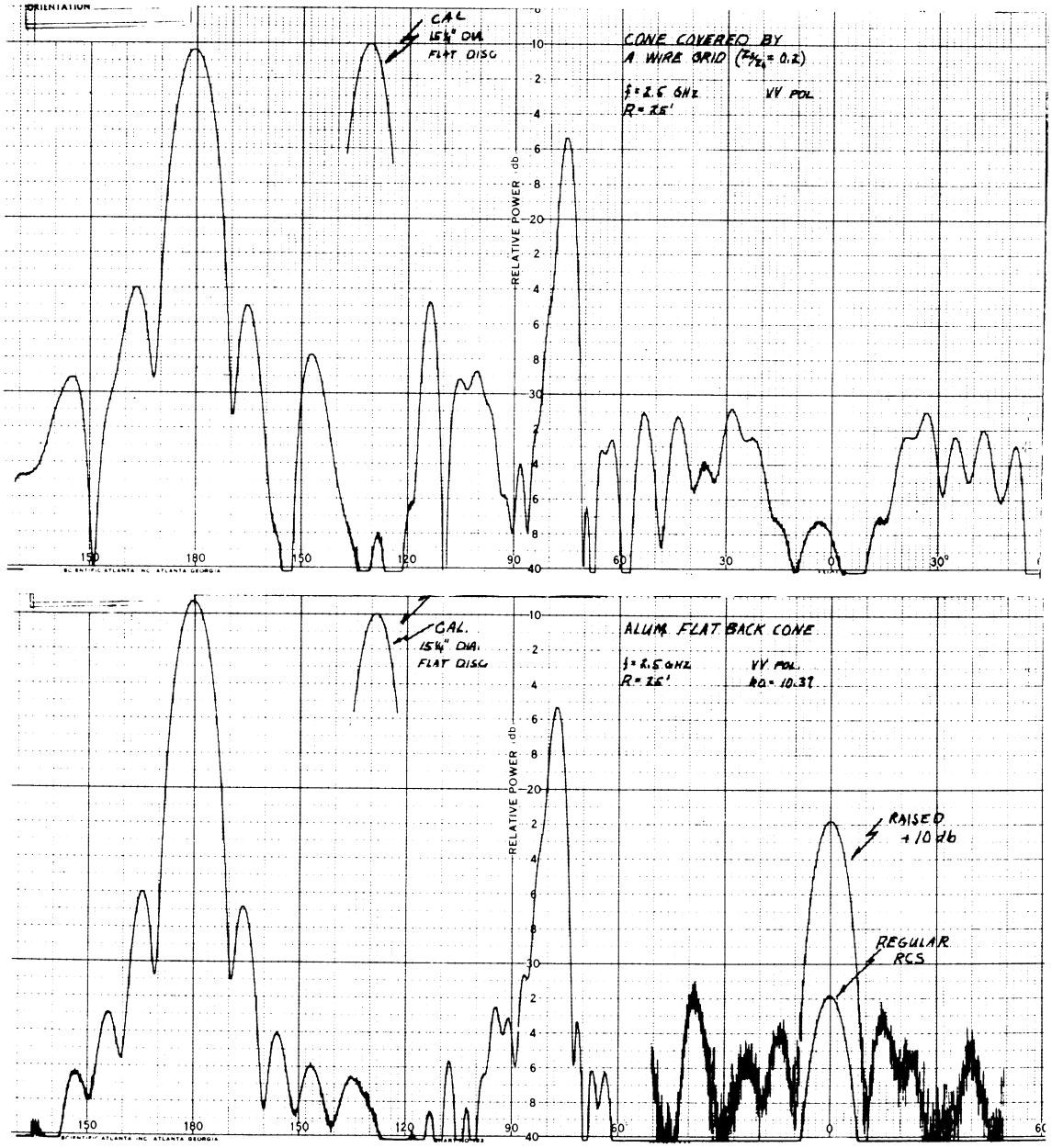

FIG. 2-19: RCS PATTERNS FOR FLAT-BACK CONE (a) WITH WIRE GRID (b) WITHOUT GRID, f = 2.5 GHz, VV POLARIZATION.

(a)

(b)

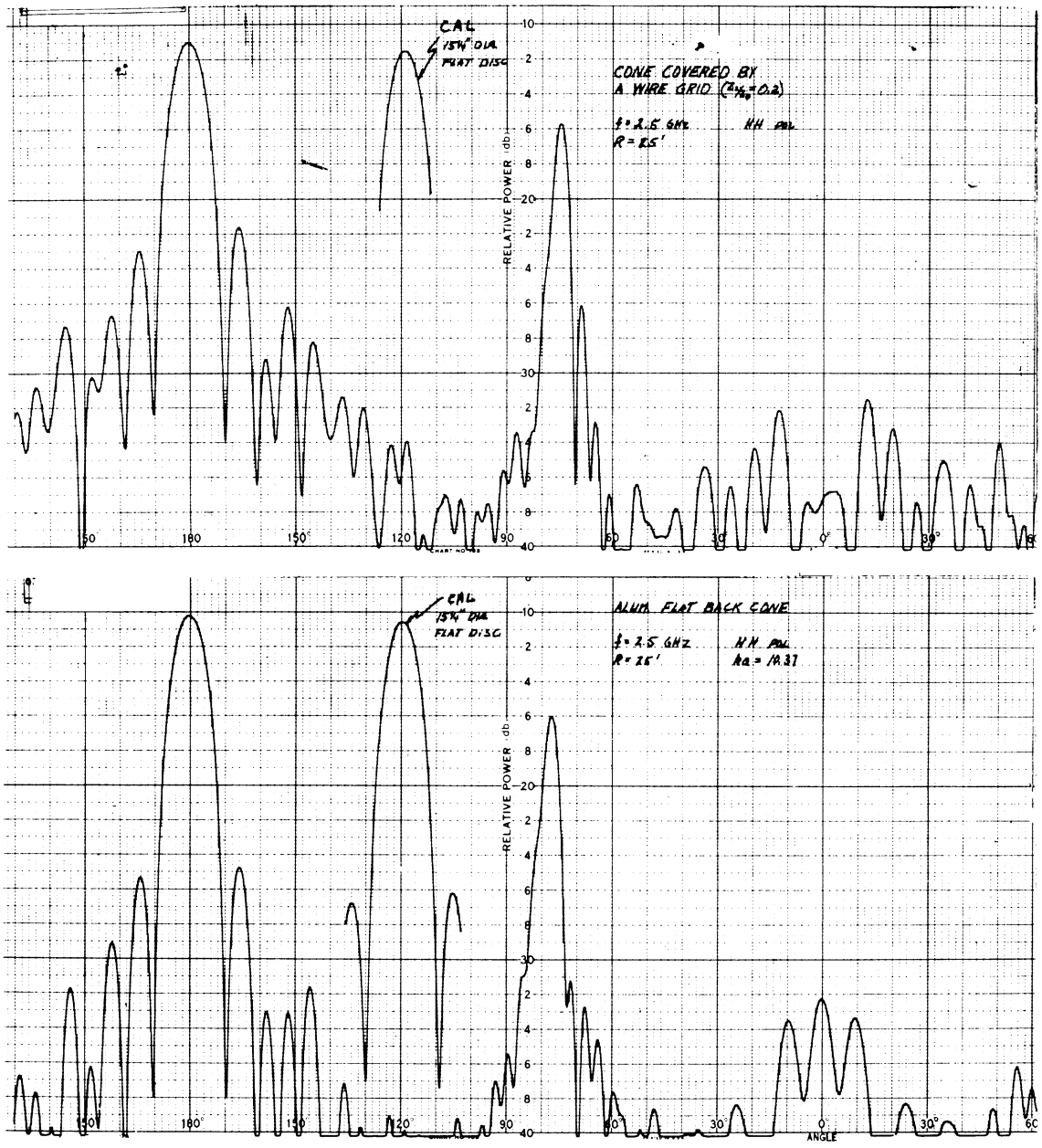

FIG. 2-20: RCS PATTERNS FOR FLAT-BACK CONE (a) WITH WIRE GRID (b) WITHOUR BRID, f = 2.5 GHz, HH POLARIZATION.

(a)

(b)

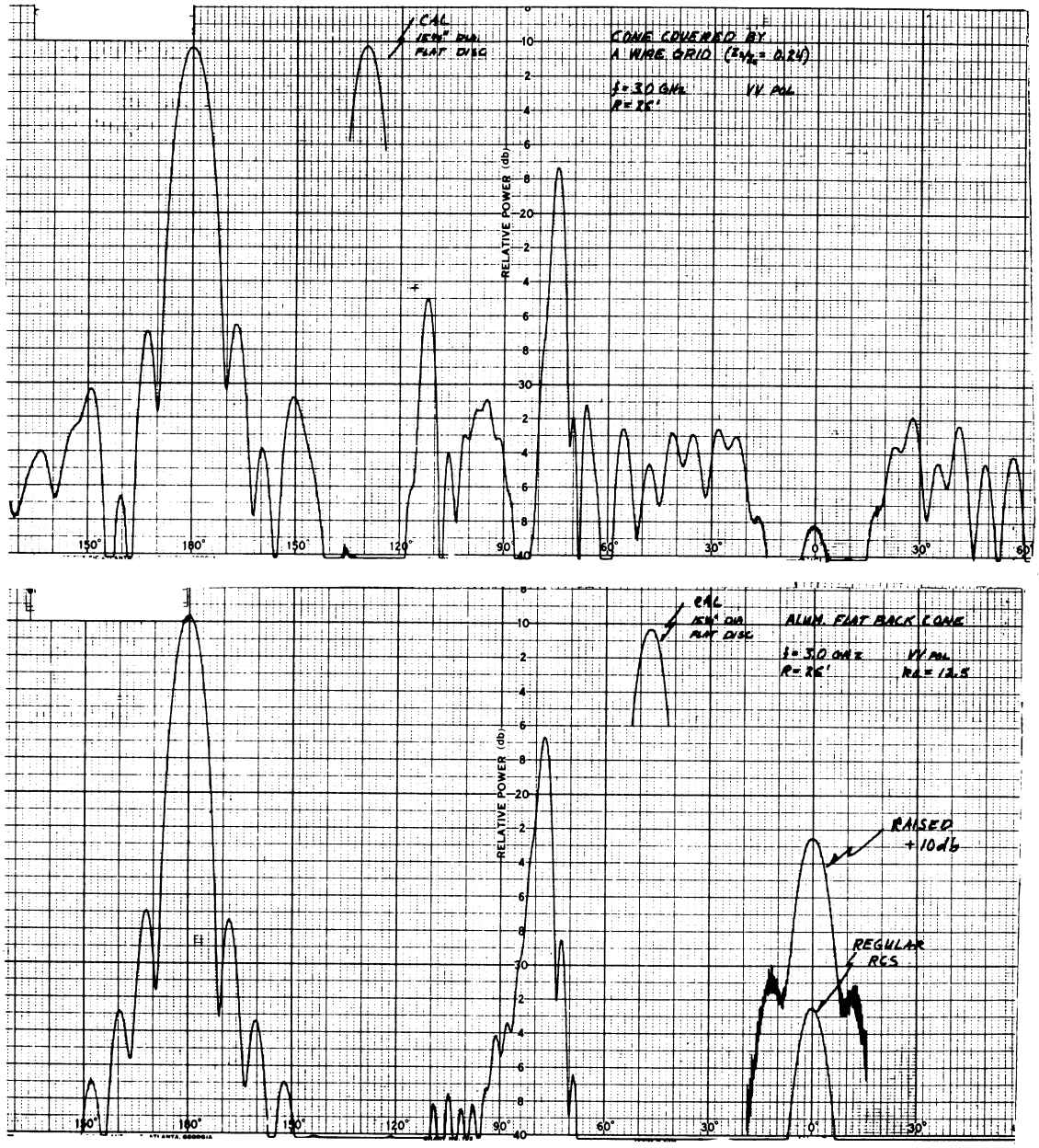

FIG. 2-21: RCS PATTERNS FOR FLAT-BACK CONE (a) WITH WIRE GRID (b) WITHOUT GRID, f = 3.0 GHz, VV POLARIZATION.

(a)

(b)

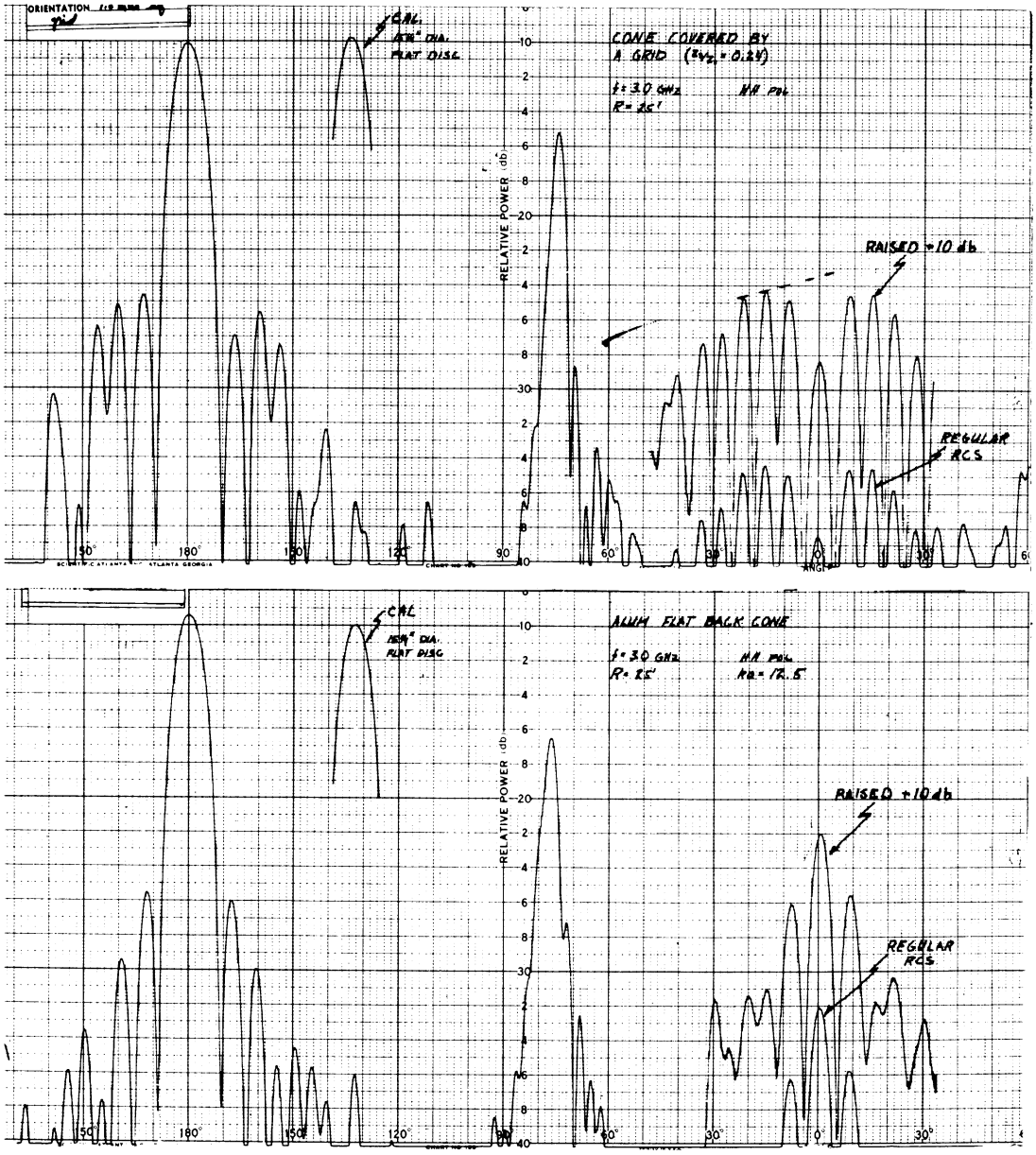

FIG. 2-22: RCS PATTERNS FOR FLAT-BACK CONE (a) WITH WIRE GRID (b) WITHOUT GRID, f = 3.0 GHz, HH POLARIZATION.

return which corresponds to the same level as the rest of the pattern and the term "Raised 10 db" means that 10 db of attenuation was removed from the receiver in order to raise the return so that more of the lobe structure can be observed.

(U) The aspect positions θ of the model for all the scattering patterns is such that $\theta = 0^{o}$ is nose-on, $\theta = 90^{o} - \alpha$ is broadside, and $\theta = 180^{o}$ is end-on or the back of the cone. In the discussion which follows all cross-section values will be normalized to the end-on return at $\theta = 180^{o}$. If for any reason the absolute value is desired, it can be determined by calculating the radar cross section for the flat circular disc from the expression

$$\sigma_{disc} = \pi\ a^{2}\ (ka)^{2} \qquad (2.1)$$

where a is the radius of the disc and k is the wavenumber $2\pi/\lambda$.

2.5.3 Analysis and Evaluation of Conical Measurements.

(U) Unfortunately no worthwhile theoretical model has been developed to predict the radar cross section for the flat-back cone when it is covered by a wire gird. For that matter we still are unable to completely explain the behavior of the flat plate covered with a wire grid, although as pointed out earlier we are still working on the flat geometry problem and hope to have a better understanding of it before the final report.

(U) Even with a better understanding of the coated flat plate problem, there is no assurance that this will enable us to comprehend this problem better in the conical geometry. It has hoped that there would be an opportunity to study the cylinder problem in order to gain an insight into the coupled mode behavior before attempting to do the coated cone, but time will not allow this approach.

(U) Since no theoretical mode is available for determining the radar cross section of the coated flat-back cone careful calibrations were made with the perfectly conducting (aluminum) cone before each test on the coated cone as indicated in Fig. 2-17 through 2-22. Broadside and nose-on comparison are made between theory and data for the base cone. All comparisons are normalized to the end-on return which is given by the expression in Eq. (2.1).

(U) When a flat-back cone is large compared to wavelength λ, the return at nose-on ($\theta = 0^{o}$) is determined by the rim return which is well approximated by (Siegel, 1960)

$$\sigma(0^{o}) = \pi a^{2}\left[(3/2 + \alpha/\pi)\ \sin\left(\frac{2\pi}{3/2 + \alpha/\pi}\right)\right]^{-2} \quad . \tag{2.2}$$

A more accurate expression which takes into account second order diffraction from the rim has been presented by Keller (1960).

(U) At broadside, $\theta = 90^{o} - \alpha$, the radar cross section for a large cone is approximately (Crispin et al, 1959).

$$\sigma(90 - \alpha) = \frac{4}{9\ \cos\alpha}\ ka\ L^{2} \tag{2.3}$$

when L is the slant-length of the cone. For half cone angles α less than 20^{o}, Eq. (2.2) is about 1/2 the broadside return of a right circular cylinder whose radar cross section is $ka\ L^{2}$.

(U) After expressions (2.2) and (2.3) are normalized to (2.1), they become

$$\frac{\sigma(0^{o})}{\sigma(180^{o})} = \left[ka\,(3/2 + \alpha/\pi)\ \sin\left(\frac{2\pi}{(3/2 + \alpha/\pi)}\right)\right]^{-2} \tag{2.4}$$

and

$$\frac{\sigma(90^{o} - \alpha)}{\sigma(180^{o})} = \frac{4}{9\pi \text{ ka cos } \alpha} (L/a)^{2} \quad . \tag{2.5}$$

These two equations are plotted in Fig. 2-23 as solid lines along with experimental data taken from the b patterns of Figs. 2-17 through 2-22. Figure 2-23 discribes the relationship between radar cross section at nose-on and broadside relation to end-on as a function of frequency.

(U) The agreement between theory and data is good for the bare cone and therefore it is expected that the data for the cone covered with the wire grid is as reliable. There is some question about the behavior of the wire grid near the cone tip, but since in the case of large ka and kL the dominant return is from the rim at the cone base where the wire grid behaves like it does in the flat plate geometry, it will be assumed that wire grid does simulate a thin, lossless plasma sheath until we can prove otherwise.

(U) After one examines all the patterns in Figs. 2-17 through 2-22 in the aspect region between $\pm 60^{o}$, two general comments can be made:

(a) The nose-on return with the grid present is reduced 4 to 13 db compared to the bare cone case

(b) the lobe-peaks away from nose-on are increased as much as 10 to 15 db for the cone covered with the grid compared to the bare cone.

In more realistic plasmas, collision effects (losses) are present and these would tend to reduce the effects of statement (b) and in general would reduce the over all radar cross section. Also it is noticed that the return at broadside, $\theta = 90^{o} - \alpha$, is about the same with or without the grid present. This is similar to behavior of the flat plate at normal incidence.

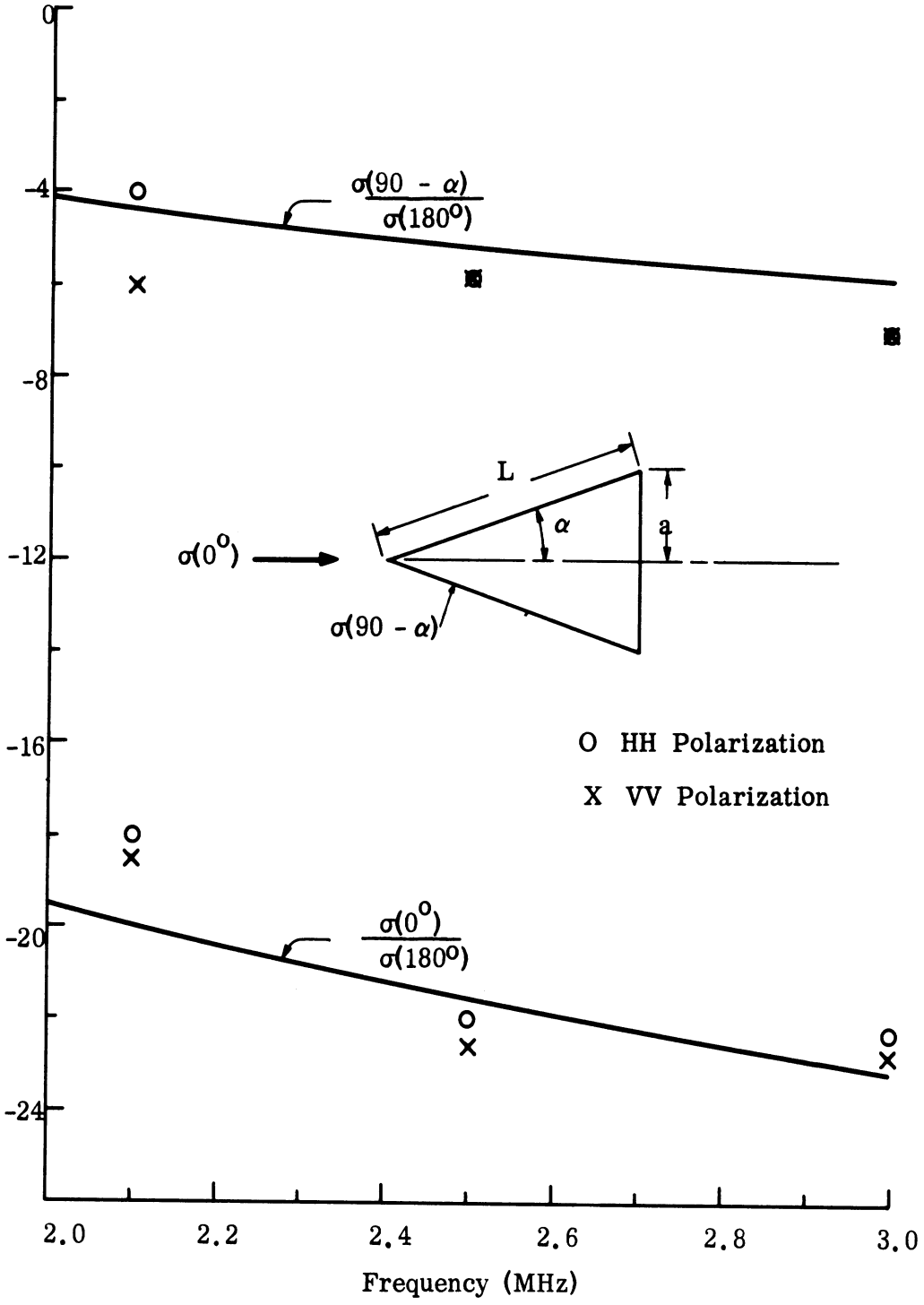

FIG. 2-23: COMPARISON BETWEEN THEORY AND EXPERIMENT FOR THE PERFECTLY CONDUCTING FLAT-BACK CONE.

(U) The preliminary test results shown in Figs. 2-17 through 2-22 indicate that a thin, lossless plasma coating around a flat-back cone can effect the radar cross section in the nose-on region in an appreciable way. These experimental results show enough change in radar cross section to make further theoretical investigations worthwhile. In the time that remains in the contract our efforts will be directed towards trying to explain the measured results we have on the flat and conical models covered with the simulated plasma sheaths.

III

TASK 3: THEORETICAL INVESTIGATIONS

3.1 Radar Cross Section of Conical Vehicles with Indented Rear Caps

3.1.1 Introduction

(S) In the investigation of the radar scattering behavior of conical vehicles with indented rear caps, similar to that of the Mk-12 re-entry vehicle, the background studies reported in Goodrich et al (1967a) and the continuing study reported in Goodrich et al (1967b) used expressions for the creeping wave and the join contributions which were conceptually erroneous. In these next two sections, the correct expressions are derived and set forth explicitly for the indented rear cap model (referred to in the tet as an ID model) viewed at nose-on incidence. In Section 3.1.4 a comparison is made of these analytical results and radar cross section data.

3.1.2 The Creeping Wave Contribution for a Non-spherical Body - With Application to Indented Rear Cap

(U) The profile of the rear part of an indented base model is shown in Fig. 3-1. As regards the longitudinal curvature (in the plane of the paper), the radius is b from the join back to beyond the rear-most point, and then changes abruptly to a radius c through the indentation. Models ID-1 and ID-2 have the same value of b, but different values of c. At all junctions in the profiles, however, the tangents are continuous.

(U) Since the half-cone angle α is small, the radius of the body at the shadow boundary is insignificantly different from that of a pure cone-sphere, and will therefore be denoted by a. For each model, a = 2.210 in., b = 0.553 in. Thus, b is small compared with a, suggesting that we use a cylindrical analogy in the derivation of the creeping wave component. The expression for the far field amplitude that then results is

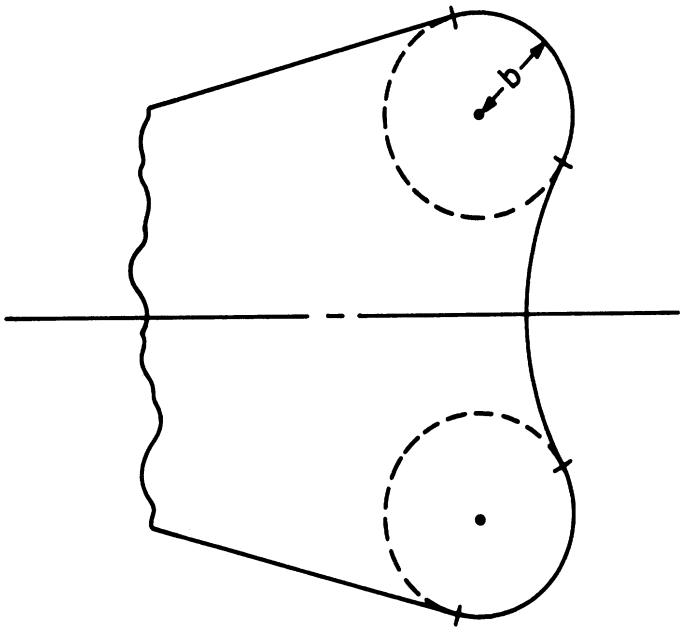

FIG. 3-1: PROFILE OF INDENTED CAP.

$$S = -\pi\, ka\, e^{i\pi kb}\, \frac{e^{2ik(a-b)+i\pi/4}}{\sqrt{2k(a-b)}}\, \left(\frac{kb}{2}\right)^{2/3} \left[\hat{q}(\xi) + \right.$$

$$\left. + \frac{e^{i\pi/6}}{30\sqrt{\pi}}\, \frac{2^{1/3}}{(kb)^{2/3}} \sum_s \frac{1}{\left\{Ai(-\beta_s)\right\}^2}\, (1 + 3/\beta_3^3)\, \exp\left(-\xi\beta_s e^{-i\frac{\pi}{6}}\right) \right]^2 \qquad (3.1)$$

where $\xi = \pi/2\,(kb/2)^{1/3}$, the β_s are the zeros of the Airy function derivative, i.e. $Ai'(-\beta_s) = 0$, and $\hat{q}(\xi) = \hat{q}^{(o)}(\xi)$ is the function tabulated in Table T, pp. 8 through 18, of Logan (1959).

(U) An elementary explanation of the various factors in the expression for S is as follows. A surface wave is "born" at the shadow boundary with birth weight B and travels a distance $\pi/2$ b around the surface, decaying as it goes. It is there launched with a launch factor L. The energy thus radiated

is subject to a "space" variation

$$i \frac{e^{i\left(kR - \frac{\pi}{4}\right)}}{\sqrt{kR}} ,$$

where R is the distance from the launch point. Note that this is a cylindrical approximation, as is the approximation to all other factors employed in the analysis. The above energy strikes the surface again when $R = 2(a - b)$, leading to a new creeping wave which proceeds around the remainder of the surface to the shadow boundary. Energy radiated at this point contributes to the backscattered return, but to get the total contribution we must add up the returns from elements all around the ring. The factor introduced by this addition is denoted by F.

(U) For a hard cylinder of radius b, using only the sth creeping wave:

$$B = \frac{1}{\beta_s \, Ai(-\beta_s)} \quad , \quad L = \frac{1}{2Ai(-\beta_s)} (kb/2)^{1/3} e^{i\pi/3}$$

and the decay rate is $\beta_s/kb\,(kb/2)^{1/3} e^{i\pi/3}$. Thus, a birth-progress-launch procedure leads to a product

$$e^{ik\frac{\pi}{2}b} \frac{1}{2\beta_s \left\{Ai(-\beta_s)\right\}^2} (kb/2)^{1/3} e^{i\frac{\pi}{3}} e^{i\xi\beta_s}$$

which, on summing over s, becomes

$$-i\sqrt{\pi}\, e^{ik\frac{\pi}{2}b} (kb/2)^{1/3} \hat{q}(\xi)$$

since

$$\hat{q}(\xi) \sim \frac{e^{5i\frac{\pi}{6}}}{2\sqrt{\pi}} \sum_s \frac{\exp\left\{i\xi\beta_s e^{i\pi/3}\right\}}{\beta_s\left\{Ai(-\beta_s)\right\}^2} .$$

After the first launch the energy is modified by the "space" factor

$$i\,\frac{e^{i\left\{2k(a-b)-\pi/4\right\}}}{\sqrt{2k(a-b)}}$$

before experiencing the above product of factors again. It is then "focussed" via a factor F = ka, and the net result is the expression given in Eq. (3.1) with the terms in square brackets replaced by $\hat{q}(\xi)$ alone. We remark that the additional terms, representing a correction to $\hat{q}(\xi)$, are provided by the second decay terms in the creeping wave expansions, which terms are known to be important (Senior, 1965) when kb is not large.

(U) Inasmuch as the above expression for S is an asymptotic one for large kb, it is to be expected that its accuracy will decrease as kb gets smaller, and based upon our experience with the expression for the sphere creeping wave, the best that we can hope for is that (3.1) will be numerically effective for $kb \geq 0.7$. Unfortunately, for the ID models, this restriction limits us to $ka \geq 2.8$ and leaves an appreciable range of ka not covered by our formulas. Nevertheless, it is necessary to employ the formula (3.1) for all values of ka of interest, including those less than 2.8, and to appreciate the behavior of the far field amplitude, Eq. (3.1) has been computed in amplitude and phase (degrees) for a variety of $ka \geq 1.0$. A selection of the computed values is given in Table III-1. It will be observed that the phase is, over an extended range of ka, almost a linear function of ka, and thus, for $5.0 \leq ka \leq 10.0$, the best fit straight line is

$$\arg S = 137.028\,ka + 187.385 \text{ (degrees)}, \tag{3.2}$$

with a maximum error of less than 1.4^{o} over the above range of ka. Bearing in mind that the geometrical path length is

$$\pi b + 2(a - b), \tag{3.3}$$

the effective (average) phase velocity of the creeping wave implied by (3.2) is 0.9433 c.

(U) We also observe from Table III-1 that S continues to increase with ka until ka is almost 20, and only beyond this value does the decrease provided by the exponential decay for large ka overwhelm the increase produced by the algebraic factors. The maximum value of S (approximately 0.407) is somewhat less than the maximum value 0.450 achieved by the creeping wave for a pure sphere, and in Fig. 3-2 we show the moduli for the two creeping waves. If the creeping wave were the only contributor to the nose-on backscattering cross-section, the cross-section of the ID model would be less than that of the corresponding cone-sphere for $ka < 9.4$, but greater for $ka \geq 9.4$; there is, however, a join contribution as well, and since this is different for the two bodies (Senior, 1967), no immediate conclusion about the relative values of the nose-on return is possible.

3.1.3 The Join Contribution for Perturbed Cone-Spheres - With Application to Indented Rear Cap.

(U) As emphasized by Senior (1967), the join contribution S_j is critically dependent on the geometrical properties of the cap in the immediate vicinity of its junction with the cone, and the formula

$$S_j = \frac{i}{4} \sec^2 \alpha \, e^{2ikh}, \tag{3.4}$$

TABLE III-1: Creeping Wave Contribution for ID Models

ka	|S|	arg S (degrees)
1.0	0.14795	256.273
1.1	0.15000	275.939
1.2	0.15326	295.077
1.3	0.15671	313.561
1.5	0.16368	348.953
1.8	0.17702	399.660
2.0	0.18522	432.038
2.5	0.20690	509.993
3.0	0.22679	584.960
3.5	0.24460	658.078
4.0	0.26178	729.887
4.5	0.27615	800.855
5.0	0.29044	871.060
5.5	0.30237	940.824
6.0	0.31376	1008.119
6.55	0.32487	1085.980
7.0	0.33249	1147.865
7.5	0.34149	1216.276
8.0	0.34886	1284.567
8.5	0.35515	1352.743
9.0	0.36189	1420.638
9.5	0.36749	1488.468
10.0	0.37205	1556.251
15.0	0.40144	2229.094
20.0	0.40696	2897.420
25.0	0.40060	3563.325

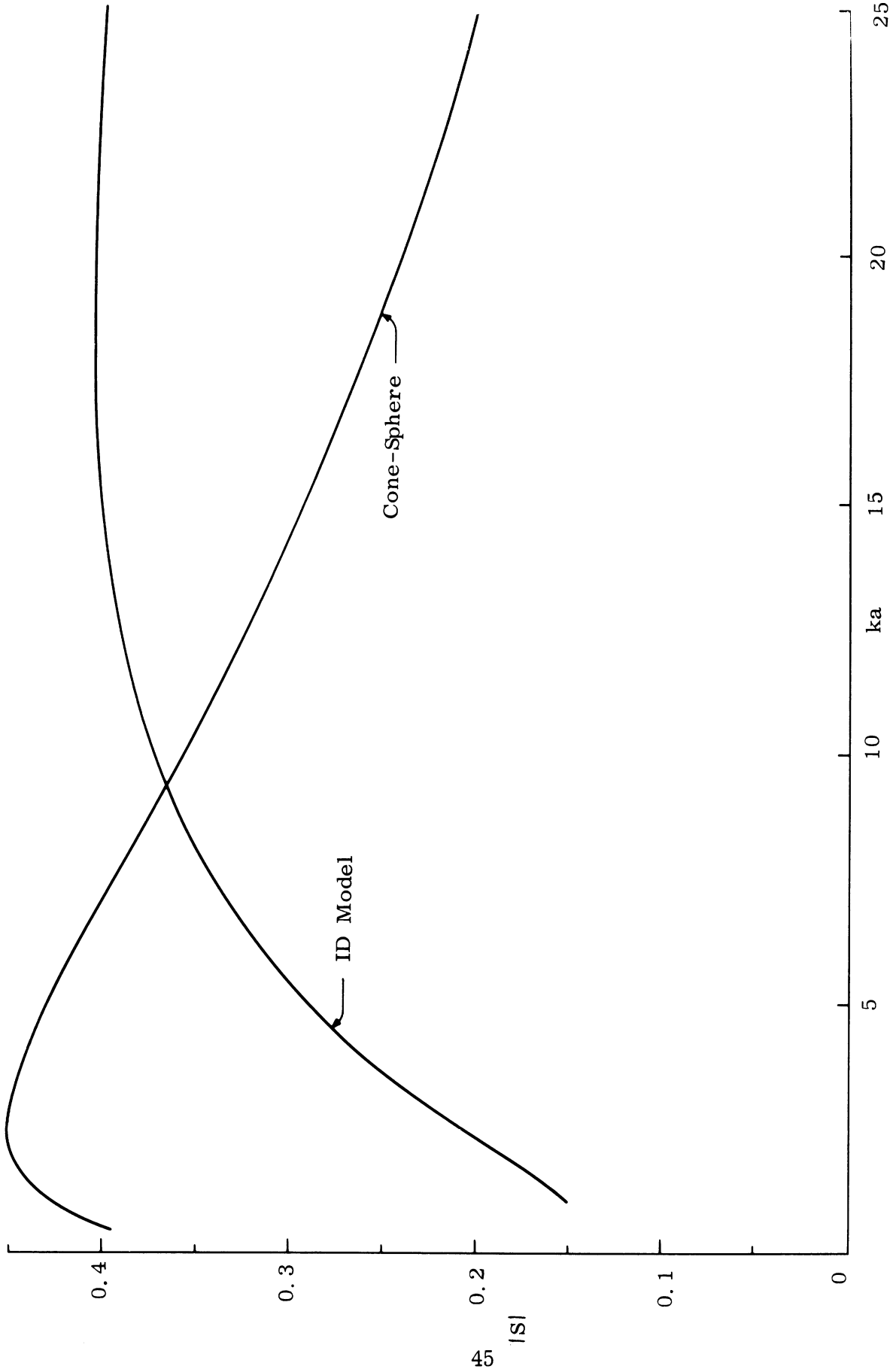

FIG. 3-2: MODULI FOR CREEPING WAVES ON ID MODEL AND CONE-SPHERE MODEL.

where α is the half-angle of the cone and h is its vertical height, is valid only for a pure cone-sphere. In particular, for the ID models, the appropriate join contribution differs considerably from this, and has a significant effect on the backscattering cross section for near nose-on angles of incidence. It is therefore desirable that we set down the required expression for the ID shape, and since we can approximate the oblique incidence behavior as we did for a pure cone-sphere by using a Bessel function factor J_o, it is sufficient to confine attention to nose-on incidence.

(U) Consider a plane wave at nose-on incidence on a conical body consisting of a cone of half-angle α and vertical height h, terminated in a cap whose profile is defined as

$$\rho = \rho(z) , \tag{3.5}$$

where z is a coordinate running along the axis of the body from an origin at the tip. If the tip is also chosen as the origin of phase, the scattering amplitude associated with the join is (Senior, 1967)

$$S_j = -\frac{i}{4}\tan^2\alpha\,(2ikh - 1)e^{2ikh} + ik^2 \int_h e^{2ikz}\,(\rho\frac{\partial\rho}{\partial z})\,dz . \tag{3.6}$$

The first group of terms originates with the cone, and the integral with the cap. Note that the integral is to be evaluated only at a lower limit, z = h, from which it is evident that only the profile in the immediate vicinity of the join is significant as regards the join contribution. It follows immediately that the ID models, all of which have the same profile from the join back to beyond the shadow boundary, all lead to the same expression for S_j.

(U) For a pure cone-sphere, the profile of the cap is part of a circle of radius $h \tan\alpha \sec\alpha$ with center at $z = h \sec^2\alpha$. With the ID models, the cap profile for some considerable distance beyond the join is also part of a circle, but of smaller radius b (say), and since the tangents are continuous at the join, geometrical considerations require that the center of the circles be at $\rho = h \tan\alpha - b \cos\alpha$, $z = h + b \sin\alpha$. The equation of this part of the profile is therefore

$$(\rho - h \tan\alpha + b \cos\alpha)^2 + (z - h - b \sin\alpha)^2 = b^2 , \qquad (3.7)$$

implying

$$\rho = h \tan\alpha - b \cos\alpha + \sqrt{b^2 \cos^2\alpha + 2(z - h)b \sin\alpha - (z - h)^2} . \qquad (3.8)$$

Note that the overall radius of the body at its shadow boundary, that is, its maximum radius, is $h \tan\alpha + b(1 - \cos\alpha)$, and for small α this is insignificantly less than for a pure cone-sphere.

(U) For use in Eq. (3.6) it is ρ^2, rather than ρ, that we require, and from (3.8) we have

$$\rho^2 = h^2 \tan^2\alpha + 2(z - h)h \tan^2\alpha - (z - h)^2 + 2Xb \cos\alpha \left\{ b \cos\alpha + \right.$$
$$\left. + (z - h) \tan\alpha - \sqrt{b^2 \cos^2\alpha + 2(z - h)b \sin\alpha - (z - h)^2} \right\} \qquad (3.9)$$

where

$$X = 1 - \frac{h}{b} \tan\alpha \sec\alpha . \qquad (3.10)$$

Since X is zero for a pure cone-sphere, the first group of terms in Eq. (3.9) are those appropriate to a cone-sphere, with the remaining terms showing the modification to ρ^2 produced by the indentation.

(U) We have now only to insert (3.9) into (3.6) to determine S_j. It is convenient, however, to make use of the general result (Senior, 1967) which says that if, in the vicinity of the join, ρ^2 is expanded in the Taylor series

$$\rho^2 = \sum_{n=0}^{\infty} a_n (z-h)^n , \tag{3.11}$$

then

$$\int_h e^{2ikz} \left(\rho \frac{\partial \rho}{\partial z}\right) dz = \frac{1}{2} \sum_{n=1}^{\infty} a_n \frac{n!}{(-2ik)^n} e^{2ikh} . \tag{3.12}$$

As regards the first three terms on the right hand side of (3.9) $a_o = h^2 \tan^2\alpha$, $a_1 = 2h \tan^2\alpha$, $a_2 = -1$ and hence, from (3.6),

$$S_j = \frac{i}{4} \sec^2\alpha \, e^{2ikh} + 2ik^2 Xb \cos\alpha \int_h e^{2ikz} \left(\rho_1 \frac{\partial \rho_1}{\partial z}\right) dz \tag{3.13}$$

with

$$\rho_1^2 = b\cos\alpha + (z-h)\tan\alpha - \sqrt{b^2\cos^2\alpha + 2(z-h)b\sin\alpha - (z-h)^2} . \tag{3.14}$$

As expected, the first term in the expression for S_j is simply the result for a pure cone-sphere.

(U) The expansion of ρ_1^2 in a Taylor series of the form (3.11) is a tedious but straightforward task, and for the first seven coefficients we obtain

$$a_o = 0 , \qquad a_1 = 0$$

$$a_2 = \frac{1}{2b\cos^3\alpha} \qquad a_3 = -\frac{\tan\alpha}{2b^2\cos^4\alpha}$$

$$a_4 = \frac{1 + 5\tan^2\alpha}{8b^3\cos^5\alpha} \quad , \quad a_5 = -\frac{3(1 + 7\tan^2\alpha)\tan\alpha}{8b^4\cos^6\alpha}$$

$$a_6 = \frac{(1 + 14\tan^2\alpha + 21\tan^4\alpha)\tan\alpha}{16\,b^5\cos^7\alpha} \quad .$$

Insertion into (3.12) and thence into (3.13) now gives for the join contribution:

$$S_j = \frac{i}{4}\sec^2\alpha\, e^{2ikh}\left[1 - X\left\{1 - i\,\frac{3\tan\alpha}{2\,kb\cos\alpha} - \frac{3(1+5\tan^2\alpha)}{(2\,kb\cos\alpha)^2} + \right.\right.$$

$$+ i\,\frac{45(1 + 7\tan^2\alpha)\tan\alpha}{(2\,kb\cos\alpha)^3} + \frac{45(1 + 14\tan^2\alpha + 21\tan^4\alpha)}{(2\,kb\cos\alpha)^4} +$$

$$\left.\left. + O\left[(2\,kb\cos\alpha)^{-5}\right]\right\}\right] \quad . \qquad (3.15)$$

(U) Unfortunately, we have now run into the sort of difficulty that so often confronts us. If $X \neq 0$, that is, if the body is not a pure cone-sphere, the expansion on the right hand side of (3.15) is feasible for computation only when $2kb\cos\alpha$ is large compared with unity, and this is true even for small α. In contrast, it is values of kb near unity (say $0.5 < kb < \alpha$) which are of most practical interest.

(U) To investigate further the nature of the expansion in (3.15) it is necessary to compute terms beyond those shown above, and because of the increasing complication of the terms as their order increases, any exact computation rapidly becomes extremely tiresome. On the other hand, if α is so small that terms involving $\tan^2\alpha$ can be neglected (so that, for example, a_6 is approximated as $\tan\alpha/16b^5\cos^7\alpha$), the calculations are rather trivial. Thus we have that $a_o = a_1 = 0$

$$a_{2n+2} \simeq \frac{(2n)!}{n!\,(n+1)!} \frac{\sec^2 \alpha}{(2b \cos \alpha)^{2n+1}} , \qquad n \geq 0$$

$$a_{2n+1} \simeq -\frac{(2n)!}{(n!)^2} \frac{\sec^2 \alpha \tan \alpha}{(2b \cos \alpha)^{2n}} , \qquad n \geq 1$$

and hence, from Eqs. (3.12) and (3.13)

$$S_j \simeq \frac{i}{4} \sec^2 \alpha\, e^{2ikh} \left[1 - X \left\{ 1 + (1 + 2ikb \sin \alpha) \times \right.\right.$$

$$\left.\left. \times \sum_{n=1}^{\infty} \frac{(2n)!\,(2n+1)!}{(n!)^2} \frac{(-1)^n}{(4kb \cos \alpha)^{2n}} \right\} \right] . \qquad (3.16)$$

The asymptotic nature of the expansion is now apparent, and for given kb the mere insertion of additional terms into (3.15) provides no guarantee of improved accuracy. Indeed, for ka as small as 2 (or even 1), it is possible that the best numerical extimate that can be obtained from (3.16) is that computed using the first term in the infinite expansion, namely

$$S_j \simeq \frac{i}{4} \sec^2 \alpha\, e^{2ikh} \left[1 - X \left\{ 1 - \frac{3(1 + 2ikb \sin \alpha)}{(2\,kb \cos \alpha)^2} \right\} \right] . \qquad (3.17)$$

(U) For kb still smaller than this, we can seek an alternative expression for S_j as a series of increasing positive powers of kb. Inserting (3.14) into (3.13) we have

$$S_j = \frac{i}{4} \sec^2 \alpha\, e^{2ikh} + ik^2 Xb \cos \alpha \int_h e^{2ikz} \left\{ \tan \alpha + \right.$$

$$\left. + \frac{z - h - b \sin \alpha}{\sqrt{b^2 - (z - h - b \sin \alpha)^2}} \right\} dz \qquad (3.18)$$

which can be reduced to

$$S_j = \frac{i}{4} e^{2ikh} \left\{ \sec^2 \alpha + 2ik Xb \sin \alpha + 4k^2 b^2 X \cos \alpha \cdot \right.$$
$$\left. \cdot \int_{-\alpha} e^{2ikb(\sin \beta + \sin \alpha)} \sin \beta \, d\beta \right\} \qquad (3.19)$$

by evaluating the first term in the integrand of (3.18) exactly, and making the substitution $z - h - b \sin \alpha = b \sin \beta$ in the second term. If $kb \ll 1$, the exponential in (3.19) can be expanded as a power series, giving

$$\int_{-\alpha} e^{2ikb(\sin\beta + \sin\alpha)} \sin\beta \, d\beta = \cos\alpha + ikb(\alpha + \sin\alpha \cos\alpha) + O\left[(kb)^2\right] .$$

Hence

$$S_j = \frac{i}{4} \sec^2 \alpha \, e^{2ikh} \left[1 + 2ik Xb \cos^2 \alpha \left\{ \sin \alpha - 2ik b \cos^2 \alpha + \right. \right.$$
$$\left. \left. + 2(kb)^2 (\alpha + \sin \alpha \cos \alpha) + O\left[(kb)^3\right] \right\} \right] , \qquad (3.20)$$

but from the nature of the higher order terms in this expansion it is probably that the region of mathematical validity is limited to $kb < 0.2$. Values of kb as small as this are of little practical concern and, in addition, are such as to give little confidence in the validity of the physical optics approximation on which Eq. (3.6), and consequently Eq. (3.20), are based. Indeed, whereas Eq. (3.20) indicates that S_j approaches the join contribution for a pure cone-sphere, modified by only the numerical factor $1 - 2ikh \sin^2 \alpha$, as $kb \to 0$, physical reasoning would suggest that the contribution in this limit should resemble the flat-backed cone result, namely

$$S_j\Big|_{\text{flat}} = -\frac{i}{4}\tan^2\alpha\, e^{2ikh}(2ikh - 1) \quad . \tag{3.21}$$

In contrast, from Eq. (3.20)

$$S_j \underset{kb \to 0}{\longrightarrow} -\frac{i}{4}\tan^2\alpha\, e^{2ikh}(2ikh - \operatorname{cosec}^2\alpha) \, , \tag{3.22}$$

and the difference between (3.21) and (3.22) is numerically significant* for small α.

(U) In spite of these difficulties, Eqs. (3.17) and (3.20) are the only ones at our command for the estimation of the join contribution associated with an ID model, and we have no alternative but to use them for cross section prediction purposes at all frequencies of interest. Each ID model is such that $b \simeq a/4$, where a is the base radius of the corresponding cone-sphere. Thus, $X = -3$ and if we write

$$S_j = \frac{i}{4} A(kb) \sec^2\alpha\, e^{2ikh} \, , \tag{3.23}$$

then according to Eq. (3.17)

$$A(kb) = 4 - \frac{9\, i \tan\alpha \sec\alpha}{2kb} - \frac{9 \sec^2\alpha}{(2kb)^2} \, , \tag{3.24}$$

whereas according to Eq. (3.20)

$$A(kb) = 1 - 6ikb \sin\alpha \cos^2\alpha - 12(kb)^2 \cos^4\alpha -$$

$$- 12\, i\, (kb)^3 \cos^2\alpha\,(\alpha + \sin\alpha\cos\alpha) \, . \tag{3.25}$$

---

*To the leading order in kh (high frequencies), however, (3.21) and (3.22) are identical.

These expressions have been computed in modulus and phase a functions of kb, and the results are shown in Fig. 3-3. Note that the cross-over point for the moduli is almost identical (at kb $\simeq$ 0.58) to the cross-over point for the phase, suggesting that Eq. (3.25) should be used for kb $\leq$ 0.58, and Eq. (3.24) for kb $\geq$ 0.58. Mathematically at least this is quite satisfying, but the nature of the resulting (combined) curve is sufficiently peculiar to cast doubt on the meaningfulness of the computed values for (say) kb < 1. On the other hand, for kb > 2 (say), the results seem unquestionable, and the quite large values of $|A(kb)|$, asymptotic to 4 as kb $\rightarrow \infty$, will be the source of quite substantial increase in the scattering from an ID model in comparison with that from a pure cone-sphere.

3.1.4 Nose-on Radar Backscattering Cross Section of ID Models - Comparison of Analysis and Experimental Data.

(U) We shall now employ the new results described in the previous two sections in the computation of the nose-on cross section and compare the prediction with measured data. It is convenient to begin with a few remarks about the experimental data available for the ID models, Values of the nose-on backscattering cross section have been measured at a series of discrete frequencies for each of the models ID-1 and ID-2. These two models are characterized by the same half-cone angle α, the same radius, a, of original spherical cap (i.e. transverse radius of curvature at the shadow boundary), and the same radius, b, of cap at the join (i.e. longitudinal radius of curvature at the shadow boundary). Only the radius c of the concave indentation serves to distinguish them, and since the theoretical estimates of the join and creeping wave contributions are functions of a and b alone, and are independent of c, it is to be expected that the measured values of the nose-on (and also oblique angle) cross sections the two models will be identical. This turns out to be the case.

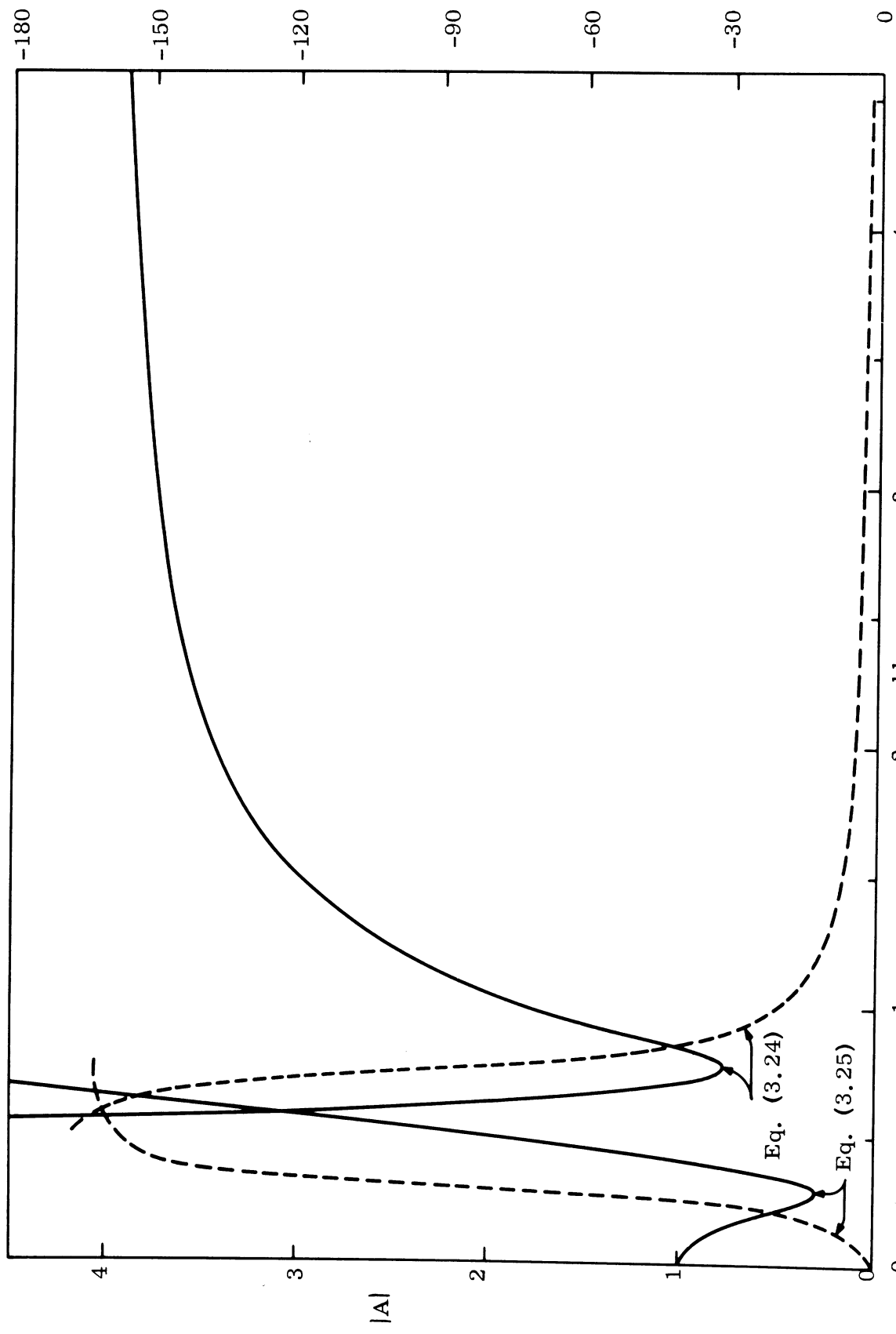

FIG. 3-3: MODULUS (——) AND PHASE (---) OF JOIN CONTRIBUTION FACTOR A(kb) FOR ID MODEL.

(U) In Table III-2 are shown measured values for the nose-on cross section of model ID-1. The measured values for model ID-2, are plotted as functions of ka in Fig. 3-4, and superimposed are the points appropriate to model ID-1. The agreement is very good and confirms the conclusions of the theory.

TABLE III-2: Nose-on Cross Section of Model ID-1.

ka	Frequency (GHz)	Pattern No.	σ/λ^2 (db)
2.98	2.53	3969	-11.8
3.96	3.37	3978	- 4.8
4.51	3.83	3980	- 3.6
6.74	5.73	3962	- 0.4

(U) In order to appreciate the change in the nose-on cross section produced by the indentation, the curve based on the experimental values for model ID-2 is reproduced in Fig. 3-5 along with the theoretical curve for a pure cone-sphere of the same base radius. The latter curve is known to constitute an accurate estimate, and has been taken directly from Fig. 3-6 with the creeping wave enhancement given by the standard empirical factor. We observe that the locations of the maxima and minima are different for the two bodies, thereby emphasizing the futility of using isolated measurements of the cross section to determine the merits of either body, and that on average the indentation has increased the nose-on scattering by (about) 8 db over this range of ka.

(U) Let us now compare the measured data for the nose-on cross sections of models ID-1 and 2 with the theoretical estimate based on the formulae in Sections 3.1.2 and 3.1.3. The theoretical expression from which to com-

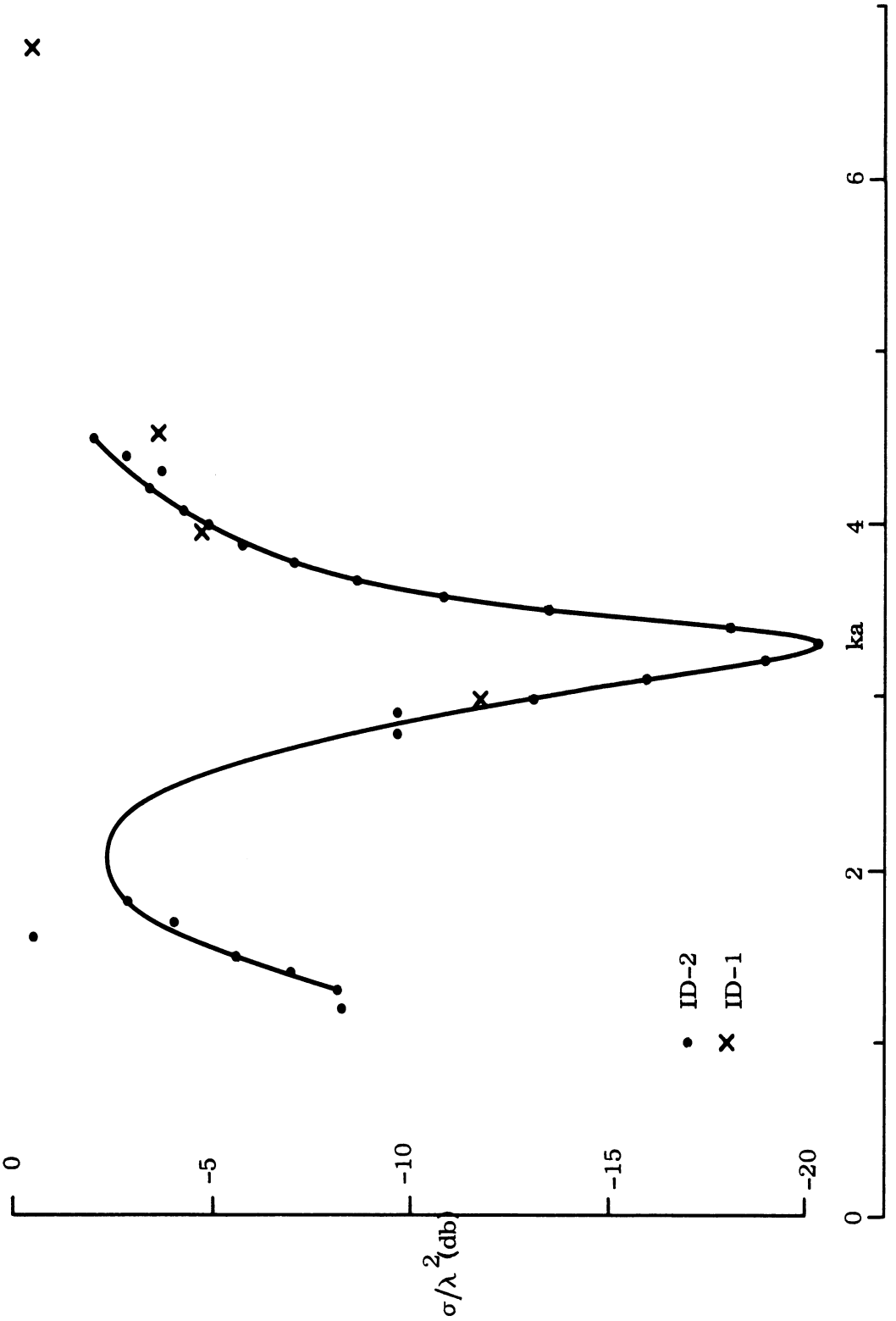

FIG. 3-4: MEASURED NOSE ON BACKSCATTERING CROSS SECTIONS OF MODELS ID-1 AND ID-2. The curve has been drawn through the ID-2 points and exists only to guide the eye.

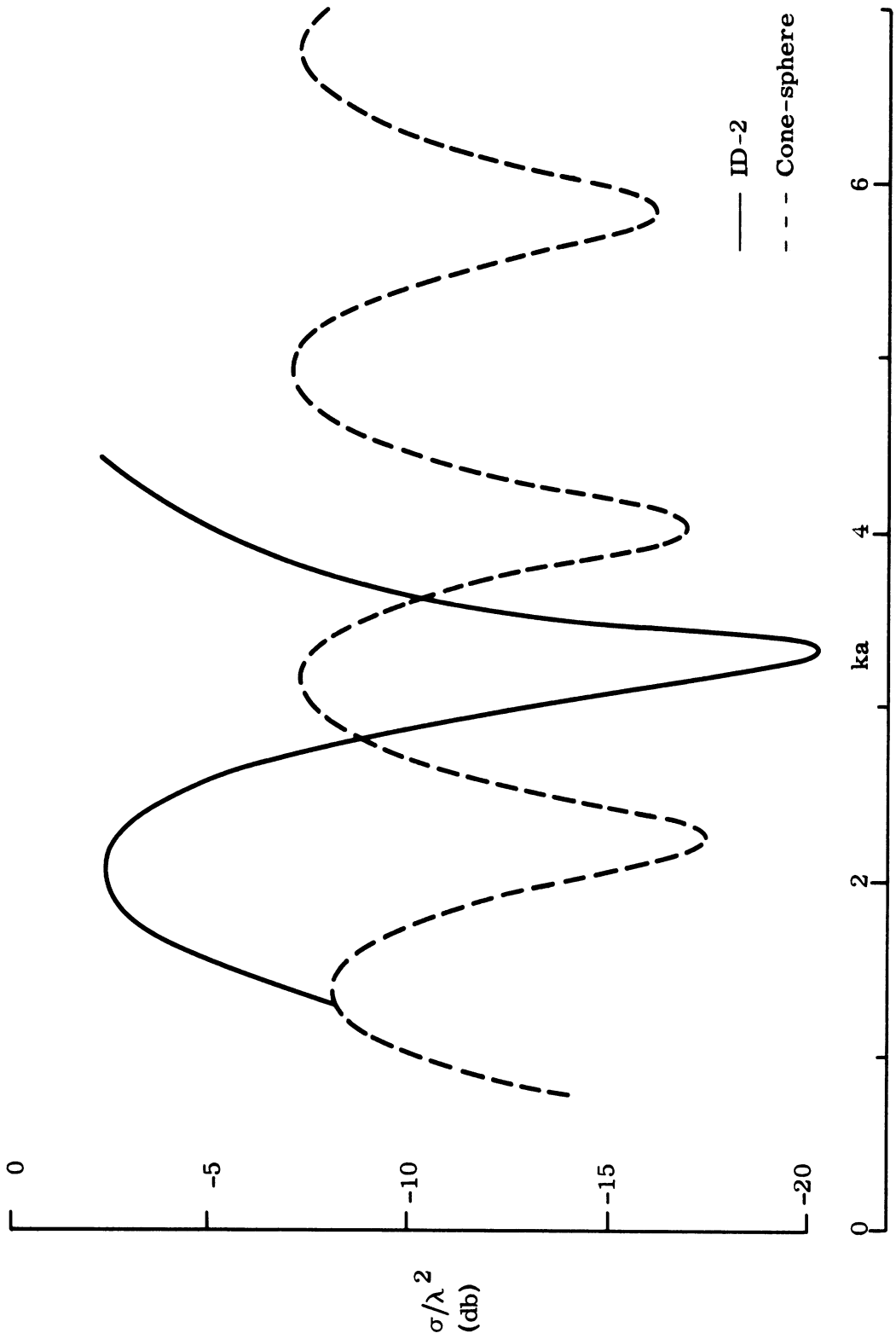

FIG. 3-5: MEASURED NOSE-ON BACKSCATTERING CROSS SECTIONS OF MODEL ID-2, COMPARED WITH THE THEORETICAL RETURN FOR A PURE CONE-SPHERE OF THE SAME SIZE.

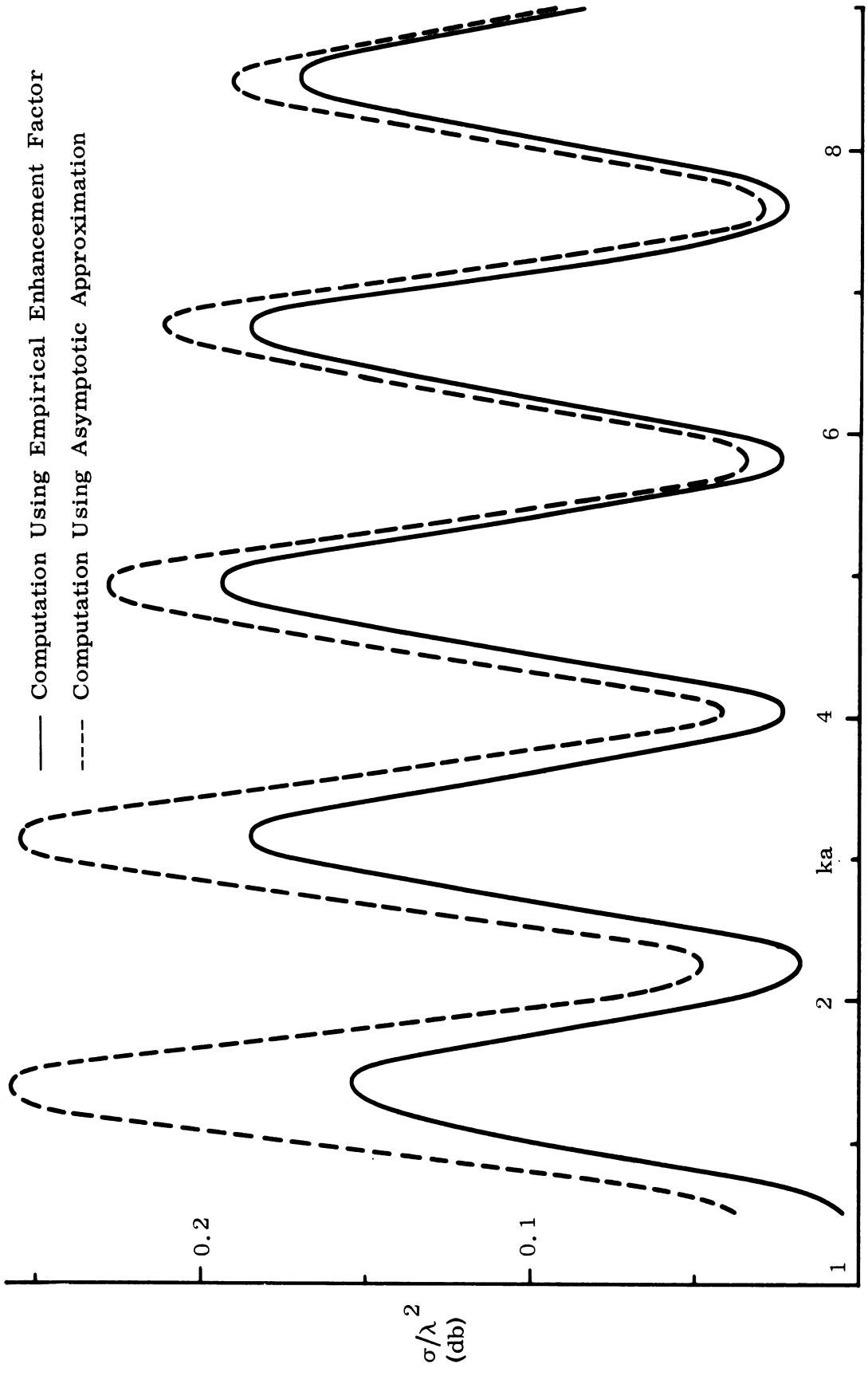

FIG. 3-6: THEORETICAL NOSE-ON BACKSCATTERING CROSS SECTION FOR A CONE-SPHERE WITH 7.5^{o} CONE HALF ANGLE.

pute the estimate is

$$\sigma/\lambda^2 = \frac{1}{\pi}\left|S_1 + S_2 + S_3\right|^2$$

where*

$$S_1 = -\frac{i}{4}\tan^2\alpha\, e^{-2ik(a\cot\alpha\cos\alpha + b\sin\alpha)}$$

is the tip contribution;

$$S_2 = \frac{i}{4}\sec^2\alpha\, e^{-2ikb\sin\alpha}\, A(kb)$$

is the join contribution, with the factor A(kb) as given in Section 3.1.3 and S_3 is the net creeping wave contribution which differs from the function discussed and computed following section 3.1.2 only in an enhancement factor. This last arises from the "overflow" of the traveling wave on the side of the cone, and is expected to be identical to the factor γ for a pure cone-sphere. For large ka, γ can be computed from its asymptotic approximation given below:

$$\gamma \simeq \left[2\left(1/3 + \int_0^B Ai(-x)\,dx\right)\left\{1 + 1/2(ka/2)^{2/3}\alpha^2 e^{-i\pi/3}\right\}\right.$$

$$\left. + (ka/2)^{2/3}\alpha^2 e^{-i\pi/3} Ai(-B)\right]\exp\left\{-(ka/2)^{1/3}\alpha\beta e^{-i\pi/6}\right\} \qquad (3.26)$$

but for small ka (< 3, say), the empirical formula must be used; for convenience, therefore, we shall use the empirical formula for γ throughout the range of ka required for the reproduction of the ID model data.

---

* For each contributor, the origin of the phase has been taken to be at the shadow boundary.

(U) As noted in Section 3.1.3, the range of ka spanned by the experimental data is a difficult one because of the relatively small values of the corresponding kb. Indeed, the break point between the low and high frequency approximations for A(kb) falls right in the middle of this range and, in truth, there is no real basis for confidence in the accuracy of either formula. Nevertheless, it is necessary for us to compute A(kb) in order to predict the nose-on scattering, and to see which of the several possible approximations for A(kb) is most effective is reproducing the measured data, a preliminary computation was performed in which (i) the (small) tip contribution S_1 was neglected, (ii) the creeping wave enhancement factor γ was replaced by unity, and (iii) A(kb) was determined first from the union of the high and low frequency approximations (see Fig. 3-3, Section 3.1.3), and then was taken to be 4 (leading term in the high frequency expansion) throughout the entire range of ka covered by the experimental data. The two curves resulting from these preliminary computations are superimposed upon the experimental points in Fig. 3-7. Not surprisingly, the curves differ considerably from one another for ka less than (say) 4, but are in very close agreement for the larger ka. With A(kb) taken equal to 4 for all ka, the curve fits the experimental data quite well near to the maxima in its oscillation, but does not reproduce the deep minimum centered on ka = 3.3. On the other hand, the more complete high frequency expression for A(kb) does reproduce the minimum, but is less accurate at the maxima; and since the low frequency expression for A(kb) appears quite irrelevent the composit (low/high frequency) expression is unsatisfactory. Indeed, the best agreement with experiment is obtained by using the high frequency expression for A(kb) for ka > 2 (approx), and then transfering to the value 4 for A(kb) for values of ka less than 2. This leads to a continuous curve for the theoretical estimate, albeit one having a discontinuity in slope at the transition point, and constitutes a tolerable approximation to

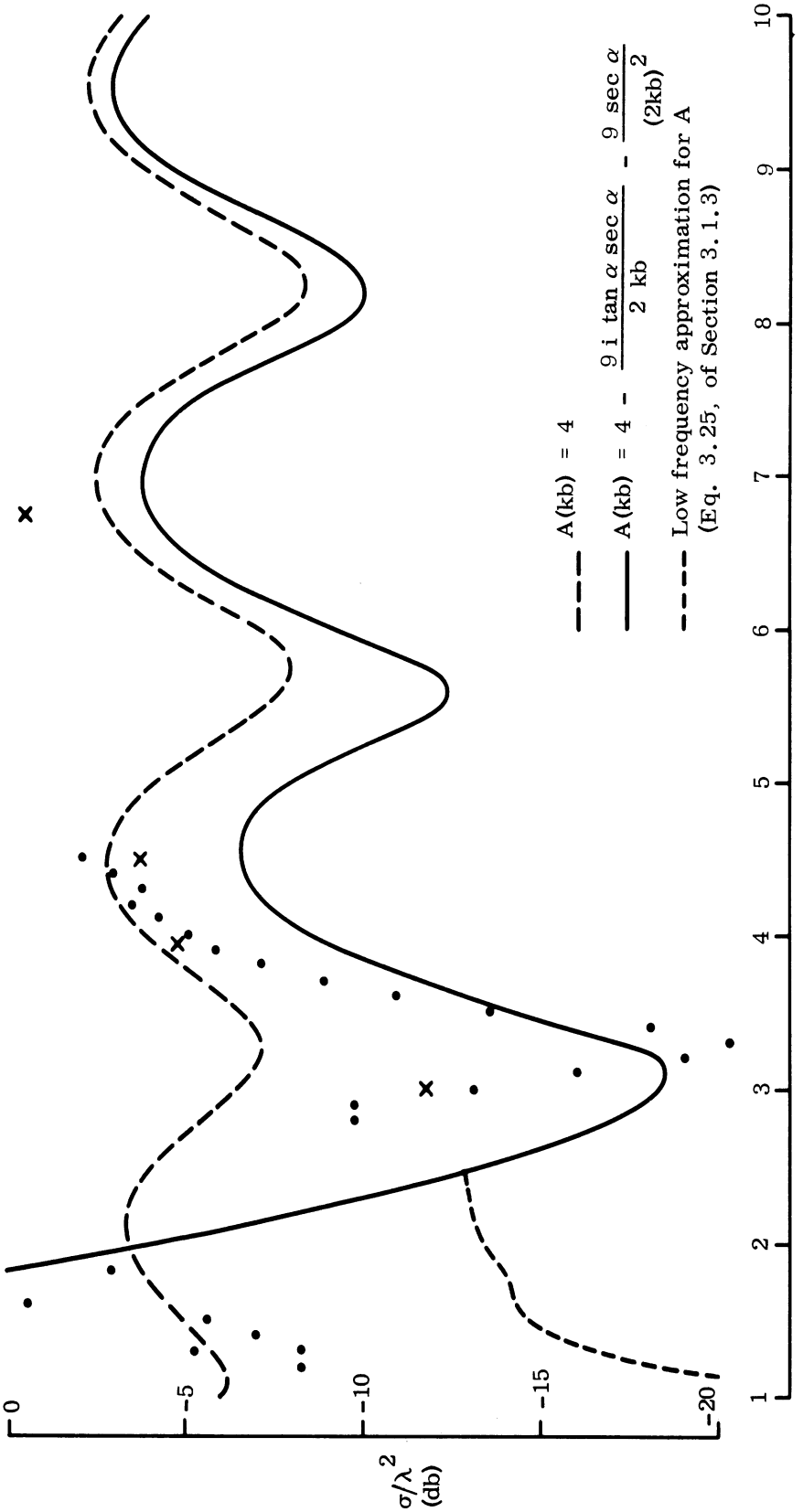

FIG. 3-7: COMPARISON OF NOSE-ON CROSS SECTION OF ID MODEL COMPUTED USING VARIOUS APPROXIMATIONS FOR A(kb) WITH MEASURED DATA FOR ID-1 (xxx) AND ID-2 (●●).

the measured data. This is, in fact, the approximation that will be used hereafter, and for a model with concave indentation in the base the postulated expressions for A(kb) are

$$kb < kb_1 \quad : \quad A(kb) = 1 - X$$

$$kb > kb_1 \quad : \quad A(kb) = 1 - X\left\{1 - \frac{3(1 + 2ikb)\sin\alpha}{(2kb\cos\alpha)^2}\right\}$$

with $X = 1 - a/b$. The value of kb_1 is chosen to provide continuity of the resulting cross section estimate for the body, and for an ID model with $b = 0.2502\,a$ ($X \simeq 3$), $kb_1 \simeq 0.50$.

(U) With the tip return included, the creeping wave contribution duly enhanced using the empirical factor, and A(kb) defined as above, the nose-on cross section of an ID model has been computed, and is shown as a function of ka in Fig. 3-8. The agreement with the measured data is adequate, though not exceptional, and in defense we note again the quite small values of the associated kb throughout the range covered by Fig. 3-8.

3.2 Backscattering Cross Section of FB Models

3.2.1 Introduction

(U) The FB models are rounded flat-backed cones of the character shown in Fig. 3-9. A cone of half-angle 9^o and base radius, a, of 1.878 in, is smoothly terminated in a toroidal portion of (longitudinal) radius b, which portion is itself smoothly terminated in a flat back. Tangents are continuous at all joins and consequently, on the assumption of perfect tolerances and modeling, the parameters of the body are as follows:

overall length = $a \cot\alpha + b(1 + \sin\alpha)$

maximum radius = $a + b(1 - \cos\alpha)$

Radius of flat back = $a - b\cos\alpha$

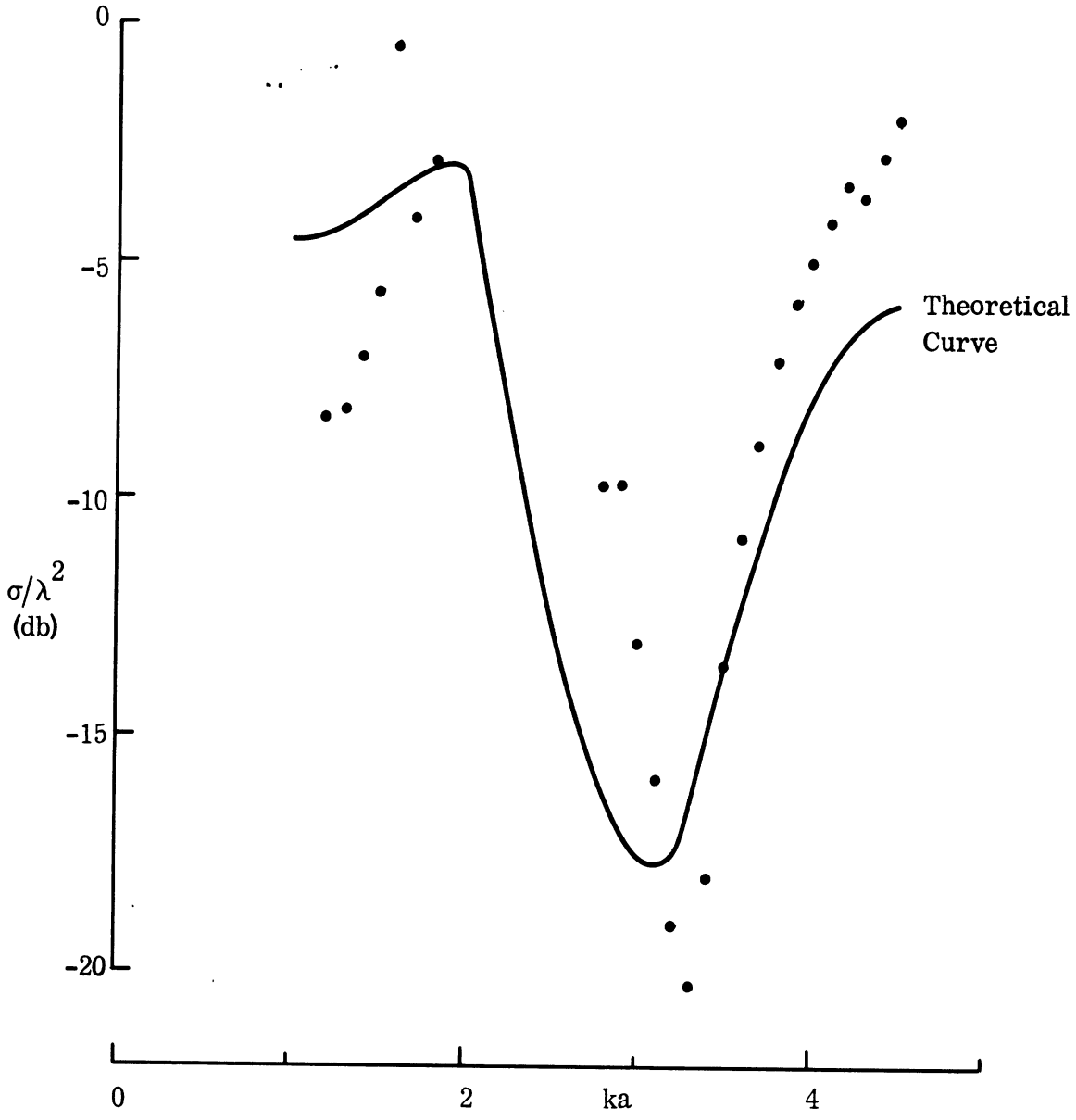

FIG. 3-8: COMPARISON BETWEEN THEORY AND EXPERIMENT FOR MODEL ID-2.

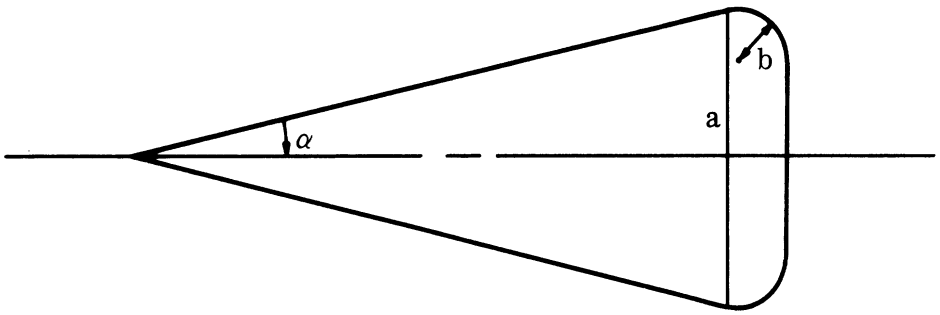

FIG. 3-9: BASIC FB SHAPE.

where α is the half-cone angle ($=9^{o}$). Each of the models which have been constructed have the same a and α, but differ in their values of b. Some pertinent dimensions are given in Table III-3. It will be observed that even for

TABLE III-3: Dimensions of FB Models.

Model	a(in.)	b(in.)	a/b	$b(1 - \cos\alpha)$, in.	$a \cot\alpha + b(1 + \sin\alpha)$, in.
FB-1	1.878	0.188	10	0.0023	12.075
FB-2	1.878	0.376	5	0.0046	12.292
FB-3	1.878	0.564	3.33	0.0069	12.510
FB-4	1.878	0.751	2.5	0.0092	12.726

model FB-4 the maximum radius exceeds the radius of the conical base by less than one-half percent, and accordingly it is sufficient for all purposes of computation to treat a as the maximum radius, which is therefore the same for the four bodies. The analysis which is reported in the next two sections is continuing. It is anticipated that better agreement of computed data with experimental data will result as the analysis develops.

3.2.2 Nose-on Backscattering Cross Section of FB Models

(U) Complete backscatter patterns have been measured at a series of frequencies spanning the range $1.0 \leq ka \leq 5.8$, and from these the values of the nose-on cross section have been read. The results are plotted as functions of ka in Figs. 3-10 and 3-11. There are several features that should be noted. For each model the data points show a regular cyclical variation as a function of ka, with no evidence of any superposed oscillation of higher frequency, and it is therefore concluded that the scattering is made up of two dominant contributors whose amplitudes (and associated phase centers) vary only slowly as functions of ka. In particular, there is no indication of any abrupt change in the character of the curves within this range of ka. The positions of the maxima and minima show a slight but systematic displacement to larger values of ka as b/a decreases, and this is consistent with the reduction in the path length of any wave circumscribing the base.

(U) For ka less than the value corresponding to the first maximum in the cross section, the scattering is almost independent of b/a -- and, incidentally, very similar to that for a flat-backed cone of the same base radius. As ka increases, however, the differences between the results for the four models become more pronounced. Thus, for model FB-1 (b/a small), the first minimum is realtively shallow and the second maximum much higher than the first (by about 6 db): in this respect the results are comparable to those for a flat-backed cone. But as b/a decreases, the second maximum rapidly falls to a level little more than that of the first maximum, with the minima becoming much more pronounced. Indeed, for model FB-4 the first minimum is 18 db down on the level of the maximum, and the second minimum is 2 db lower still. Clearly, for this model the two contributors must be almost equal in magnitude at the position of the minima and, hence, may well be comparable throughout the intervening region as well.

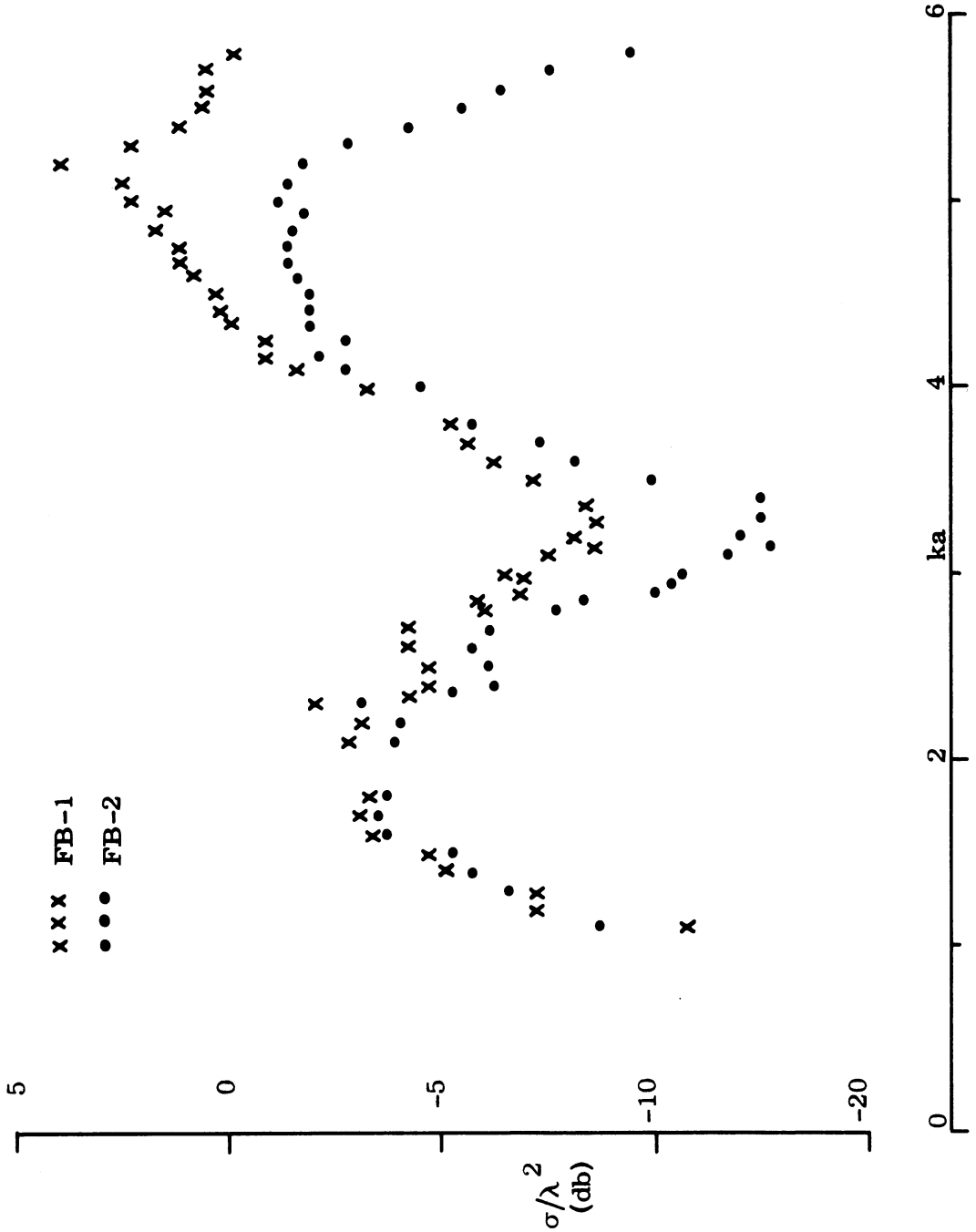

FIG. 3-10: MEASURED NOSE-ON SCATTERING DATA FOR MODELS FB-1 AND FB-2.

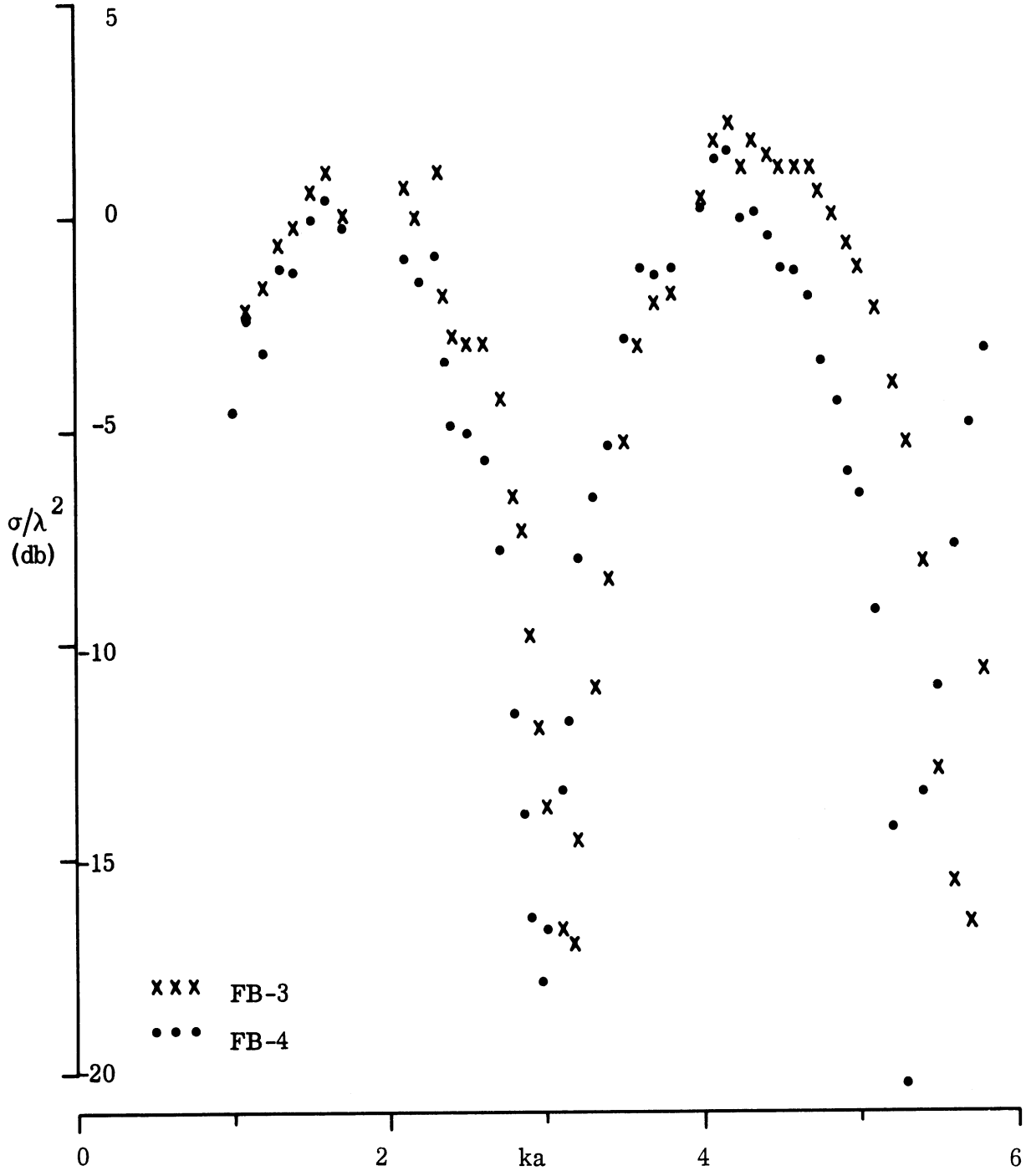

FIG. 3-11: MEASURED NOSE-ON SCATTERING DATA FOR MODELS FB-3 AND FB-4.

(U) If the measured nose-on scattering cross section of model ID-2 (see Fig. 3-4 of Section 3.1.4) is compared with the data in Figs. 3-10 and 3-11, the curve is found to lie mid-way between the curves derived from the data points for FB-2 and FB-3. This is entirely reasonable since, for model ID-2, b/a = 4, and confirms that the indentation has no effect on the cross section at least for nose-on incidence.

(U) The theoretical prescription for the cross section is, of course, the same regardless of whether the back is flat or indented, and depends only on the values of ka and a/b. It will be recalled that the numerical estimate based on this prescription was in tolerable agreement with the measured nose-on data for models ID-1 and ID-2; unfortunately, for the more extensive FB data shown in Figs. 3-10 and 3-11, the estimates are not satisfactory and the theoretical formula (notwithstanding its obvious accuracy for sufficiently large values of ka) fails entirely to predict the character of the data as a function of b/a for ka in the range 2.5 to 6. It does not, for example, predict the increasing depth of the minimum near ka = 5.5 as b/a decreases, and accordingly it is necessary to seek a modification of the theory for such values of ka.

3.2.3 Specular Flash and Rear-on Backscattering Cross Section of FB Models.

(U) From the backscatter patterns measured for each of the FB models at 51 frequencies from 1.00 to 5.80 GHz, corresponding to $1.0 \leq ka \leq 5.8$, where a is here the radius of the cone at its base, the values of the cross sections at specular and rear-on aspects have been read, and it is the purpose of this section to compare the specular and rear-on cross sections with the theoretical estimates derived from formulae given heretofore.

(U) Figure 3-12 shows the measured values of the specular flash cross section σ/λ^2 plotted as functions of ka, where, for clarity of presentation, the values for models FB-2, FB-3 and FB-4 have been reduced by 5, 10 and 15 db respectively. The results for the four bodies are virtually indistinguishable, and certainly there is no evidence of any dependence on b. This is in accordance with the theoretical picture and included in Fig. 3-12 is the curve representing the theoretical estimate computed from the formula

$$\sigma_o/\lambda^2 = K\,(ka)^3 \qquad (3.27)$$

(Senior, 1967) with

$$K = \frac{\operatorname{cosec}^2 \alpha \sec \alpha}{9\pi^2} = 0.4646 \quad \text{for } \alpha = 9^o .$$

The agreement is good, particularly for the larger ka, and certainly any discrepancies average no more than a fraction of a db. In particular, there is no apparent need for any refinement of the formula when ka is large. Nevertheless, for the smaller ka (approaching unity), the formula does underestimate the measured values by as much as 2 or 3 db, and throughout the range the data does show some evidence of a small but systematic oscillation as a function of ka. This may be attributable to the influence of the creeping waves on the cone, and any prediction of this effect is beyond the scope of a simple formula such as that in Eq. (3.27).

(U) The nature of the discrepancy between theory and experiment for the specular flash is clearly shown in Fig. (3-13) in which the ratio of the measured flash cross section to the theoretical estimate given in (3.27) is plotted versus ka. Each data point is the result of averaging the measured cross sections for the four FB models, and the trend revealed by Fig. 3-13 is

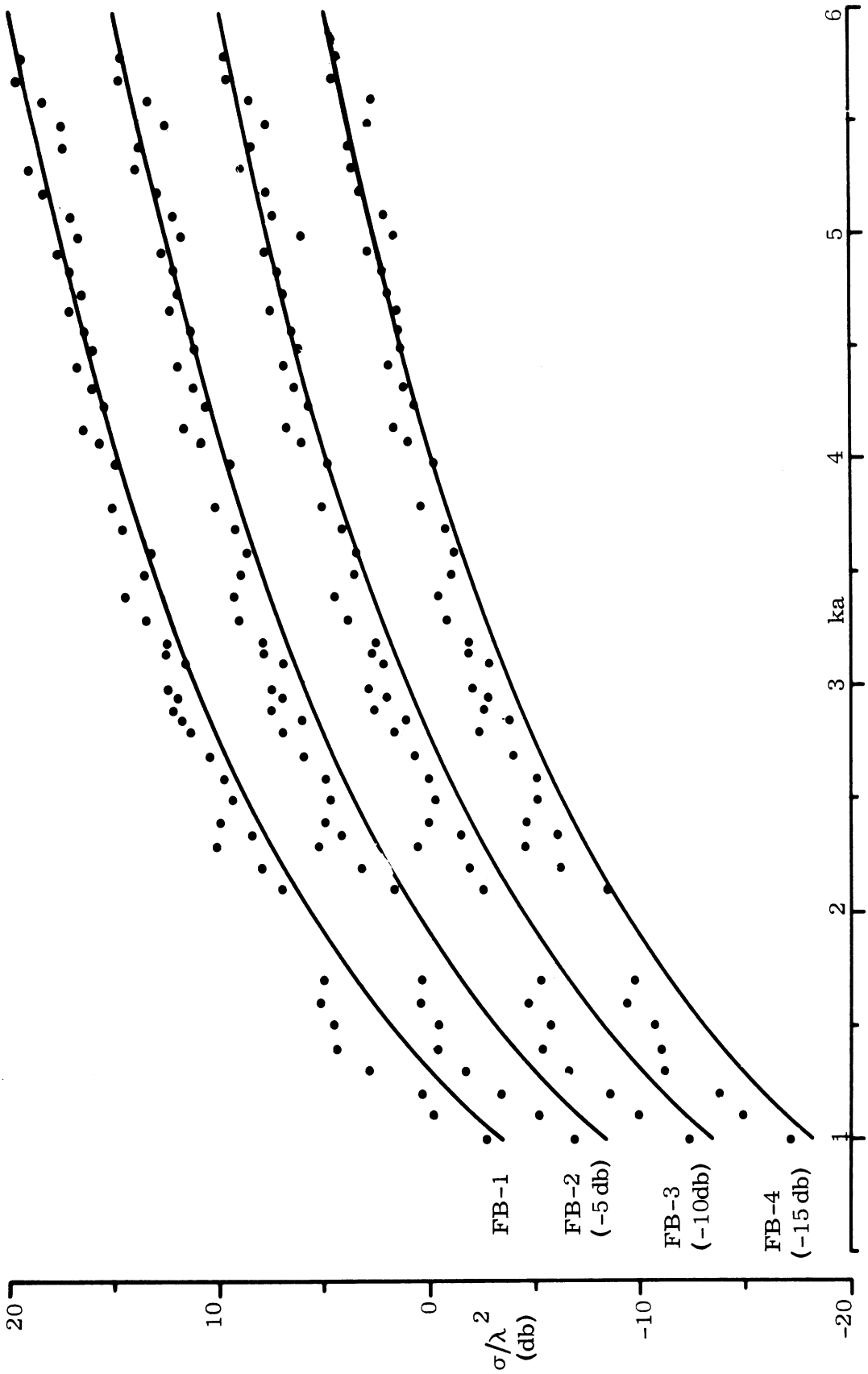

FIG. 3-12: MEASURED DATA FOR THE SPECULAR FLASH CROSS SECTION COMPARED WITH THEORETICAL ESTIMATE.

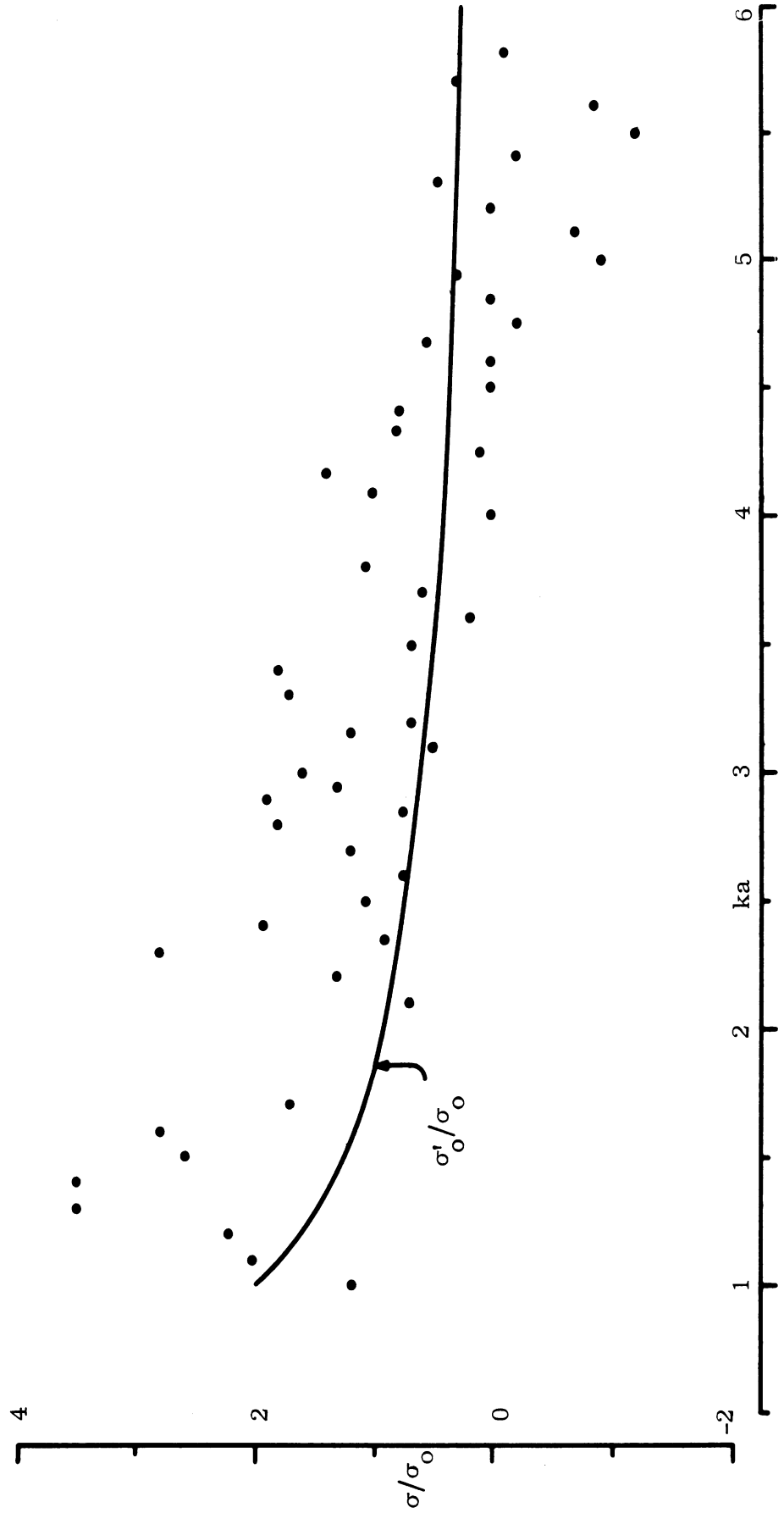

FIG. 3-13: RATIO OF MEASURED TO THEORETICAL SPECULAR FLASH CROSS SECTIONS.

probably due to experimental error, there is nevertheless a residual discrepancy much of which is removed if we base our theoretical estimate on a cylinder approximation instead of physical optics. As noted by Senior (1967), the specular return from the cone can be interpreted as a return from a right circular cylinder whose length is the slant length of the cone, and whose radius is $\frac{4}{9}$ a secα. Rather than estimate the return from such a cylinder using physical optics, we can instead employ the exact expression for the currents borne by a cylinder of infinite length and the above radius, and integrate these currents over the finite length of the equivalent cylinder. The resulting cross section is (Senior and Knott, 1964):

$$\sigma_o'/\lambda^2 = \frac{1}{4\pi^2} A(\tfrac{4}{9} ka \sec\alpha)(ka \operatorname{cosec}\alpha)^2 = \frac{A(x)}{x} \cdot \frac{\sigma_o}{\lambda^2} \qquad (3.28)$$

where

$$A(x) = \frac{4}{\pi} \left| \sum_{n=-\infty}^{\infty} (-1)^n \frac{J_n(x)}{H_n(x)} \right|^2$$

and $x = \frac{4}{9} ka \sec\alpha$. A(x) has been computed for x = 0.1(0.1)10.0, and using these results it is a simple matter to calculate the ratio of the modified cross section σ_o' to the physical optics cross section σ_o as a function of ka. The curve is shown in Fig. 3-13, and it is seen that the modification to the theoretical estimate provided by Eq. (3.28) does improve the agreement with experiment.

(U) For rear-on incidence, the measured values of the backscattering cross section of the four models are plotted as functions of ka in Fig. 3-14 where, for clarity, we have again separated the data points by reducing those for models FB-2, FB-3 and FB-4 by 5, 10 and 15 db respectively. Although

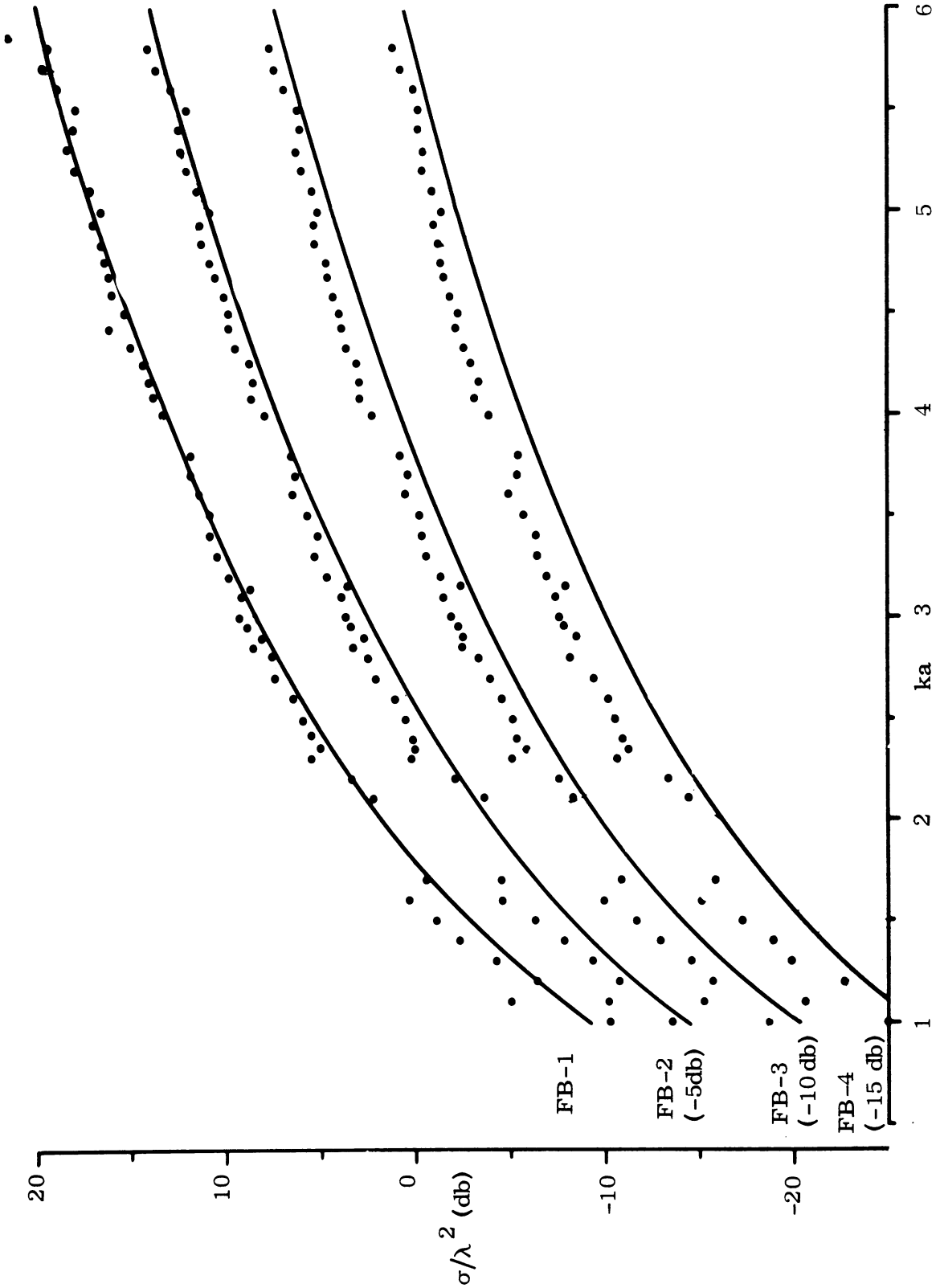

FIG. 3-14: MEASURED DATA FOR THE REAR-ON CROSS SECTION COMPARED WITH THEORETICAL ESTIMATE.

the results for all four models are similar, there are some slight differences which appear to indicate a systematic dependence on b. Some such dependence is, indeed, predicted by the theoretical formula, and we have included in Fig. 3-14 the theoretical curves computed from the physical optics gormula given in Eq. (3.32). The agreement is good, particularly for the more sharply-curved model FB-1 and in general for all models for the larger ka. As ka decreases, however, a systematic discrepancy is evident, which discrepancy increases with kb.

(U) A more striking illustration of the differences between theory and experiment is provided by Fig. 3-15, in which the ratios of the measured and theoretical cross sections are plotted as functions of ka, with σ_o determined from (3.32). For model FB-1 the agreement could hardly be improved upon, and most of the discrepancies here are undoubtedly experimental, but as b/a increases the theoretical formula for the smaller ka under-estimates the measured values by an amout which, for model FB-4, averages about 2 db for ka near unity. The explanation clearly lies in the high frequency nature of Eq. (3.32).

3.2.4 Physical Optics Estimate of the Rear-on Return of Flat Back Model

(U) A valid estimate of the rear-on backscattering cross section of an FB model is provided by physical optics, and the derivation of the appropriate expression is a straightforward task using the techniques described by Senior (1967).

(U) With the coordinates and notation illustrated below, the expression for the far field amplitude is (Senior, 1967)

$$S = ik^2 \left\{ \int_0^{a-b} \rho \, d\rho + \int_0^{b} e^{2ikz} \left(\rho \frac{\partial \rho}{\partial z}\right) dz \right\} , \qquad (3.29)$$

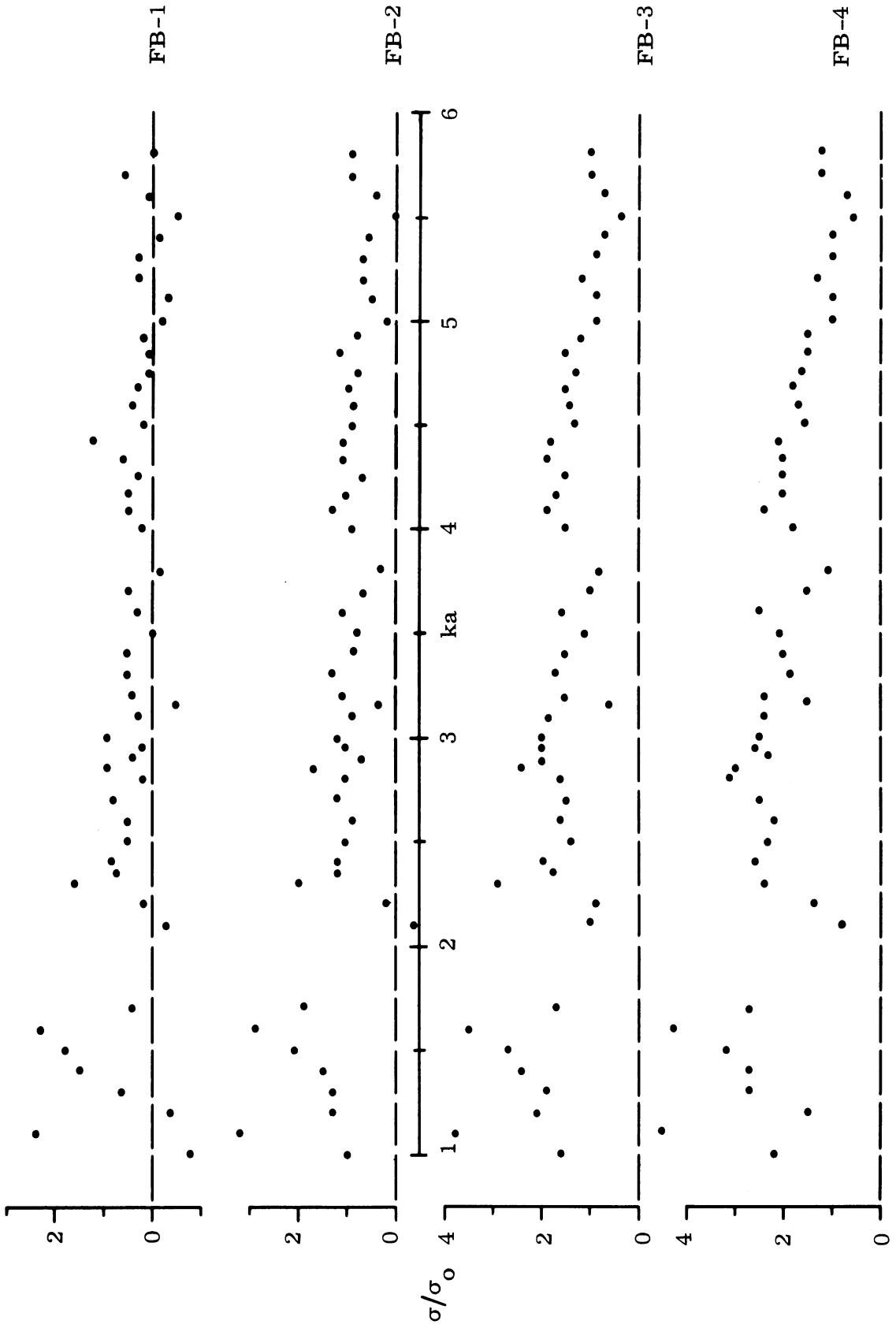

FIG. 3-15: RATIO OF MEASURED TO THEORETICAL REAR-ON CROSS SECTIONS.

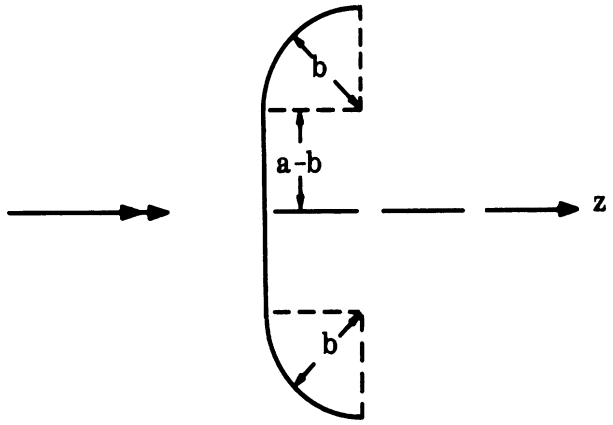

where the time dependence $e^{-i\omega t}$ has been assumed. The first integral on the right-hand side of (3.29) arises from the flat portion of the back, and is trivially performed; the second, in which

$$(\rho - a + b)^2 + (z - b)^2 = b^2 \quad , \tag{3.30}$$

arises from the toroidal portion, and since the upper limit of integration corresponds to the shadow boundary (where the physical optics current is in error), our main interest centers on the contribution provided by the lower limit, corresponding to the join of the flat and curved portions.

(U) Substituting (3.30) into (3.29) we have, after carrying out some simple steps,

$$S = ik^2 \left\{ \frac{1}{2}(a-b)^2 - \int_0 e^{2ikz}(a-b)\left(1 + \frac{a-b}{\sqrt{z(2b-z)}}\right) dx \right\}$$

$$\sim ik^2 \left\{ \frac{1}{2}(a-b)^2 + (a-b)\sqrt{b/2} \int_0 \frac{e^{2ikz}}{\sqrt{z}} dz \right\}$$

in which we have retained only that term resulting from the lower limit of

integration that is dominant at high frequencies. The transformation $s^2 = 2kz$ now reduces the integral to a standard form, and gives

$$S = \frac{i}{2} k^2 (a - b)^2 \left\{ 1 + \frac{1}{a - b} \sqrt{\frac{\pi b}{k}}\, e^{i\pi/4} \right\} . \qquad (3.31)$$

Note that the first term is merely the result for a circular disc of radius (a - b), and that the second term is one half the standard expression for a torus (Crispin et al, 1959). The required expression for the rear-on cross section is therefore

$$\sigma/\lambda^2 = \frac{1}{4\pi}(ka)^4 (1 - \tfrac{1}{n})^4 \left\{ 1 + \frac{1}{1 - \frac{1}{n}} \sqrt{\frac{2\pi}{nka}} + \frac{1}{(1 - \frac{1}{n})^2} \frac{\pi}{nka} \right\} \qquad (3.32)$$

where, for convenience, we have written b = a/n.

3.3 Computer Program for Current on Rotationally Symmetric Metal Body

3.3.1 Introduction

(U) In evaluating multi-dimensional integrals, as in the case of the computer program for solving the Maue equation for the surface current induced on rotationally symmetric metallic bodies, movable singularities occur.

(U) A number of ad hoc methods exist for removing final singularities in an integral (Davis, P.J. and P. Rabinowitz, 1967; McNamee, J., 1964) but there appear to be no general procedures. In this section we develop and discuss a general procedure using a transformation of the independent variables. The procedure is effective not only for removing fixed singularities in a integral, but also for removing movable singularities, that is, singularities which may depend on one or more parameters. We are able to transform the original integral I_o into a product GI_1 where G is a function depending only on the parameters and I_1 is a new integral. The singular behavior of I_o is con-

tained in G while I_1 exists for all values of the parameters. The procedure is also quite flexible, in that it allows the use of a variety of weight functions in I_1, and thus enables us to pick that weight function which leads to the most suitable existing quadrature scheme. The integral I_o may be one of the integrals in the process of repeated integration, and the parameters in G may depend on other independent variables. In this case GI, is in the form suitable for treatment in later integrations.

(U) In Section 3.3.2 we develop the general procedure. In the following sections we apply this to the evaluation of the integral

$$\int_{-1}^{1} \frac{f(x)\,dx}{\sqrt{(1 - x^2)(1 - k^2x^2)}} \tag{3.33}$$

where f(x) is entire and k is a parameter such that $0 \leq k < 1$. In the process we shall develop some new quadrature schemes and some effective methods of evaluating incomplete elliptic integrals.

3.3.2 The General Procedure

(U) Consider the evaluation of the integral

$$I_o = \int_{-1}^{1} \frac{w_o(x)\,dx}{\prod_{i=1}^{m}(1 - \lambda_i x)^{\omega_i}} \tag{3.34}$$

where the ω_i are real constants and $w_o(x)$ is defined for all complex x such that $w_o(x) < 0$ for x in the interval (-1, 1). The λ_i are parameters in an open domain Λ such that for each fixed $(\lambda_1, \ldots \lambda_m) \in \Lambda$ the integral

$$\int_{-1}^{1} \frac{w_o(x)\,dx}{\prod_{i=1}^{m}(1 - \lambda_i x)^{\omega_i}} \tag{3.35}$$

exists and such that the λ_i may approach ± 1. For the purpose of simplification of the development in this section we shall assume that f is entire*, real when x is real, and that $\prod_{i=1}^{m} (1 - \lambda_i x)^{\omega_i}$ is real when $x \in \Lambda(-1, 1)$ and $(\lambda_1, \ldots, \lambda_m) \in \Lambda$.

(U) We briefly describe a norm on the error of quadrature which influences our choice of a transformation on (3.34). Let $E_n(g)$ be the error of a quadrature scheme, i.e.

$$E_n(g) = \int_{-1}^{1} w(x)\, g(x)\, dx - \sum_{j=1}^{n} w_j\, g(x_j) \tag{3.36}$$

where $|w(x)|$ is integrable over (-1, 1), the w_j are weights and the x_j are points on the closed interval $[-1, 1]$ such that $E_n(g) = 0$ whenever g is a polynomial of degree p. Let g(z) be holomorphic in the ellipse $\mathcal{E}_\rho$ (of complex numbers $z = x + iy$) with foci at $z = \pm 1$ and sum of semi-axes equal to ρ, and let g(x) be real. Define

$$A = \int_{-1}^{1} |w(x)|\, dx\,, \qquad B = \sum_{j=1}^{n} |w_j|$$

$$M(\rho) = \sup_{z \in \mathcal{E}_\rho} |\mathrm{Re}\; g(z)| \tag{3.37}$$

Then we have

Lemma 2.1:

$$E_n(g) < \frac{8(A + B)}{\pi} \frac{M(\rho)}{\rho^{\rho+1}}\,. \tag{3.38}$$

*In practice the function f(x) may have singularities in the finite x plane provided that these are far from the region of integration relative to those displayed in (3.34).

Proof: The proof is similar to that of Theorem 4 in Stenger F. (1966) and is omitted.

Corollary 2.1: Of the set of all n-point quadrature schemes (3.36) that are exact for polynomials of degree p the Gaussian scheme minimizes the right of (3.38). For Gaussian quadrature with $w(x) > 0$ the bound

$$|E_n(g)| < \frac{16\mu_o}{\pi} \frac{M(\rho)}{\rho^{2n}} \quad ; \quad \mu_o = \int_{-1}^{1} w(x)\, dx \,, \tag{3.39}$$

holds.

(U) Quadrature schemes that are exact for degree p are most extensively tabulated. In what follows we shall, therefore, attempt to construct transformations on (3.34) which reduce (3.34) to another integral that can be evaluated by Gaussian quadrature and for which the error bound (3.39) is relatively small. Best results would be achieved in this respect by choosing

$$w_1(x) = w_o(x) \Big/ \prod_{i=1}^{m} (1 - \lambda_i x)^{\omega_i}$$

as a weight function and constructing a set of Gaussian quadrature formulas using polynomials orthogonal over $(-1, 1)$ with respect to $w_1(x)$. We could achieve this by constructing quadrature formulas for certain fixed values of the parameters and then obtain formulas for intermediate values of the parameters by use of polynomial interpolation. However we expect that this procedure is worthwhile only if it is necessary to evaluate (3.34) for a large number of different functions f.

(U) Let $\mathcal{P}_x$ be a path in the complex x plane such that the segment of $\mathcal{P}_x$ joining -1 and 1 is a straight line, such that the integral

$$\int_{-1}^{x} \frac{w_o(t)\,dt}{\prod_{i=1}^{m}(1-\lambda_i t)^{\omega_i}} \tag{3.40}$$

taken along $\mathcal{P}_x$ exists for each x on $\mathcal{P}_x$, and such that the points $x_o, x_1, \ldots x_r$ are on $\mathcal{P}_x$, where $x_o = 1$. Let w(y) be a function defined for complex y such that $w(y) > 0$ if $-1 < y < 1$. Let $\mathcal{P}_y$ be a path in the complex y plane such that the segment of $\mathcal{P}_y$ joining -1 and 1 is a straight line and such that the r + 1 distinct points $\{y_i\}_{i=o}^{r}$ with $y_o = 1$ are on $\mathcal{P}_y$. Let $\{h_j(y)\}_{j=o}^{r}$ be a set of functions such that $h_o(t) = 1$, such that $h_j(y)$ is real when y is real, such that each integral

$$H_{ij} = \int_{-1}^{y_{i-1}} w(t)\,h_{j-1}(t)dt \qquad (i,\ j=1,\ 2,\ \ldots\ r+1) \tag{3.41}$$

taken along $\mathcal{P}_y$ exists, and such that the square matrix $[H_{ij}]$ of order r + 1 is non-singular for all $(\lambda_1, \ldots, \lambda_m) \in \bar{\Lambda}$, the closure of Λ, where H_{ij} is the (i, j)'th element of $[H_{ij}]$.

(U) Note that $\mathcal{P}_x$ and $\mathcal{P}_y$ may depend continuously upon $(\lambda_1, \ldots \lambda_m) \in \bar{\Lambda}$, provided that the above conditions are satisfied. Note also that the functions w_o and w may restirct the choice of $\mathcal{P}_x$, $\mathcal{P}_y$ or r. For example, if $w(y) \equiv 0$ for all y $[-1, 1]$ it is necessary to take $y_j \in [-1, 1]$ if we want $r > 0$; if we do not want $y_j \in [-1, 1]$ for $j > 0$ it is necessary to take $r = 0$.

(U) Let us put

$$\int_{-1}^{x} \frac{w_o(t)\,dt}{\prod_{i=1}^{m}(1-\lambda_i t)^{\omega_i}} = \int_{-1}^{y} \left(\alpha_o + \sum_{j=1}^{r} \alpha_j h_j(t)\right) w(t)\,dt\ . \tag{3.42}$$

In this equation the constants α_j on the right are determined such that $y = y_j$ when $x = x_j$, $j = 0, 1, \ldots r$. Note that since $\left[H_{ij}\right]$ is non-singular there exists a unique set of α_j's for all $(\lambda_1, \ldots, \lambda_m) \in \Lambda$.

Theorem 2.1: Let $x = x(y)$ be determined by (3.42) as described above. This transformation reduces the integral (3.34) to the integral

$$I_o = \int_{-1}^{1} \left[\alpha_o + \sum_{j=1}^{r} \alpha_j h_j(y)\right] w(y) f\left[x(y)\right] dy \ . \qquad (3.43)$$

Proof: The proof follows by direct substitution of (3.42) into (3.34). The constants α_j in general depend on the parameters λ_i. Hence if $r > 0$ (3.43) offers no advantage over (3.34) if we attempt to evaluate (3.43) using

$$\left[\alpha_o + \sum_{j=1}^{r} \alpha_j h_j (y)\right] w(y)$$

as a weight function. We may however have gained over (3.34) if we either

(i) replace (3.43) by $r + 1$ new integrals choosing $h_{j-1}(y)\, w(y)$ as a weight function in the j'th, or

(ii) choose $w(y)$ as a weight function to evaluate (3.43).

(U) In order to minimize the bound (3.38) it is preferable in each of these cases that $x(y)$ be an analytic function in as large a region as possible. In the cases (ii) we also want the function $h_j(y)$ to be analytic in as large a region as possible.

(U) Let $\mathcal{E}_\rho^{(x)}$ and $\mathcal{E}_\rho^{(y)}$ be ellipses of complex numbers with foci at ± 1 in the x and y planes respectively such that for each ellipse the sum of its semiaxes is ρ and such that $x(y)$ is analytic for $y \in \mathcal{E}_\rho^{(y)}$. Let $w = F(y)$ be a conformal map of $\mathcal{E}_\rho^{(y)}$ onto $|w| < 1$ such that $F(-1) = 0$. If we suppose that $x(y) \in \mathcal{E}_\rho^{(x)}$ whenever $y \in \mathcal{E}_\rho^{(y)}$, Schwarz's Lemma (Caratheordory, C. 1958),

applied to the function $G[F(y)] = F[x(y)]$ yields $|G[F(y)]| \leq |F(y)|$ for all $y \in \mathcal{E}_\rho^{(y)}$. Since moreover $G[F(1)] = F(1)$ Schwarz's Lemma yields $G[f(y)] \equiv F(y)$, from which $x(y) \equiv y$.

(U) We have thus proved the following negative result:

Lemma 2.2: Let $x(y)$ be analytic in $\mathcal{E}_\rho^{(y)}$. Unless $x(y) \equiv y$ there exists points $y \in \mathcal{E}_\rho^{(y)}$ such that $x(y) \in \mathcal{E}_\rho^{(x)}$.

(U) Hence if $x(y) \not\equiv y$ then given any positive number B there exist entire functions f(t) such that

$$\sup_{y \in \mathcal{E}_\rho^{(y)}} |f(y)| = B \quad \text{while} \quad \sup_{y \in \mathcal{E}_\rho^{(y)}} |f[x(y)]| > B.$$

(U) We have considerable freedom of choice in picking the weight function w(t). In practice we would be apt to pick a weight function for which quadrature formulas are extensively tabulated. On the other hand since the bound (3.37) can in general be made smaller when x(y) is analytic in a larger domain, picking a weight function w(t) for which quadrature formulas are tabulated does not always yield the most rapidly converging quadrature scheme.

(U) By Lemma 2.2 the bound (3.38) applied to (3.43) in either case (i) or case (ii) above is in general minimal when $x(y) \equiv y$. Since the construction of high degree Gaussian quadrature formulas is no longer a formidable task (Gautschi, W. 19) it is worthwhile to keep in mind the following result, the proof of which illustrates a construction of x(y):

Theorem 2.2: Corresponding to any positive number ϵ any compact subset S of the parameter domain Λ can be covered by a finite number of N neighborhoods U_j, $j = 1, 2, \ldots, N$ such that for $(\lambda_1, \ldots \lambda_m) \in U_j$ there exists a function w(t) and a set of functions $h_j(t)$ with the property that if x(y) is defined by (3.42) then $|x(y) - y| < \epsilon$, $-1 \leq y \leq 1$.

Proof: Let $(\lambda_1^o, \ldots \lambda_m^o)$ be a point of S and let $\delta > 0$ define

$$U_j = \left\{(\lambda_1, \ldots \lambda_m) : \sum_{j=1}^{m} \left|\lambda_j - \lambda_j^o\right|^2 < \delta\right\} \cap \Lambda \tag{3.44}$$

Putting

$$w(t) = \frac{w_o(t)}{\prod_{i=1}^{m} (1 - \lambda_i^o t)^{\omega_i}} \tag{3.45}$$

we choose $\alpha_o, \alpha_1, \ldots, \alpha_r$ $(r \leq m)$ in (3.42) such that

$$y = 1 \text{ when } x = 1$$

$$y = 1/\lambda_i^o \text{ when } x = 1/\lambda_i, \quad i = 1, 2, \ldots, r \quad . \tag{3.46}$$

Here we assume thar $r \geq 0$ is taken sufficiently small such that only integrable singularities are included on each side of (3.45) and such that in (3.42) $y = 1/\lambda_i^o$ is a singularity of the same type as $x = 1/\lambda_i$. By our hypotheses on the independence of $h_i(t)$ the conditions (3.46) uniquely determine α_j, $j = 0, 1, \ldots, r$ as continuous functions of $\lambda_1, \ldots, \lambda_m$. When $(\lambda_1, \ldots, \lambda_m) = (\lambda_1^o, \ldots, \lambda_m^o)$ we have $\alpha_o = 1$ and $\alpha_j = 0$, $j = 1, 2, \ldots, r$. Consequently if δ is chosen sufficiently small, α_j can be made of differ by as little as we please from its value when $(\lambda_1, \ldots, \lambda_m) = (\lambda_1^o, \ldots, \lambda_m^o)$. Hence if δ is sufficiently small the assention of Theorem 2.2 follows for $(\lambda_1, \ldots, \lambda_m) \in U_j$. That S can be covered by a finite number of the U_j is a consequence of the Heine-Borel Thoerem.

Corollary 2.1: If the integral on the left of (3.42) becomes unbounded as some of the λ_i approach ± 1 then at least one of the α_j on the right of (3.42) becomes unbounded.

Proof: That at least one of the α_j's must become unbounded follows from the fact that

$$\int_{-1}^{1} h_j(t)\, w(t)\, dt$$

exists for all $j = 0, 1, \ldots r$ and for all $(\lambda_1, \ldots, \lambda_m) \in \Lambda$.

(U) We conclude this section with some additional remarks concerning the transformation (3.42).

Remarks: 1. The resulting transformation is often analytic in a larger domain if the ω_i are chosen such that $-1 < \omega_i$. This choice can always be made by use of the following identity:

$$\frac{f(x)}{(1-ux)^{\omega}} = \sum_{k=0}^{\mu-1} \frac{f^{(k)}(1/u)}{k!} (x - \frac{1}{u})^k + \frac{F(x)}{(1-ux)^{\omega-\mu}} \qquad (3.47)$$

where $\mu = [\omega]$. Given f(x) (3.47) defines F(x); further with the exception of $x = 1/u$ the singularities of F(x) are of the same type as those of f(x), and F(x) is holomorphic wherever f(x) is holomorphic.

2. The transformation (3.42) has practical merit only if it enables us to easily express x as a function of y.

3. If $r = 0$ the transformation (3.42) is a one-to-one mapping of $-1 \leq x \leq 1$ onto $-1 \leq y \leq 1$. If $r > 0$ the transformation (3.42) may cease to be one-to-one for all values of the parameters.

4. In the notation of Theroem 2.2 it is often the case that relatively few sets U_j are required to cover S, particularly if instead of "nearness of x(y) to y" we only require "analytivity of x(y) in some domain."

5. In order to produce a holomorphic function $x = x(y)$ it is not always necessary to match singularities as in the proof of Theorem 2.2. As is readily verified we need not require a singularity of y to match up with $x = 1/\lambda_i$ when $\omega_i = (n - 1)/n$, where n is a positive integer.

3.3.3 Examples

(U) In this section we illustrate the developments of Section 3.3.2 with some examples. In section 3.3.3.1 we give two examples illustrating that the theory of Section 3.3.2 does in fact include and extend well-known procedures. In Section 3.3.3.2 we develop some formulas to evaluate the integral (3.33).

3.3.3.1 Well-known Examples

(U) Consider evaluating the integral

$$I = \int_0^1 \frac{f(x)}{\sqrt{x}}\, dx \quad . \tag{3.48}$$

where f(x) is analytic and does not have singularities near the interval of integration. Actually (3.48) is already in a form suitable for Gaussian quadrature with weight function $1/\sqrt{x}$.

(U) Denoting ξ_j and w_j to be the corresponding Legendre-Gauss zeros and weights ($\xi_{-n} < \xi_{-n+1} < \ldots < \xi_{-1} < 0 < \xi_1 < \ldots < \xi_n$) for 2n-point quadrature over (-1, 1) we have

$$I = 2 \sum_{j=1}^{n} w_j f(\xi_j^2) + E_n(f) \tag{3.49}$$

where, with $|f(x)| \leq e^{\beta|x|}$, x complex (f(x) is real where x is real) (3.39) yields

$$\left| E_n(f) \right| < \frac{16\, e^{\beta/2}}{\pi} (e\beta/8n)^{2n} \qquad (3.50)$$

after minimization with respect to ρ.

(U) On the other hand we may remove the $1/\sqrt{x}$ singularity by setting

$$\int_0^x \frac{dt}{\sqrt{t}} = \alpha \int_0^y dt$$

choosing α such that $y = 1$ when $x = 1$. This yields $\alpha = 2$ and $x = y^2$, so that (3.48) becomes

$$I = 2 \int_0^1 f(y^2)\, dy \quad . \qquad (3.51)$$

We can now use Gauss-Legendre quadrature directly on this integral; since $f\left[(-y)^2\right] = f(y^2)$ and since $\xi_{-j} = -\xi_j$ we again need not evaluate $f(y^2)$ when $\xi_j < 0$. Using (3.39) with $\left| f(y^2) \right| \leq e^{\beta |y^2|}$ and minimizing with respect to ρ we again obtain (3.50).

(U) We next examine the integral

$$I = x \int_0^1 \frac{f(t)\, dt}{1 - xt} \quad , \qquad 0 \leq x < 1 \quad . \qquad (3.52)$$

The usual method of subtracting out the singularity in this integral is to write

$$I = -f(1/x) \ln(1 - x) + x \int_0^1 \frac{f(t) - f(1/x)}{1 - xt}\, dt \qquad (3.53)$$

for x near 1. Note that the integrand in the integral on the right is now en-

tire and we may use Legendre-Gauss quadrature to evaluate it. Using a n-point formula we get the error bound

$$\left|E_n(f)\right| < \frac{16}{\pi} e^{\beta\left(\frac{1}{x}+\frac{1}{2}\right)} \left(\frac{e\beta}{8n}\right)^{2n} ; \quad |F(x)| \leq e^{\beta x} . \tag{3.54}$$

On the other hand putting

$$x \int_0^t \frac{d\tau}{1 - x\tau} = \alpha \int_0^y d\tau \tag{3.55}$$

and choosing α such that $y = 1$ when $t = 1$ we obtain

$$\left.\begin{aligned} t &= \frac{1 - (1 - x)^y}{x} \quad ; \qquad \alpha = -\ln(1 - x) \\ I &= -\ln(1 - x) \int_0^1 f\left(\frac{1 - (1 - x)^y}{x}\right) dy \end{aligned}\right\} \tag{3.56}$$

On evaluating

$$I_1 = \int_0^1 f\left(\frac{1 - (1 - x)^y}{x}\right) dy$$

by n-point Legendre-Gauss quadrature we get the error bound

$$\left|E_n(f)\right| < \frac{16}{\pi} e^{\beta/x} \left[\frac{e \ln(1 - x)}{4 \ln \frac{2n x}{\beta}}\right]^m \tag{3.57}$$

(U) Note that the function $f = f(y)$ defined by (3.56) is an entire function of y. Note also that although the bound on the right of (3.54) approaches zero faster as $n \to \infty$ than that given by (3.57). The form (3.56) has an advantage

over (3.53) in the case when I is part of a repeated integral and integration with respect to x is required next,* since an effective numerical integration of (3.53) with respect to x requires two different procedures while the integration of (3.56) requires only one: Gaussian quadrature using log (1 - x) as a weight function.

(U) Note also that by Remark 1 of the previous section the transformation (3.53) can also be obtained by our procedure.

3.3.3.2 The Numerical Evaluation of

(U)

$$I = \int_{-1}^{1} \frac{f(x)\,dx}{\sqrt{(1 - x^2)(1 - k^2 x^2)}} \qquad (3.58)$$

In this integral of I of (3.58) k is a parameter such that $0 \leq k < 1$. We shall assume that f(x) is an entire function, real when x is real.

(U) We (the authors) feel that an effective method of evaluating (3.58) would be of considerable value because of the frequenct occurance of elliptic integrals in practice. The above problem arose in our attempt to evaluate a three dimensional integral connected with the solution of the reduced wave equation $(\nabla^2 + \lambda^2)u = 0$ in three dimensions (Honl, H., et al, 1961). In that case I was an inner integral and k a function of two other variables. As it was necessary to integrate the result also with respect to these other variables a knowledge of the type of singularity that I has as $k \to 1$ was important. In evaluating (3.58) we wanted the number of evaluation points to be small since the evaluation of I was an often used subroutine in a larger program. Also it was necessary to compute I very accurately -- to within 10^{-7}.

---

*Consider the case when f(t) = f(t, x)

(U) In what follows we illustrate several procedures for evaluating I. Some of these procedures are effective over the whole range of k, while others are effective only over a part of the range $0 \leq k < 1$.

3.3.3.3 A Method for Small and Intermediate k

(U) We apply Chebychev quadrature to (3.58) in the form

$$I = \frac{\pi}{n} \sum_{j=1}^{n} F(x_j) + E_n(F), \quad x_j = \cos\left[\frac{(2j-1)\pi}{2n}\right] \tag{3.59}$$

where

$$F(x) = f(x) \,/\, \sqrt{1 - k^2 x^2} \ . \tag{3.60}$$

On applying the error norm of Section 3.3.2 we get

$$\left| E_n(f) \right| < \frac{16\, e^{\beta/2}}{\sqrt{1 - k^2 (4n/\beta)^2}} \left(\frac{e\beta}{4n}\right)^{2n} \quad (\beta/4n < k) \tag{3.61}$$

$$\text{or} \quad < 16 \sqrt{\frac{2n\,e}{\sqrt{1-k^2}}} \left[\frac{k}{1 + \sqrt{1-k^2}}\right]^{2n} e^{\beta/k}, \quad 0 < k < 1 \ .$$

Thus convergence is quite rapid when k is small. However when k is a function of other variables and additional integrations are required with respect to these variables the above method has a disadvantage for k near 1 since it does not display the singularity of I as a function of k.

3.3.3.4 A Method for Large k.

(U) In this section we use the procedure of Section 3.3.2 to develop a method suitable for ka near 1. The method is in fact suitable for all k in the range $0 \leq k < 1$ although the rate of convergence is not as rapid for that of some of the other methods for intermediate and small values of k.

(U) In view of (3.58) we have

$$I = \int_0^1 \frac{F(x)\,dx}{\sqrt{(1-x)(1-kx)}} \quad ; \tag{3.62}$$

$$F(x) = \frac{f(x) + f(-x)}{\sqrt{(1+x)(1+kx)}} \quad .$$

Thus F(x) has a singularity at the point x = -1; by our assumptions of Section 3.3.2 this is the nearest singularity of F(x) to the integration strip $[0,1]$.

(U) In (3.62) we put

$$\int_x^1 \frac{dt}{\sqrt{(1-t)(1-kt)}} = \alpha \int_y^1 \frac{dt}{\sqrt{1-t}} \tag{3.63}$$

choosing α so that x = 0 when y = 0. We then obtain

$$\frac{1}{\sqrt{k}} \sinh^{-1} \sqrt{\frac{k(1-x)}{1-k}} = \alpha \sqrt{1-y} \quad ;$$

$$\alpha = \frac{1}{\sqrt{k}} \sinh^{-1} \sqrt{\frac{k}{1-k}} = \frac{1}{\sqrt{k}} \ell n \left(\frac{1+\sqrt{k}}{\sqrt{1-k}} \right) \tag{3.64}$$

$$x = 1 - \frac{1-k}{k} \sinh^2 \left[\alpha \sqrt{k(1-y)} \right] \quad .$$

With this transformation (3.62) becomes

$$I = \alpha \int_0^1 \frac{F[x(y)]}{\sqrt{1-y}}\, dy \tag{3.65}$$

where x(y) and α are given by (3.64).

(U) Note that x(y) defined by (3.64) is an entire function of y and also a one-one function mapping $0 \leq 4 \leq 1$ onto $0 \leq x \leq 1$. Hence, the integral on the right of (3.65) exists for all values of k. The dominant portion of the singularity of (3.58) as a function of k is contained in α; this being a particularly desirable feature from the point of view of repeated integration.

(U) The integral on the right of (3.65) can now be evaluated by use of Gaussian quadrature with $1/\sqrt{1 - y}$ as a weight function (see 3.48, 3.49). Setting

$$I = \alpha \left[\sum_{j=1}^{n} w_j F\left[x(y_j)\right] + E_n(F) \right] \tag{3.66}$$

we obtain

$$\left| E_n(F) \right| < \frac{64\, n\, e^{1 + \beta/\pi}}{\alpha \sqrt{(1 + k)(2 - y_o)}} \left(y_o + \sqrt{y_o^2 - 1}\right)^{-2n} ;$$

$$y_o = 1 + \left(\frac{\sinh^{-1} \sqrt{\frac{2k}{1 - k}}}{\alpha \sqrt{k}} \right)^2 , \tag{3.67}$$

assuming again that $|f(x)| \leq e^{\beta |x|}$. The above bound is obtained again by use of (3.39) and minimization with respect to ρ. The bound on F used is $|F(x)| \leq 2\, e^{\beta |x|} / (1 + x)$, $-1 < x \leq 0$. Under the transformation (3.64) the singularity at $x = -1$ in (3.62) becomes a function of k and approaches the region of integration arbitrarily closely as $k \longrightarrow 1$. Note however that $E_n(f) \longrightarrow 0$ as $k \longrightarrow 1$.

3.3.3.5 A Method for Intermediate and Large k

(U) Let us make the transformation $x = x(y)$ in (3.58), where $x(y)$ is determined from

$$\int_0^x \frac{dt}{\sqrt{(1-t^2)(1-k^2t^2)}} = \int_0^y \frac{(\alpha+\beta t^2)\,dt}{\sqrt{(1-t^2)(1-k_o^2t^2)}} \,. \tag{3.68}$$

In (3.68) k_o is fixed, and α and β are determined such that

(i) $y = 1$ when $x = 1$

(ii) $y = 1/k_o$ when $x = 1/k$, $0 < k,\ k_o < 1$. (3.69)

We thus attempt to match up the singularities as described in Section 3.3.2. Using the notations

$$F(x,k) = \int_0^x \frac{dt}{\sqrt{(1-t)^2(1-k^2t^2)}}, \quad E(x,k) = \int_0^x \sqrt{\frac{1-k^2t^2}{1-t^2}}\,dt \tag{3.70}$$

together with

$$\left.\begin{aligned} &F(1,k) = K\,, && F(1,k_o) = K_o \\ &E(1,k) = E\,, && E(1,k_o) = E_o \\ &k' = \sqrt{1-k^2}\,, && F(1,k') = K',\quad F(1,k'_o) = K'_o \\ &E(1,k') = E'\,, && E(1,k'_o) = E'_o \\ &F(1/k,k) = K + iK'\,, && E(1/k,k) = E + i(E'-K') \end{aligned}\right\} \tag{3.71}$$

we find on substituting (3.69) into (3.68) that α and β satisfy a simultaneous pair of linear equations whose determinant is

$$E_o K'_o + E'_o K_o - K'_o K_o = \pi/2 \,, \tag{3.72}$$

the Lagrange identity. Thus the condtions (3.69) uniquely determine α and β in (3.67) and we obtain

$$F(x, k) = \frac{K}{K_o} F(k, k_o) + \frac{2}{\pi} \left[K_o K' - K'_o K\right] \left[\frac{E_o}{K_o} F(y, k_o) - E(y, k_o)\right] \tag{3.73}$$

or

$$x = sn\left\{\frac{K}{K_o} F(y, k_o) + \frac{2}{\pi} \left[K_o K' - K'_o K\right] \left[\frac{E_o}{K_o} F(y, k_o) - E(y, k_o)\right]\right\} . \tag{3.73'}$$

The integral (3.58) is thus transformed into the integral

$$I = \int_{-1}^{1} \frac{(\alpha + \beta y^2) F\, x(y)}{\sqrt{(1 - y^2)(1 - k_o^2 y^2)}}\, dy \tag{3.74}$$

where

$$\alpha = \frac{K}{K_o} + \frac{2}{\pi} (K_o K' - K_o' K) \frac{E_o}{K_o}$$
$$\beta = -\frac{2k_o^2}{\pi} (K_o K' - K_o' K) \tag{3.75}$$

and where x(y) is given by (3.73').

(U) Let us check whether (3.73') is a one-to-one transformation. To this end we have

Lemma: The Transformation (3.73) maps $-1 \leq y \leq 1$ onto $-1 \leq x \leq 1$ in a one-to-one manner if and only if k is such that

$$\frac{K}{K'} \geq \frac{K_o E_o}{K_o' E_o - \frac{\pi}{2}} \quad . \tag{3.76}$$

Proof: It is readily seen by use of (3.68) that (3.73) is one-to-one if and only if both of the requirements (i) $\alpha \geq 0$ and (ii) $(\alpha + \beta) \geq 0$ are satisfied. For if $\alpha < 0$ we must have $\beta > 0$ in order to meet the first of (3.69); in this case $\alpha + \beta y^2$ has a simple zero in (-1, 1) similarly if $\alpha = 0$ then $\beta > 0$. Clearly $\alpha + \beta \geq 0$ implies that $\alpha + \beta y^2 \geq 0$, $-1 \leq y \leq 1$, since there is at most one y in (0, 1) such that $\alpha + \beta y^2 = 0$. Consequently if $\alpha + \beta < 0$ then $\alpha + \beta y^2 < 0$ for $|y|$ ($|y| < 1$) sufficiently near 1. The inequality $\alpha + \beta \geq 0$ yields

$$K \left[E_o' - k_o^2 K_o'\right] + K' \left[E_o - (1 - k_o^2) K_o\right] \geq 0 \, . \tag{3.77}$$

Since

$$E_o - (1 - k_o^2) K_o = k_o^2 \int_0^{K_o} cn^2 u \, du \tag{3.78}$$

where cn u [= cn (u, k_o)] is defined by cn u = $\sqrt{1 - 2n^2 u}$, $-K_o < y \leq K_o$ it follows that $E_o - (1 - k_o^2) K_o \geq 0$ (> 0) for all k_o in $0 \leq k_o < 1$ ($0 < k_o < 1$). Similarly $E_o' - k_o^2 K_o' \geq 0$. Therefore the only condition which may not be satisfied for all k in $0 \leq k < 1$ is the condition $\alpha \geq 0$. Using (3.75) we see that this condition is satisfied for all k such that (3.76) holds.

(U) For example, when $k_o = 1/\sqrt{2}$ (3.76) holds for all k such that $0.059\ldots \leq k < 1$.

(U) Similarly we are able to deduce the behavior of x = x(y) defined by (3.73) when y is complex by use of formulas in Byrd, P.F. and M.D. Friedman, (1954). These formulas were used to obtain one of the graphs of

Fig. 3-16. Let $k_o = 1/\sqrt{2}$ and let $\mathcal{E}_\rho$ be defined as in Section 3.3.2. Then Fig. 3-16 enables us to obtain for any given k in $0 < k < 1$ the value of ρ with the property that x(y) is bounded if and only if $y \in \mathcal{E}_\rho$. In Section 3.3.3.6 we shall describe a method of using the graph for obtaining error bounds.

(U) Table III-4 is a table of zeros and weights for applying Gaussian quadrature to (3.74), with weight function

$$1/\sqrt{(1 - y^2)(1 - k_o^2 y^2)}$$

and with $k_o = 1/\sqrt{2}$. Gautschi's method (Gautschi, W. 1967) was used to obtain these formulas.

3.3.3.6 A Method for all k

(U) In this section we describe the transformation

$$\int_0^x \frac{dt}{\sqrt{(1 - t^2)(1 - k^2 t^2)}} = \int_0^y \frac{\alpha \, - dt}{\sqrt{1 - t^2}} \qquad (3.79)$$

choosing α such that $x = 1$ when $y = 1$. We thus obtain $\alpha = 2K/\pi$, and

$$x = \mathrm{sn}\left[\frac{2K}{\pi} \sin^{-1} y\right] , \qquad (3.80)$$

and (3.58) is transformed into the integral

$$I = \frac{2K}{\pi} \int_{-1}^{1} \frac{f\left(\mathrm{sn}\left[\frac{2K}{\pi} \sin^{-1} y\right]\right)}{\sqrt{1 - y^2}} \, dy \quad . \qquad (3.81)$$

We evaluate the integral I by use of n-point Chebychev quadrature to obtain

$$I = \frac{2K}{\pi}\left[\frac{\pi}{n} \sum_{j=1}^{n} f\left(\mathrm{sn}\left[\frac{(n - 2j + 1)K}{n}\right]\right) + E_n(f)\right] \qquad (3.82)$$

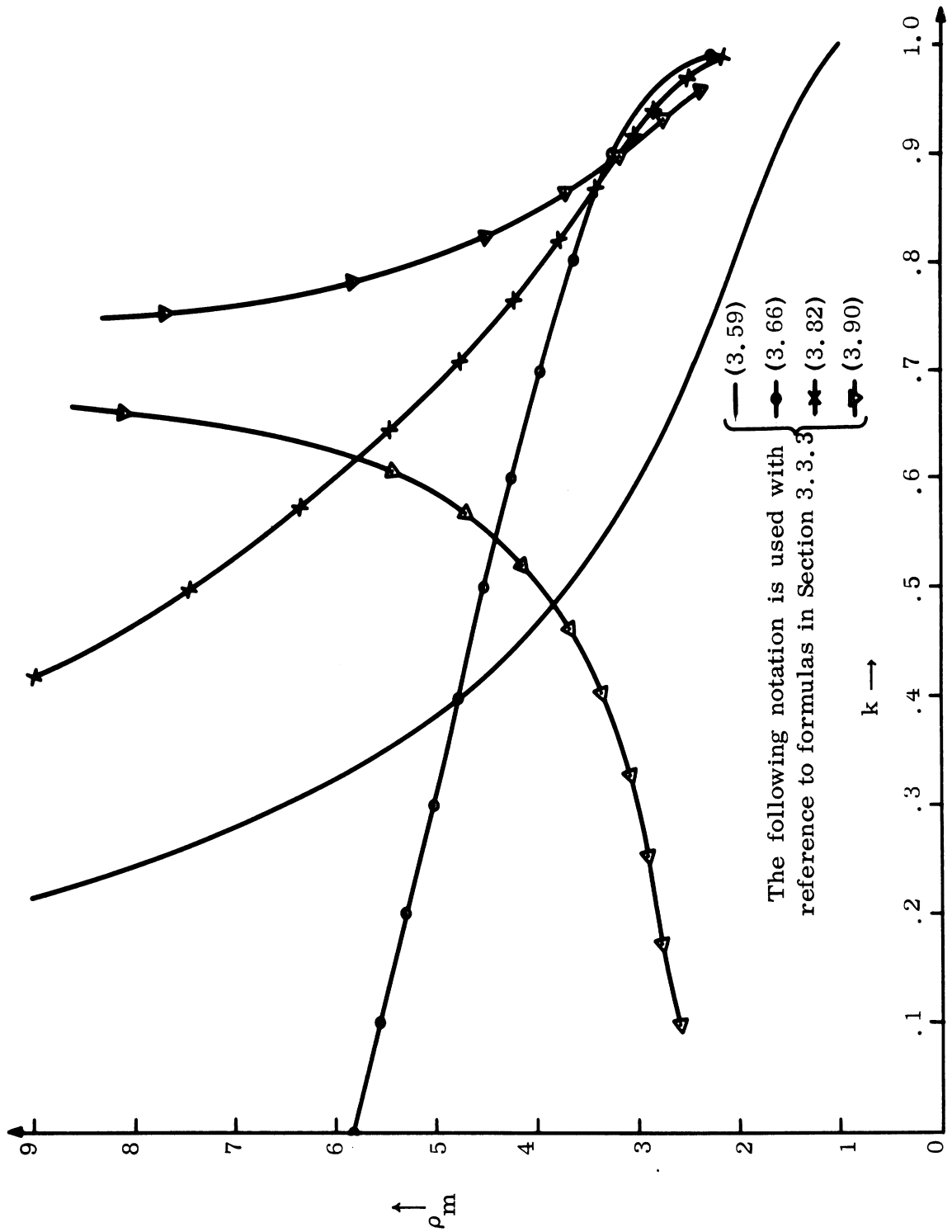

FIG. 3-16: IN THE APPROXIMATION OF $\int_{-1}^{1} w(y)F(y)\,dy$ BY $\sum_{j=1}^{n} w_j F(y_j)$ THESE GRAPHS SHOW

$\rho_m = \max\{\rho : F(y) \text{ IS ANALYTIC IN } \mathcal{E}_\rho\}$ AS A FUNCTION OF k.

TABLE III-4: A Tabulation of Zeros and Weights for the Formula (3.90).

x_i	w_i
n = 2	
0.7369 21582 63652	1.854 07467 73012
n = 4	
0.3954 69781 80571	0.8425 64689 98211
0.9301 23603 28663	1.0115 09987 3191
n = 6	
0.2649 51597 16405	0.5451 74977 20330
0.7170 91637 67463	0.6099 34460 36376
0.9680 02002 48077	0.6989 65239 73418
n = 8	
0.1986 21001 15531	0.4036 60738 26268
0.5632 97934 36302	0.4324 38866 30620
0.3372 28694 04480	0.4845 76717 20760
0.9817 02539 55180	0.5333 98355 52475
n = 10	
0.1587 15892 17121	0.3207 08661 04100
0.4596 28626 03537	0.3357 07997 14341
0.7131 04989 96760	0.3647 39149 50250
0.8944 27331 04644	0.4019 89917 80663
0.9881 69228 53536	0.4309 28951 80771
n = 32	
0.0492 92858 71437	0.0986 84761 02046
0.1473 94213 81454	0.0991 54111 01528
0.2440 47560 36271	0.1000 94187 01064
0.3383 04451 55721	0.1015 06874 34035
0.4292 41652 76928	0.1033 92706 97865
0.5159 70971 01291	0.1057 47763 89022
0.5976 48818 41601	0.1085 58977 12039
0.6734 85408 86576	0.1117 97486 80229
0.7427 53450 03188	0.1154 09842 42554
0.8047 96126 79396	0.1193 07377 72279
0.8590 34069 81790	0.1233 55206 02390
0.9049 70875 26986	0.1273 64117 31767
0.9421 96641 28673	0.1310 90854 28518
0.9703 89031 67376	0.1342 53453 52388
0.9893 11727 28378	0.1365 66149 66189
0.9988 10853 58111	0.1377 90808 16210

We illustrate two methods of obtaining a bound on $E_n(f)$

Method I:

(U) Here we use the usual notation

$$q = e^{-\pi K'/K} \tag{3.83}$$

for the nome q. The transformation $x = sn\left[\frac{2K}{\pi} \sin^{-1} y\right]$ maps the ellipse $\mathcal{E}_\rho$ in the y plane conformally Kober, H. (1960) onto the circle $|x| \leq 1/\sqrt{k}$, where $\rho = q^{-1/4}$. Thus by use of (3.39) we have

$$\left|E_n(f)\right| < 16\, M^* q^{-n/2} \tag{3.84}$$

where

$$M^* = \max_{|x| \leq 1/\sqrt{k'}} \left|\text{Re } f(x)\right| \quad . \tag{3.85}$$

Thus for example, for the case $|f(x)| \leq e^{\alpha|x|}$, x complex and f(x) real when x is real we have

$$\left|E_n(f)\right| < 16\, e^{\alpha/\sqrt{k}}\, q^{n/2} \quad . \tag{3.86}$$

Method II:

(U) Here we note that $sn\left[\frac{2K}{\pi} \sin^{-1} i y\right] = sn\left[\frac{2iK}{\pi} \ell n\, r\right]$, where $r = y + \sqrt{y^2 + 1}$, $y \geq 0$. The expansion

$$sn\left[\frac{2iK}{\pi} \ell n r\right] = \frac{\pi i}{kK} \sum_{j=0}^{\infty} \frac{r^{2j+1} - r^{-(2j+1)}}{q^{-(j+1/2)} - q^{(j+1/2)}} \tag{3.87}$$

yields the estimate

$$\left|sn\left[\frac{2iK}{\pi} \ell n r\right]\right| \leq \frac{\pi}{kK} \frac{q^{1/2} r}{1 - q r^2}, \quad 1 \leq r < q^{-1/2} \tag{3.88}$$

Using this inequality we replace

$$\max_{y \in \mathcal{E}_r} \left| \text{Re } f\left(\text{sn}\left[\frac{2K}{\pi} \sin^{-1} y\right]\right)\right| = M(r)$$

by a function g(r) which exceeds M(r) and then minimize $16\, q(r)\, r^{-2n}$ with respect to r to obtain a bound on $E_n(f)$. For example, with $|f(x)| \leq e^{\alpha|x|}$ we get

$$\left|E_n(f)\right| < 16\, e^{\sqrt{\frac{4\pi\alpha n}{kK}}}\, q^n \quad , \tag{3.89}$$

a bound which is usually smaller than (3.85), although not quite as simple to obtain.

(U) Method II has the advantage that it may also be used to obtain a bound on the error of the quadrature scheme developed in the previous section. For if (3.74) is evaluated by the formula

$$\int_{-1}^{1} \frac{(\alpha + \beta y^2)\, F[x(y)]\, dy}{\sqrt{(1 - y^2)(1 - k_o^2 y^2)}} = \sum_{j=1}^{n} w_j (\alpha + \beta y_j^2)\, F(x(y_j)) + E_n(F) \tag{3.90}$$

where the w_j and y_j are obtained from Fig. 3-17, we may obtain an estimate on $E_n(F)$ as follows. We first determine ρ from Fig. 3-16 and set $q^* = q(k^*) = 1/\rho^2$. Corresponding to k^* we find $K^* = K(k^*)$ and then minimize

$$\frac{32\, K_o}{\pi}\left[\alpha + \beta\left(\frac{r - r^{-1}}{2}\right)^2\right] F^*\left[\frac{2iK^*}{\pi} \ell n r\right] r^{-2n}$$

with respect r ($1 \leq r \leq 1/q^{*1/2}$) to obtain an estimate on the bound of $E_n(F)$, where $F^*\left[\frac{2iK^*}{\pi} \ell n r\right]$ bounds $F\left[\frac{2K^*}{\pi} \sin^{-1} y\right]$ in the ellipse $\mathcal{E}_r$ ($r = y + \sqrt{1 + y^2}$ if y is imaginary).

3.3.3.7 A Method of Computing Elliptic Integrals and Elliptic Functions.

(U) Two disadvantages of the method in Section 3.3.3.5 are that it requires the computation of Elliptic integrals and elliptic function sn. The method of Section 3.3.3.5 also requires the computation of m. We suggest computing snu = sn (u, k) by use of the formula (Copson, E.T., 1950)

$$\operatorname{sn} u = \frac{2}{\sqrt{k}} \frac{\sum_{n=0}^{\infty} (-1)^n q^{(n+1/2)^2} \sin \frac{(2n+1)\pi u}{2K}}{1 + 2 \sum_{n=1}^{\infty} q^{n^2} \cos \frac{n\pi u}{2K}} \tag{3.91}$$

where K can be computed by the method of Section 3.3.3.3 for moderate values of k and by the method of Section 3.3.3.4 for k near 1. We then use (3.83) to find q and (3.91) to find sn u.

(U) The methods developed in the previous sections also provdie effective procedures for computing the elliptic integrals (3.70) we obtain

$$F(x, k) = \int_0^1 \frac{x\, du}{\sqrt{(1 - x^2u^2)(1 - k^2x^2u^2)}} \tag{3.92}$$

and

$$E(x, k) = \int_0^1 \sqrt{\frac{1 - k^2x^2u^2}{1 - x^2u^2}}\, x\, du \quad . \tag{3.93}$$

We now make the transformation

$$\int_0^u \frac{x\, d\tau}{\sqrt{1 - x^2\tau^2}} = \alpha \int_0^y \frac{d\tau}{\sqrt{1 - \tau^2}} \tag{3.94}$$

choosing α so that u = 1 when y = 1. We then obtain

$$u = \frac{1}{x} \sin\left[\frac{2}{\pi} (\sin^{-1} x) \sin^{-1} y\right] \quad . \tag{3.94'}$$

This transformation changes (3.92) and (3.93) into the integrals

$$F(x,k) = \frac{2}{\pi} \sin^{-1} x \int_0^1 \frac{1}{\sqrt{1 - k^2 \sin^2\left[(\frac{2}{\pi} \sin^{-1} x)\sin^{-1} y\right]}} \frac{dy}{\sqrt{1 - y^2}} \tag{3.92'}$$

and

$$E(x,k) = \frac{2}{\pi} \sin^{-1} x \int_0^1 \sqrt{1 - k^2 \sin^2\left[(\frac{2}{\pi} \sin^{-1} x) \sin^{-1} y\right]} \frac{dy}{\sqrt{1 - y^2}} \tag{3.93'}$$

respectively.

(U) Both integrals (3.92') and (3.93') are now suitable for Chebchev quadrature. On noting that each integrand in (3.92') and (3.93') is on even function of y we may use an even number of evaluation points to obtain

$$F(x,k) = \frac{\sin^{-1} x}{n} \sum_{j=1}^{n} 1/M_j (x,k) + E_n(F) \tag{3.95}$$

and

$$E(x,k) = \frac{\sin^{-1} x}{n} \sum_{j=1}^{n} M_j (x,k) + E_n(E) \tag{3.96}$$

where

$$M_j(x,k) = \sqrt{1 - k^2 \sin^2\left[\frac{(2j - 1)}{2n} \sin^{-1} x\right]} \quad . \tag{3.97}$$

Proceeding similarly as in Section 3.3.3.3 we obtain

$$\sqrt{\frac{\sqrt{1-k^2}}{4ne}}\,\left|E_n(F)\right| \;,\; \left|E_n(E)\right| \leq 16\left[\frac{k}{1+\sqrt{1-k^2}}\right]^{4n} \quad , \quad (3.98)$$

bounds which are uniformly valid for all x in $-1 \leq x \leq 1$. For example when $k = 1/\sqrt{2}$ we have the bounds

n	$E_n(F)$	$E_n(E)$
5	2.7×10^{-6}	3.5×10^{-7}
6	2.6×10^{-8}	1.0×10^{-9}

We expect that the above method competes well with that described in Fair, W.G. and Y.L. Luke, (1967) or that described in National Bureau of Standards (1964).

3.3.4 Conclusion

(U) This section describes an analytic procedure for treating movable singularities in an integral. Some methods for treating fixed singularities in special quadrature schemes are known and are currently being developed (Fox, L., 1967, and the references therein), but ours is more general since it is independent of the quadrature scheme and since we do not require the singularities to be fixed.

(U) The examples given for evaluation of the integral (3.33) are not the only ones that we tried on a computer. For example, we also expanded F(x) in a power series and applied term-by-term integration using formulas given in Byrd, P.F. and M.D. Friedman (1954). We found that while these produced good results for k near 1 they were unstable for smaller values of k. Although effective methods for evaluating elliptic functions and integrals exist (we have in fact developed an effective method of evaluating elliptic integrals in Section 3.3.3.7) routines for evaluating these on a computer are not as

accessible as routines for evaluating elementary functions. Thus while the method of Section 3.3.3.5 produces very rapid convergence for intermediate and large k and while the method of Section 3.3.3.6 is effective for all k in $0 \leq k < 1$ we prefer the methods in Sections 3.3.3.3 and 3.3.3.4 since for these the evaluating of x(y) can be achieved more simply on a computer.

(U) The variety of transformations obtained for the integral (3.33) point to the non-uniqueness of our procedure. We believe this to be an asset, rather than a handicap.

3.4 Plasma Re-entry Sheath (Task 3.1.5)

3.4.1 Introduction

(U) One of the key problems in obtaining the nose-on or near nose-on incident, backscattered return from a plasma sheathed conical vehicle, is the determination of the return from the base. The plasma will partially or completely shield the base thus reducing its cross-section. Of the two types of bases rounded or flat-backed, the latter should be treated first for two reasons, (1) the flow fields around the base are better known, and (2) there are more dynamic re-entry backscattered measurements available for such vehicles.

(U) The choice of electromagnetic model for the plasma in the vicinity of the rear shoulder of the vehicle depends upon the flow fields. As pointed out by Weiss and Weinbaum (1966), there is a rapid expansion and separation of the hypersonic boundary layer at the rear shoulder of a blunt based re-entry body (see Fig. 3-17). In the outer portion of this expansion region (the free shear layer), the electrom density will rapidly decrease beyond the shoulder, whereas in the inner portion, and the recirculation region the electron density may be quite large. Due to the complexity of the problem, some simplified models should be treated first. For the direct backscattered return from the rear edge, the effect of the electron density in the recirculation region and the portion of the free inviscid layer adjacent to it, will play a

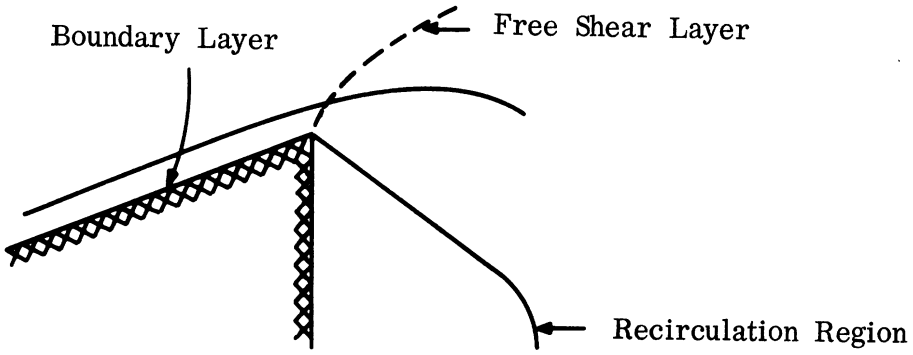

FIG. 3-17: HYPERSONIC BOUNDARY LAYER SEPARATION FOR FLAT-BACKED CONES.

minor role. Such regions are important when multiple scattering across the base is taken into account. In addition it will be assumed that the expansion will be sufficiently rapid in the remaining section of the free shear layer, so that the electron density becomes insignificant a short distance (compared to wavelength) back of the rear shoulder or edge. Thus a first order model of the sheath in the vicinity of the rear edge would be a finite conical slab as given in Fig. 3-18. The usefulness of such a model will depend mainly upon

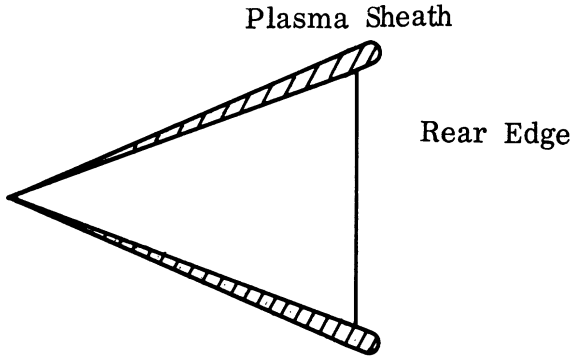

FIG. 3-18: FIRST ORDER MODEL OF SHEATH TO TAKE INTO ACCOUNT THE BACKSCATTERING FROM THE REAR EDGE.

the rate of expansion (or decrease in electron density) beyond the rear edge, compared to the incident wavelength. Thus, such a model is more useful at lower frequencies. The theoretical approach to the calculation of the back-scattered return from the rear of such a model falls in several degrees of approximation. The first crude approximation to the direct return from the base, is obtained by employing physical optics. Computations are being performed, using the physical optics technique combined with the local reflection coefficients calculated for a plasma sheathed pointed cone, and the results will be given in the final report.

(U) However since the physical optics technique will only give "ball-park" answers, more accurate techniques are required. A theoretical treatment is being carried out using the integral equation approach. The integral equation approaches has been applied to the non-homogeneous planar sheath, in order to yield physical insight into the physical approximations that can be applied to the more difficult cases. The results were presented in the Second Quarterly, and some additional results are given in the next section of this quarterly. The application of the integral equation to the rear edge is also given.

(U) To assist in the theoretical analysis for the base return, experimental measurements have been made for a finite cone coated with a simulated plasma sheath. The results are presented in the experimental section.

3.4.2 Integral Equation Approach

(U) In the last quarter, the integral equation approach was applied to the problems of reflection by a planar inhomogeneous sheath. It was found that a thin inhomogeneous sheath of permittivity $\epsilon(z)$, where z represents the distance normal to the surface, can be replaced by a homogeneous sheath with a "mean" relative permittivity ϵ_1. In the first polarization case treated,

electric polarization perpendicular to the plane of incidence, the mean permittivity ϵ_1 was obtained in the form

$$\epsilon_1 = (3/\delta^3) \int_0^\delta t^2 \, \epsilon(t) \, dt \, , \tag{3.99}$$

where δ denotes the thickness of the sheath. This represents a first approximation valid when $\left| \kappa_1 \delta \right| \ll 1$, where $\kappa_1^2 = k\left[\epsilon_1 - \sin^2\theta\right]$. The results derived for the other polarization case, however, are not in agreement with the above expression when normal incidence is considered. For this reason we have reconsidered the case where the incident electric field is polarized in the plane of incidence.

(U) We orient a Cartesian coordinate systems so that the positive z axis is normal to the sheath of thickness δ, with the $z = 0$ plane being the conducting surface. The angle of incidence is denoted by θ and the plane of incidence is the x - z plane.

(U) For electric polarization in the plane of incidence, the magnetic field has the general form

$$\underline{H} = \hat{y} \, e^{ikx \sin\theta} \, H(z) \, . \tag{3.100}$$

outside the slab ($z > \delta$), the field is comprised of the incident and reflected waves in which case H(z) has the explicit form

$$H(z) = \exp\left[-ikz\cos\theta\right] + R \exp\left[ik(z - 2\delta)\cos\theta\right] \, . \tag{3.101}$$

In the slab the function H(z) must satisfy the differential equation

$$\epsilon \frac{d}{dz}\left(\frac{1}{\epsilon}\frac{dH}{dz}\right) + k^2(\epsilon - \sin^2\theta) H = 0 \tag{3.102}$$

subject to the boundary condtions

$$\frac{dH}{dz} = 0 \text{ at } z = 0, \quad H, \quad \frac{1}{\epsilon}\frac{dH}{dz} \text{ continuous at } z = \delta \quad . \tag{3.103}$$

(U) In order to express Eq. (3.102) as an integral equation, we introduce a constant ϵ_1 and write the differential equation in the form

$$\frac{d^2H}{dz^2} + \kappa_1^2 H = -\frac{d}{dz}\left[(\epsilon_1 - \epsilon)\left(\frac{1}{\epsilon}\frac{dH}{dz}\right)\right] + k^2 \sin^2\theta \, \frac{\epsilon_1 - \epsilon}{\epsilon} H, \tag{3.104}$$

where

$$\kappa_1^2 = k^2(\epsilon_1 - \sin^2\theta) \quad . \tag{3.105}$$

The following integral equations satisfying the required boundary condition at $z = 0$ may now be obtained in the form

$$H(z) = H_o \cos\kappa_1 z - \int_0^z \frac{\epsilon_1 - \epsilon(t)}{\epsilon(t)} \left\{ \cos\kappa_1 (z - t) \frac{dH(t)}{dt} - \frac{k^2 \sin^2\theta}{\kappa_1} \sin\kappa_1 (z - t) H(t) \right\} dt \quad , \tag{3.106}$$

$$\frac{1}{\epsilon(z)}\frac{dH(z)}{dz} = -\frac{H_o \kappa_1}{\epsilon_1}\sin\kappa_1 z + \frac{\kappa_1}{\epsilon_1}\int_0^z \frac{\epsilon_1 - \epsilon(t)}{\epsilon(t)} \left\{ \sin\kappa_1 (z - t)\frac{dH(t)}{dt} + \frac{k^2 \sin^2\theta}{\kappa_1} \cos\kappa_1 (z - t) H(t) \right\} dt \quad . \tag{3.107}$$

The continuity conditions at $z = \delta$ yield two equations involving the two unknown quantities H_o and R :

$$H_o \cos \kappa_1 \delta - \int_0^\delta \frac{\epsilon_1 - \epsilon}{\epsilon} \left\{ \cos \kappa_1 (\delta - t) \frac{dH}{dt} - \frac{k^2 \sin^2 \theta}{\kappa_1} \sin \kappa_1 (\delta - t) H \right\} dt = e^{-ik\delta \cos\theta} \left[1 + R\right]$$

$$- \frac{H_o \kappa_1}{\epsilon_1} \sin \kappa_1 \delta + \frac{\kappa_1}{\epsilon_1} \int_0^\delta \frac{\epsilon_1 - \epsilon}{\epsilon} \left\{ \sin \kappa_1 (\delta - t) \frac{dH}{dt} + \frac{k^2 \sin^2 \theta}{\kappa_1} \cos \kappa_1 (\delta - t) H \right\} dt = e^{-ik\delta \cos\theta} \left[1 + R\right] ik \cos\theta \, .$$

By eliminating H_o we obtain the following expression involving R:

$$- \int_0^\delta \frac{\epsilon_1 - \epsilon}{\epsilon} \left\{ \kappa_1 \sin (\kappa_1 t) \frac{dH}{dt} - k^2 \sin^2 \theta \cos (\kappa_1 t) \right\} dt \, e^{ik\delta \cos\theta}$$

$$= \left[\kappa_1 \sin \kappa_1 \delta - ik \cos\theta \, \epsilon_1 \cos \kappa_1 \delta \right]$$

$$+ R \left[\kappa_1 \sin \kappa_1 \delta + ik \cos\theta \, \epsilon_1 \cos \kappa_1 \delta \right] \, . \qquad (3.108)$$

(U) The constant permittivity ϵ_1 will be chosen so that the reflection coefficient associated with a uniform slab of thickness δ and permittivity ϵ_1 will be the same as the reflection coefficient given by Eq. (3.108) for the nonuniform case. In the uniform case the reflection coefficient is given by Eq. (3.108) with the left-hand side equal to zero; thus, the mean permittivity ϵ_1 is prescribed by the equation

$$\int_0^{\delta} \frac{\epsilon_1 - \epsilon}{\epsilon} \left\{ \kappa_1 \sin(\kappa_1 t) \frac{dH}{dt} - k^2 \sin^2\theta \cos(\kappa_1 t) H \right\} dt = 0 \quad , \qquad (3.109)$$

where the functions dH(t)/dt and H(t) may be found by iterating Eq. (3.106) and (3.107). The value of ϵ_1 is thus determined by a transcendental equation.

(U) A simple solution can be obtained for sheaths thin enough that $|\kappa_1 \delta| << 1$. We further assume

$$\left| \frac{\sin^2\theta}{\delta} \int_0^{\delta} \frac{dt}{\epsilon(t)} \right| << 1 \ ,$$

then we have approximately (with $H_o = 1$) $H(z) \sim 1$, $\frac{1}{\epsilon(z)} \frac{dH(z)}{dz} \sim -k^2 z$. On applying this approximation to Eq. (3.109) we obtain the relation

$$(\epsilon_1 - \sin^2\theta) \left[\epsilon_1 (\delta^3/3) - \int_0^{\delta} \epsilon(t)\, t^2\, dt \right]$$

$$= \frac{\sin^2\theta}{k^2} \left[\delta - \epsilon_1 \int_0^{\delta} \frac{dt}{\epsilon(t)} \right] \quad , \qquad (3.110)$$

which is a quadratic equation for ϵ_1 except in the case of normal incidence ($\theta = 0$). For normal incidence the result presented in Eq. (3.99) for the other polarization case is recovered. Unlike the other polarization case, however, the first approximation to ϵ_1 given immediately above is dependent upon the angle of incidence.

(U) It is interesting to consider the case where $\epsilon(z)$ is a constant; then Eq. (3.110) may be written in the form

$$(\epsilon_1 - \epsilon)\left[\frac{k^2\delta^2}{3}(\epsilon_1 - \sin^2\theta) + \frac{\sin^2\theta}{\epsilon}\right] = 0 \quad . \qquad (3.111)$$

The exact condition that two different uniform layers have the same reflection coefficient can be written as

$$\frac{\epsilon_1}{\kappa_1}\cot\kappa_1\delta = \epsilon/\kappa \cot\kappa\delta \ , \qquad (3.112)$$

which for thin layers becomes

$$\frac{\epsilon_1}{\kappa_1^2}\left[1 - \frac{\kappa_1^2\delta^2}{3}\right] = \epsilon/\kappa^2\left[1 - \frac{\kappa^2\delta^2}{3}\right] \quad .$$

This last equation may be presented in the form

$$(\epsilon_1 - \epsilon)\left[\frac{\kappa_1^2\delta^2}{3} + \frac{k^2\sin^2\theta}{\kappa^2}\right] = 0$$

and since, for $|\epsilon| >> \sin^2\theta$ we have $\kappa^2 \sim k^2\epsilon$, it is clear that Eq. (3.111) is obtainable from the exact relation in Eq. (3.112) under the conditions we have assumed. The consistency of Eq. (3.110) is thus illustrated by the uniform layer case.

(U) Some numerical results have been calculated. Let us consider the simpler polarization case, electric vector polarized perpendicular to the plane of incidence, in which case it was shown that the effective dielectric constant ϵ_1 is given by

$$\epsilon_1 = 3/\delta^3 \int_0^\delta t^2\,\epsilon(t)\,dt \qquad (3.113)$$

provided $|\kappa_1\delta| << 1$. We will evaluate ϵ_1 for a specific permittivity

$$\epsilon(z) = 1 + (i\nu - \omega)\, A\, e^{-b\,z} \tag{3.114}$$

where ν, ω, A and b are positive constants, and investigate the validity criterion $|\kappa_1 \delta| << 1$. Evaluating Eq. (3.113) for the permittivity in Eq. (3.114) we find

$$\epsilon_1 = 1 + \left[1 - \epsilon(\delta)\right] \gamma(\phi) \tag{3.115}$$

where

$$\phi = b\,\delta \quad , \quad \gamma(\phi) = (3/\phi^3)\left[\phi^2 + 2(\phi + 1 - e^{\phi}\right] \; . \tag{3.116}$$

Using this expression for ϵ_1 in the formula for κ_1, one can show that $|\kappa_1 \delta| << 1$ may be written in the form

$$\kappa\,\delta\left\{(A\gamma\omega)^2\left[(\nu/\omega)^2 + 1\right]e^{-2\phi} + 2\,(A\gamma\omega)\cos^2\theta\, e^{-\phi} + \cos^4\theta\right\}^{1/4} << 1. \tag{3.117}$$

Hence, if $(\nu/\omega)^2 << 1$, then Eq. (3.117) reduces to

$$\kappa\,\delta\left\{\left|A\gamma\omega\, e^{-\phi} + \cos^2\theta\right|\right\}^{1/2} << 1 \; . \tag{3.118}$$

It should be noted that $\gamma(\phi) < 0$ for all $\phi > 0$.

(U) The expression in (3.113) is derived under the assumption that $E(z) \sim \kappa_1 z$; however, it is useful to investigate the effect of the error term. We find by including a higher order iteration

$$E(\delta) \sim \kappa_1 \delta\left\{1 + k^2 \int_0^{\delta} \epsilon(t)\left[(3t/2\delta) - 1\right] t\, dt\right\} + O(\kappa_1\delta)^2 \; . \tag{3.119}$$

Hence, in addition to the criterion that $|\kappa_1 \delta| << 1$, one must also have

$$\left| k^2 \int_0^{\delta} \epsilon(t) \left[(3t/2\delta) - 1 \right] t \, dt \right| << 1 \, . \tag{3.120}$$

For the permittivity in Eq. (3.115) this inequality may be written as

$$(\kappa \delta)^2 \, | \lambda (\phi) | \, A \omega \sqrt{1 - (\nu/\omega)^2} << 1 \tag{3.121}$$

where

$$\lambda (\phi) = \left[(\phi^2 + 4\phi + 6) \, e^{-\phi} + 2(\phi - 3) \right] \Big/ 2\phi^3 \tag{3.122}$$

and if $(\nu/\omega)^2 << 1$, then Eq. (3.121) becomes

$$(\kappa \delta)^2 \, A \omega \, | \lambda (\phi) | << 1 \quad . \tag{3.123}$$

(U) In the following table III-5 some numbers have been calculated. It has been assumed that $\nu << \omega$ and that $\omega = 10^8$ rad/sec, $A = 10^{-6}$ sec.; the δ is computed for several values of ϕ from Eqs. (3.118) and (3.123).

TABLE III-5

ϕ	Equation (3.118)	Equation (3.123)
1	$\delta << .4$	$\delta^2 << .7$
10	$\delta << \dfrac{3}{\sqrt{\left\lvert \cos^2 \theta - .6 \right\rvert}}$	$\delta^2 << 14$
100	$\delta << \dfrac{3}{\sqrt{\left\lvert \cos^2 \theta - 6 \cdot 10^{-4} \right\rvert}}$	$\delta^2 << 10^3$

3.4.3 Integral Equation Applied to the Base Return

(U) In obtaining the backscattered return from the base, the plasma model indicated in the introduction will be employed. The principal of local analysis will then be used, wherein, the local region of the rear edge will be approximated by a coated wedge. With this reduction to the local two dimensional geometry as shown in Fig. 3-19, the fundamental problem reduces to the obtaining of the backscattered field from the coated edge.

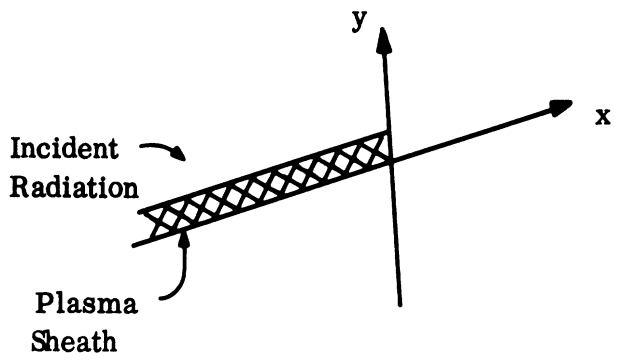

FIG. 3-19: LOCAL WEDGE GEOMETRY.

(U) The integral equation approach to this, is briefly described as follows for the case of polarization parallel to the wedge.

(U) With the z-axis taken along the edge, and the y axis normal to plasma coated surface, the incident electric intensity will have the form

$$E^i = \underline{z} \exp ik(x \cos\theta - y \sin\theta)$$

and the total (scattered plus incident) electric intensity will have the form

$$\underline{E} = \psi(x, y)\, \underline{z}$$

where ψ must vanish on the conducting surface of the body. Employing the Green's function G, which vanishes on the conducting wedge, and which satisfies the differential equation.

$$\nabla^2 G + k^2 G = -4\pi\, \delta(x - x_o)\, \delta(y - y_o)$$

the following integral equation may be developed for ψ,

$$\psi(\underline{x}_o) = \psi^o(\underline{x}_o) + \frac{1}{4\pi} \int_A k^2(\epsilon - 1)\psi(\underline{x}) G(\underline{x}, x_o)\, d\underline{x} .$$

In this expression $\epsilon(x, y)$ is the relative dielectric constant of the plasma sheath (denoted by the domain of integration A), and ψ^o is the total field generated by the incident wave on the bare conducting body. Expressions for both ψ^o and G can be found in Oberhettinger (1954).

(U) In the analysis, the variation of ϵ with regard to x will be ignored (assumed very slowly varying) in which case $\epsilon \sim \epsilon(y)$. Thin plasmas will be treated where the concept of thin plasmas is given by the relations

$$|\kappa\, \delta| < 1 , \qquad \kappa^2 = k^2 \left[3/\delta^3 \int_0^\delta t^2 \epsilon(t)\, dt - \sin^2 \theta \right] .$$

where δ is the thickness of the plasma. It was pointed out in the Second Quarterly that thin non-homogeneous plasma slabs could be replaced by a homogeneous slab of relative dielectric constant,

$$\epsilon_1 = 3\, \delta^{-3} \int_0^\delta t^2\, \epsilon(t)\, dt ,$$

under the action of incident plane waves. This was based upon the approximation, that the total electric field in the slab behaved linearly i.e.; $\psi \sim yg(x)$. Thus the best approach for the thin plasma sheath on the wedge, is to assume that

$$\psi(\underline{x}) = y\, \psi_1(x) + y^2\, \psi_2(x) + \ldots$$

such that a distance several wavelengths away from the edge ($|kx| > 1$), the dominant behavior corresponds to that of an infinite slab, i.e., $\psi(\underline{x}) \sim y\psi_1(\underline{x})$. With such an approximation, the solutions of the integral equation is to be sought, where in particular the values of $\psi(\underline{x})$ and $\frac{\partial \psi}{\partial n}$ on the surface of the slab are required. At a short distance away from the edge the following impedance boundary condition should be obtainable $\partial \psi / \partial n = \eta \psi$ where η is a constant. Thus the integral equation approach can be used to establish the approximation of thin plasma sheaths by an impedance boundary condition and the errors in such an approximation. The backscattered return for the impedance wedge is immediately obtainable from well-known solutions. The backscattered return from the plasma sheathed cone using the impedance wedge approximation, will be presented in the final report.

IV

TASK 4.0: SHORT PULSE INVESTIGATION

4.1 Introduction

(U) All aspects of the problem discussed in the previous Quarterly Report (Goodrich et al, 1967b) were continued. The new work is described under the same section headings as in the previous report. In addition investigation of short pulse returns from cone-sphere and flat-backed cones viewed nose-on were begun. These results are reported in Section 4.5 and 4.6.

4.2 Ray Optical Techniques

(U) In Goodrich et al, (1967b) a ray optical method was discussed as one technique whereby the transient scattered field due to a short pulse incident upon a scattering body could be obtained. In that report the procedure for computing the reflected field was outlined in detail. The procedure for computing the diffracted field was considered by using a frequency domain analysis and then applying a Tauberian theorem to obtain the time domain solution for a short time interval behind the pulse front. Since the last Quarterly Report work has been done on the development of a purely time domain analysis which could be used to compute the diffracted field.

(U) With the knowledge that the total field at all points is necessarily described by an analytic function of the variables in space and time we may write the functional form of the field as:

$$\bar{E}(\bar{r}, t) = \sum_{n=0}^{\infty} \frac{\bar{A}_n(\bar{r})}{n!} (t - \psi/c)^n \qquad (4.1)$$

where ψ is a surface in space on which the field is discontinuous and which must satisfy the eikonal $(\nabla\psi)^2 = 1$. The $A_n(\bar{r})$ are the discontinuities in the n'th derivatives across this surface. The $A_n(\bar{r})$ must satisfy a transport-recurrence relation:

$$2\,(\nabla\psi \cdot \nabla)\,\bar{A}_n(r) + \nabla^2\psi\,\bar{A}_n(r) = c\,\nabla^2\,\bar{A}_{n-1}(r) \qquad (4.2)$$

where $n = 0, 1, 2, \ldots$ and $A_{-1} = 0$.

(U) For the free space portions (①, ③) of the diffracted rays shown in Fig. 4-1 the procedure for evaluating the transport of the coefficients is straightforward sine the ψ, $\nabla\psi$ and $\nabla^2\psi$ are known well behaved functions.

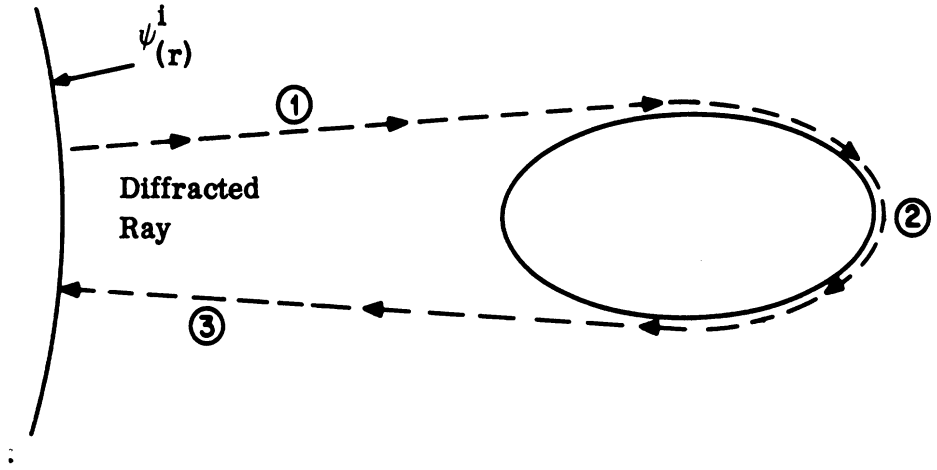

FIG. 4-1: TYPICAL DIFFRACTED RAY.

For the surface portion ② of the diffracted ray the coefficients $A_n(r)$ must satisfy the boundary conditions at the surface as well as the transport equation. A problem now presents itself in that $\nabla^2\psi$ approaches infinity on the obstacle surface. This is true if the equation of the pulse front is computed assuming that each element of the front (ψ = constant) moves with the same speed. If we consider a right circular cylinder $\nabla^2\psi$ has the form:

$$\nabla^2\psi = \frac{1}{\sqrt{r^2 - a^2}} \qquad (4.3)$$

where a is the radius of the cylinder. This singularity may be removed from

from the transport equation for n = 1, 2, . . . by writing it in the form

$$2\bar{A}_{n-1}\,(\nabla\psi\cdot\nabla)\,\bar{A}_n - \bar{A}_n\Big[2\,(\nabla\psi\cdot\nabla)\,A_{n-1} - C\,\nabla^2 A_{n-2}\Big] = C\,A_{n-1}\,\nabla^2 A_{n-1} \quad . \tag{4.4}$$

To evaluate the transport of A we must use the original equation and the problem still remains. If we remove the assumption that all elements of the ψ = constant surface travel with constant speed this problem may be alleviated. The correct situation as regards the motion of the ψ = constant surfaces can be ascertained from the CW high frequency surfaces of constant phase, but we do not see how to determine this a priori in the time domain.

(U) A second problem which remains before the method can be applied is to find out how to make the transitions between regions ① and ② and between ② and ③ . In region ① the expression for the field is known

$$\bar{E}^i(\bar{r},t) = \sum_{n=0}^{\infty} \frac{\bar{A}^i_n(\bar{r})}{n!}\,(t - \frac{\psi^i}{c})^n = \sum_{p=1} \bar{E}^i_p(r,t) \quad . \tag{4.5}$$

Let us suppose there exists a time dependent diffraction factor $D^1_{qp}(t)$ in the form of a tensor such that the surface field at the point $\tau = 0$ on the surface ray is given by the convolution:

$$\bar{E}^c_q(r,t) = \int_0^{\infty} D^1_{qp}(t - t')\,\bar{E}^i_p(t')\,dt' \tag{4.6}$$

where the superscript c denotes the surface field. This leads to the fact that:

$$A^{c}_{nq}(\bar{r}_0) = \left(t - \frac{\psi(r_o)}{c}\right)^{-n} \left[\int_0^{\infty} D^{1}_{pq}(t - t') \left(t' - \frac{\psi(r_o)}{c}\right)^{n} dt'\right] A^{i}_{pn}(\bar{r}_o) \qquad (4.7)$$

where $\psi(\bar{r}_o) = \psi^{i}(\bar{r}_o) = \psi^{i}(\bar{r}_o)$.

(U) A single factor $D^{2}_{r\ell}(t)$ can be defined for the process of re-radiation of energy in the backscatter direction. A method for determining exactly the $D^{1}_{r\ell}(t)$ and $D^{2}_{r\ell}(t)$ has yet to be discovered. If the range of the spectral function of the incident pulse only extends over large values of ω then the inverse transforms of Keller's geometrical diffraction coefficients will provide an adequate approximation to these factors.

4.3 Integral Equation Formulation of Time Dependent Scattering Problems.

(U) In Goodrich et al, (1967b) some background material for setting up an integral equation for the scalar potential in a scattering problem was presented. This has not been pursued further since we are really interested in the vector case. We therefore present below, first, the CW; i.e. frequency domain integral equations (3.8) and then the time domain equations obtained by taking Fourier transforms. The numerical integration of the CW equation is being studied on this contract (task 3.1.3) and elsewhere as well. The integration involves large matrix inversions if the scattering body has dimensions large compared to λ as well as other difficulties. It appears that, by working in the time domain, the matrix inversion can be avoided, although probably other complications will arise. The scalar version of this problem has been attacked with some success by Soules and Mitzner (1966). There does not appear to be any fundamental reason why their approach, suitably modified, cannot be used in the vector case. It is a problem worthwhile investigating but is certainly too long term to be brought to fruition during the remaining life of this contract.

(U) We derive an integral expression for the electromagnetic field scattered by a smooth finite closed three diminsional scatterer when irradiated by a linearly polarized pulse of arbitrary form.

(U) A linearly polarized plane incident pulse of arbitrary form and length T is represented by

$$\vec{\mathcal{E}}^i = \hat{a}\,\mathcal{F}^i\left(t - \frac{\hat{\alpha}\cdot\vec{r}}{c}\right), \quad \left|t - \frac{\hat{\alpha}\cdot\vec{r}}{c}\right| \leq T/2$$
$$= 0, \quad \left|t - \frac{\hat{\alpha}\cdot\vec{r}}{c}\right| > T/2 \tag{4.8}$$

where $\mathcal{F}^i$ is an arbitrary function of one real variable, $\hat{a}$ is a constant unit vector in the direction of the electric field, $\hat{\alpha}$ is a constant vector in the direction of propagation, $\vec{r}$ is the position vector of any point in space and c is the velocity of propagation.

(U) The free space time dependent Maxwell equations are

$$\text{curl}\,\vec{\mathcal{E}} = -\mu\,\frac{\partial\vec{\mathcal{H}}}{\partial t}$$
$$\text{curl}\,\vec{\mathcal{H}} = \epsilon\,\frac{\partial\vec{\mathcal{E}}}{\partial t} \tag{4.9}$$

from which we may deduce (assuming no time independent terms)

$$\vec{\mathcal{H}}^i = \frac{\hat{\alpha}\times\hat{a}}{\mu c}\,\mathcal{F}^i\left(t - \frac{\hat{\alpha}\cdot\vec{r}}{c}\right). \tag{4.10}$$

The scattering surface will be denoted by B and $\hat{n}$ is a unit normal from B to the exterior volume. We fix the origin of a Cartesian coordinate system in the interior of B. The geometry is illustrated in Fig. 4-2

(U) To find a representation of the scattered field we make use of an integral representation derived in the Second Quarterly (Goodrich et al, 1967b)

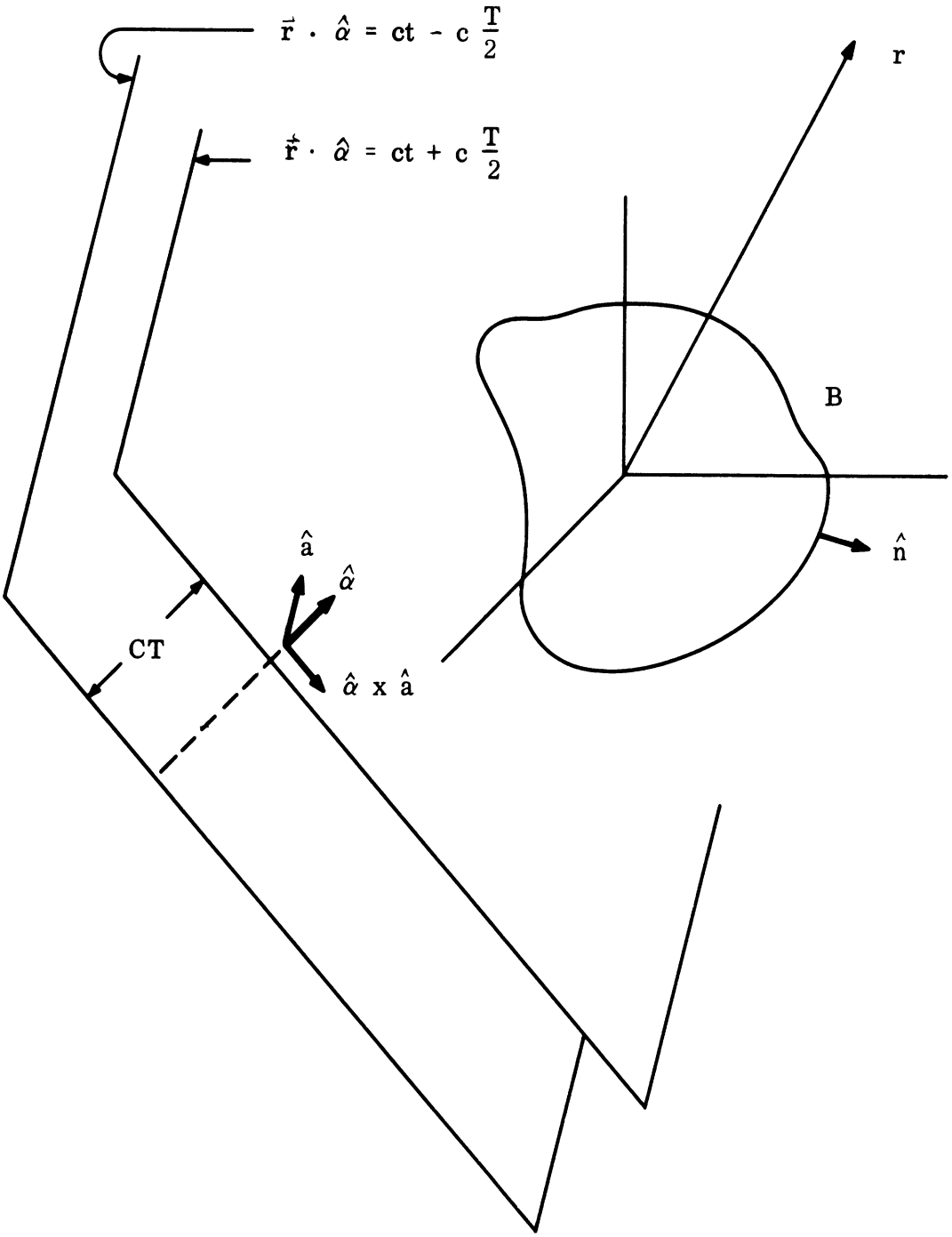

FIG. 4-2: GEOMETRY OF SCATTERER AND INCIDENT PULSE.

$$\mathcal{E}^s(t) = \int_{-\infty}^{\infty} \bar{E}^s(\omega)\, F^i(\omega)\, e^{-i\omega t}\, d\omega$$

$$\mathcal{H}^s(t) = \int_{-\infty}^{\infty} \bar{H}^s(\omega)\, F^i(\omega)\, e^{-i\omega t}\, d\omega \qquad (4.11)$$

where $\bar{E}^s(\omega)e^{-i\omega t}$ and $\bar{H}^s(\omega)e^{-i\omega t}$ are the scattered fields due to an incident time harmonic plane wave of the form $\bar{E}^i e^{-i\omega t} = \hat{a}e^{i\omega(\hat{\alpha}\cdot\hat{r}/c)}e^{-i\omega t}$, $\bar{H}^i e^{-i\omega t} = \frac{\hat{\alpha}\times\hat{a}}{\mu c} e^{i\omega(\hat{\alpha}\cdot\hat{r}/c)} e - i\omega t$ and $F^i(\omega)$ is the spectral function of the incident pulse evaluated at r = 0.

$$F^i(\omega) = \frac{1}{2\pi}\int_{-\infty}^{\infty} \mathcal{F}^i(\tau)\, e^{i\omega\tau}\, d\tau$$

$$\mathcal{F}^i(\tau) = \int_{-\infty}^{\infty} F^i(\omega)\, e^{-i\omega\tau}\, d\omega \quad . \qquad (4.12)$$

In our case $\tau = t - (\hat{\alpha}\cdot\hat{r})/c$, thus $\mathcal{F}^i$, $\bar{E}^s$, $\bar{H}^s$, $\vec{\mathcal{E}}^s$ and $\vec{\mathcal{H}}^s$ will in general be functions of position where as $F^i(\omega)$ will not. The expressions for the time harmonic scattered field may be expressed in integral form as follows. Start with Stratton (1941)*, for the field at a point P in terms of its values on a surface S enclosing V.

$$\frac{1}{4\pi}\int_S \left[i\omega\mu\,(\hat{n}\times\bar{H})\phi + (\hat{n}\times\bar{E})\times\nabla\phi + (\hat{n}\cdot\bar{E})\nabla\phi \right] da$$

$$= \begin{cases} \bar{E}(P) & \text{for P in V} \\ 0 & \text{for P not in V or on S} \end{cases} \qquad (4.13)$$

* Section 8.14 Eq. (22) and the text of 8.14 following the equation.

Here $\phi = e^{ikR}/R$ where R is the distance between P and an arbitrary point on the boundary, $\hat{n}$ is a unit outward normal to S. Taking the curl of (4.13) with respect to point P gives, via Maxwell's equation curl $\vec{E} = i\omega\mu\vec{H}$

$$\frac{-1}{4\pi}\ \text{curl}\int \phi\,(\hat{n}\times\bar{H})\,da + \frac{i}{4\pi\,\omega\mu}\ \text{curl curl}\int \phi\,(\hat{n}\times\bar{E})\,da$$

$$= \begin{cases} \bar{H}(P), & \text{for P in V} \\ 0\ , & \text{for P not in V or on S.} \end{cases} \qquad (4.14)$$

(U) To obtain an expression for fields scattered by a surface S_o one uses the fact that such fields satisfy the radiation condition

$$\lim_{r\to\infty}\left[\bar{r}\times\text{curl}\ \bar{E} + ik\,r\,\bar{E}\right] = 0 \qquad (4.15)$$

The Eqs. (4.13) and (4.14) are applied to a volume included between two surfaces B and $S_{R\,\infty}$, the latter being a large sphere enclosing B whose radius R_∞ will be permitted to tend toward infinity. From (4.13) one has

$$\bar{E}^s \simeq \int_B - \frac{1}{4\pi}\int_{S_{R\,\infty}} d\,\Omega\, e^{ik(r\,-\,\hat{r}\,\cdot\,\bar{r}_o)}$$

$$\left[\bar{r}\times\text{curl}\ \bar{E}^s + ik\,r\,\bar{E}^s\right], \qquad (4.16)$$

where $d\,\Omega$ is an element of solid angle. In the limit $R\,\infty \to \infty$ the integral over $S_{R\,\infty} = 0$.

(U) Thus for a wave scattered from a surface B bounding volume V

$$\bar{H}^S(P) = \frac{1}{4\pi} \text{ curl } \int_B \phi\, (\hat{n} \times \bar{H}^S)\, da - \frac{i}{4\pi\, \omega\, \mu}$$

$$\text{curl curl } \int_B \phi\, (\hat{n} \times \bar{E}^S)\, da \quad , P \text{ not in V or on B} \qquad (4.17)$$

where now $\hat{n}$ represents the outward normal to the volume enclosed by S_o which accounts for the sing change from (4.14).

(U) To obtain an expression for the total fields ($\vec{H}$, $\vec{E}$) which are the fields to which the boundary conditions are applicable, one takes into account the fact that incident field is a plane wave. Since a plane wave does not satisfy the radiation condition, one cannot use (4.17). However, the interior formula (4.14) can be applied to $\vec{H}^{inc}$. For a point exterior to B (4.14) gives

$$0 = \frac{1}{4\pi} \text{ curl } \int_B \phi\, (\hat{n} \times \bar{H}^{inc})\, da - \frac{i}{4\pi\, \omega\mu} \text{ curl curl } \int_B \phi (\hat{n} \times \bar{E}^{inc})\, da \qquad (4.18)$$

Adding (4.17) and (4.18) yields the desired result

$$H^S(P) = \frac{1}{4\pi} \text{ curl } \int_B \phi\, (\hat{n} \times \bar{H})\, da - \frac{i}{4\pi\, \omega\mu}$$

$$\text{curl curl } \int_B \phi\, (\hat{n} \times \bar{E})\, da \qquad (4.19)$$

If B is a perfectly conducting surface, $\hat{n} \times \bar{E} = 0$. Then

$$H^s = \frac{1}{4\pi} \text{ curl } \int_B \phi \, (\hat{n} \times \bar{H}) \, da \tag{4.20}$$

and by Maxwell's equation curl $\bar{H} = -i\epsilon\omega\bar{E}$

$$E^s = \frac{i}{4\pi\epsilon\omega} \text{ curl curl } \int_B \phi \, (\hat{n} \times \bar{H}) \, da \quad . \tag{4.21}$$

We repeat that in (4.20) and (4.21) the $\bar{H}$ under the integral sign is total $\bar{H}$ field.

(U) Substituting these expressions in (4.12) yields

$$\bar{\mathcal{E}}^s(\vec{r}, t) = \int_{-\infty}^{\infty} F^i(\omega) e^{-i\omega t} \frac{i}{\epsilon\omega} \text{ curl curl } \int_B \frac{e^{\frac{i\omega R}{c}}}{4\pi R} \hat{n}$$

$$\times \left[\vec{H}^i (\vec{r}_B, \omega) + \vec{H}^s (\vec{r}_B, \omega) \right] da \, d\omega \tag{4.22}$$

$$\bar{\mathcal{H}}^s(\vec{r}, t) = \int_{-\infty}^{\infty} F^i(\omega) \, e^{-i\omega t} \text{ curl } \int_B \frac{e^{i\frac{\omega}{c}R}}{4\pi R} \hat{n}$$

$$\times \left[\vec{H}^i (\vec{r}_B, \omega) + \vec{H}^s (\vec{r}_B, \omega) \right] da \, d\omega$$

where $\vec{r}_B$ is a point on B. Provided we may invert the order of s integration, which should be rigorously established, we obtain

$$\bar{\mathcal{E}}^s(\vec{r},\, t) = \frac{i}{\epsilon}\, \text{curl curl} \int_B \frac{\hat{n}}{4\pi R} \times \left\{ \int_{-\infty}^{\infty} F^i(\omega)\, \frac{e^{-i\omega t + (i\omega R/c)}}{\omega} \right.$$

$$\left. \times \left[\vec{H}^i(\vec{r}_B,\, \omega) + \vec{H}^s(\vec{r}_B,\, \omega) \right] d\omega \right\} dB \qquad (4.23)$$

$$\bar{\mathcal{H}}^s(r,\, t) = \text{curl} \int_B \frac{\hat{n}}{4\pi R} \times \left\{ \int_{-\infty}^{\infty} F^i(\omega)\, e^{-i\omega t + i\frac{\omega R}{c}} \right.$$

$$\left. \times \left[\vec{H}^i(\vec{r}_B,\, \omega) + \vec{H}^s(\vec{r}_B,\, \omega) \right] d\omega \right\} dB \quad .$$

Restricting our attention to the magnetic field we see that since

$$\vec{H}^i(\vec{r}_B,\, \omega) = \frac{\hat{\alpha} \times \hat{a}}{\mu c}\, e^{i\omega \frac{\hat{\alpha} \cdot \vec{r}_B}{c}} \qquad (4.24)$$

the term

$$\int_{-\infty}^{\infty} F^i(\omega)\, e^{-i\omega t + i\frac{\omega R}{c}}\, \vec{H}^i(\vec{r}_B,\, \omega)\, d\omega$$

$$= \frac{\hat{\alpha} \times \hat{a}}{\mu c} \int_{-\infty}^{\infty} F^i(\omega)\, e^{-i\omega\left(t - \frac{R}{c} - \frac{\hat{\alpha} \cdot \vec{r}_B}{c}\right)}\, d\omega$$

$$= \frac{\hat{\alpha} \times \hat{a}}{\mu c}\, \mathcal{F}^i\left(t - \frac{R}{c} - \frac{\hat{\alpha} \cdot \vec{r}_B}{c}\right) \qquad (4.25)$$

This follows from (4.12). Also from (4.11) we see that

$$\int_{-\infty}^{\infty} F^i(\omega)\, e^{-i\omega t + \frac{i\omega R}{c}}\, \vec{H}^s(\vec{r}_B, \omega)\, d\omega = \vec{\mathcal{H}}^s(\vec{r}_B, t - \frac{R}{c}) \qquad (4.26)$$

Thus

$$\vec{\mathcal{H}}^s(\vec{r}, t) = \nabla \times \int_B \frac{\hat{n}}{\mu c 4\pi R} \times (\hat{\alpha} \times \hat{a})\, \mathcal{F}^i(t - \frac{R}{c} - \frac{\hat{\alpha} \cdot \vec{r}_B}{c})\, da$$

$$+ \nabla \times \int_B \frac{\hat{n}}{4\pi R} \times \vec{\mathcal{H}}^s(\vec{r}_B, t - \frac{R}{c})\, d \qquad (4.27)$$

This is the desired integral equation giving $\vec{\mathcal{H}}^s(r, t)$ in terms of its retarded values on the surface and that of the incident field. It is expected that it can be solved by a timewise iterative procedure. As mentioned in the opening paragraph it certainly can be treated analogous to the scalar problem which has been worked through numerically for a spherical obstacle by Soules and Mitzner (1966).

4.4 Pulse Scattering from a Perfectly Conducting Sphere.

(U) Some computation of the return for a rectangular pulsed CW carrier were carried out numerically, essentially as reported in the previous Quarterly Report but with the effect of an added bandwidth limitation on reception taken into account. This was done by limiting the frequency range in the inverse Fourier transform of the weighted CW response. These isolated results are not of much use in themselves, but will be included with further ones (to be carried out in the next quarter) in the Final Report.

4.5 Pulse Scattering from a Perfectly Conducting Cone-sphere.

(U) It was decided to more or less repeat the type of calculations given in Section 4.4 for the body consisting of a finite cone with spherical base joined on in such a way that the slope is continuous

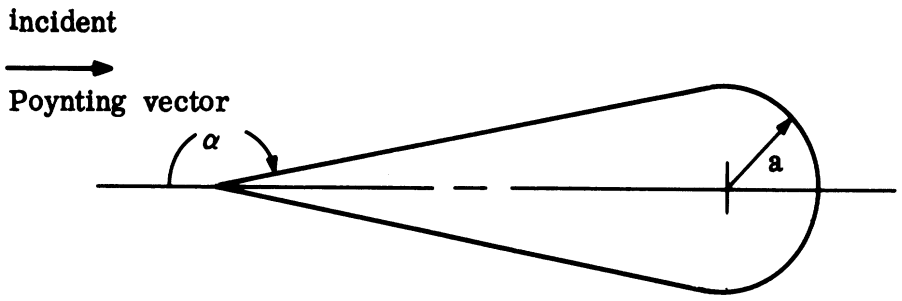

Cone - Sphere

(U) We are considering backscattering from a cone-sphere irradiated nose-on by a pulse

$$f^i(r, t) = \hat{x} \cos \omega_o t \qquad |t| \leq T/2$$
$$= 0 \qquad |t| > T/2 \tag{4.28}$$

which in the frequency domain corresponds to

$$\bar{F}^i(\omega) = \hat{x} \frac{T}{4\pi} \left\{ \frac{\sin (\omega + \omega_o) \frac{T}{2}}{(\omega + \omega_o) \frac{T}{2}} + \frac{\sin (\omega - \omega_o) \frac{T}{2}}{(\omega - \omega_o) \frac{T}{2}} \right\} \tag{4.29}$$

(U) To compute the scattered field we will assume a linear time invariant system so that in the frequency domain, the response to (4.29) will be

$$\vec{F}^{S}(r, \omega) = F^{i}(\omega)\, \vec{E}^{S}(r, \omega)$$

where $E^{S}(r, \omega)$ is the impulse responce, and is given by Senior (1965) as

$$\vec{E}^{S}(r, \omega) = \hat{x}\, \frac{e^{ikr}}{kr}\, S \tag{4.30}$$

and S is the scattering amplitude. Using the inverse Fourier transform, we can write

$$\vec{f}^{S}(\vec{r}, t) = \hat{x} \int_{-\infty}^{\infty} F^{i}(\omega)\, \vec{E}^{S}(r, \omega)\, e^{-i\omega t}\, d\omega \tag{4.31a}$$

$$= \hat{x}\, \frac{cT}{4\pi r} \int_{-\infty}^{\infty} \left\{ \frac{\sin(\omega + \omega_o)\frac{T}{2}}{(\omega + \omega_o)\frac{T}{2}} + \right.$$

$$\left. + \frac{\sin(\omega - \omega_o)\frac{T}{2}}{(\omega - \omega_o)\frac{T}{2}} \right\} \frac{e^{i\omega\left(\frac{r}{c} - t\right)}}{\omega}\, S\, d\omega \tag{4.31b}$$

Since the integral is to be carried out overall frequencies we have to specify the ranges for which S is a good approximation, and also justify the use of negative frequencies.

(U) The frequency spectrum will be divided in three regions, high, medium and low.

High Frequency Range (ka large)

(U) For high frequencies, the creeping wave contributes nothing and S can be approximated as

$$S \sim \frac{i}{4}\, \sec^{2}\alpha\, e^{-2ika \sin\alpha} \tag{4.32}$$

Thus

$$E^s(r,\omega)\, F^i(r,\omega) = \hat{x}\,\frac{T}{4\pi}\left[\frac{\sin(\omega+\omega_o)\frac{T}{2}}{(\omega+\omega_o)\frac{T}{2}} + \frac{\sin(\omega-\omega_o)\frac{T}{2}}{(\omega-\omega_o)\frac{T}{2}}\right] \frac{c}{r}\,\frac{e^{i\omega\frac{r}{c}}}{\omega} \times \frac{i}{4}\sec^2\alpha\, e^{-2ika\sin\alpha} \tag{4.33}$$

and

$$\bar{f}^s_H(r,t) = \hat{x}\, 2\,\mathrm{Re}\int_\alpha^\infty E^s F^i e^{-i\omega t}\, d\omega \quad . \tag{4.34}$$

(U) Since $E^{s*}(r,\omega) = E^s(r,-\omega)$ thus

$$\bar{f}^s_H(r,t) = -\hat{x}\,\frac{cT\sec^2\alpha}{8\pi r}\int_\alpha^\infty \left[\frac{\sin(\omega+\omega_o)\frac{T}{2}}{(\omega+\omega_o)\frac{T}{2}} + \frac{\sin(\omega-\omega_o)\frac{T}{2}}{(\omega-\omega_o)\frac{T}{2}}\right] \sin\omega\tau_1\,\frac{d\omega}{\omega} \tag{4.35}$$

$$\tau_1 = r/c - \frac{2a}{c}\sin\alpha - t \quad . \tag{4.36}$$

Intermediate Frequency Range

(U) For intermediate values of frequency, the creeping wave gives a significant contribution, and S is given by

$$S = \frac{i}{4}\sec^2\alpha\, e^{-2ika\sin\alpha} + \gamma(ka)\, S_c(ka) \tag{4.37}$$

and

$$\tilde{f}^{s}_{M}(r, t) = \tilde{f}^{s}_{M_1}(r, t) + \tilde{f}^{s}_{M_2}(r, t) \tag{4.38}$$

where $\tilde{f}^{s}_{M_2}(r, t)$ is the join contribution given by

$$\tilde{f}^{s}_{M_1}(r, t) = -\hat{x}\,\frac{cT\sec^2\alpha}{8\pi r}\int_{\beta}^{\alpha}\left[\frac{\sin(\omega+\omega_o)T/2}{(\omega+\omega_o)T/2} + \frac{\sin(\omega-\omega_o)T/2}{(\omega-\omega_o)T/2}\right]\sin\omega\tau_1\,\frac{d\omega}{\omega} \tag{4.39}$$

and $f^{s}_{M_2}(r, t)$ is the creeping wave contribution. For ka in the range $7.5 \leq ka \leq 10.5$, $\simeq 2.0$ and S_c is given approximately by

$$S_c \cong (0.5026 - 0.01467\,ka)\exp\left\{i\pi(1.0256\,ka - 0.95410)\right\} \tag{4.40a}$$

$$= (A - B\,ka)\exp\left\{i\pi(C\,ka - D)\right\}\ . \tag{4.40b}$$

Thus we can write the creeping wave contribution as

$$\tilde{f}^{s}_{M_2}(r, t) = \hat{x}\,\frac{r}{r}\,2\,\mathrm{Re}\int_{\beta}^{\alpha}\frac{e^{ikr}}{k}(A - Bka)\exp\left\{i\pi(C\,ka - D)\right\}e^{-i\omega t}\,F(r, \omega)\,d\omega \tag{4.41}$$

$$= \hat{x}\,\frac{2r}{r}\int_{\beta}^{\alpha}\frac{F^{i}(r, \omega)}{\omega}(A - B\,ka)\left\{\cos D\pi\cos ka\tau_2 + \sin D\pi\sin ka\,\tau_2\right\}d\omega \tag{4.42}$$

$$\tau_2 = \frac{r}{a} - \pi c - \frac{ct}{a} \tag{4.43}$$

(U) Since $D \gtrsim 1$

$$\bar{f}^{s}_{M_2}(r, t) \quad - \hat{x} \frac{2r}{r} \int_{\beta}^{\alpha} (A - Bka)\, F^{i}(r, \omega) \cos ka\, \tau_2 \frac{d\omega}{\omega} . \qquad (4.44)$$

and $F^{i}(r, \omega)$ is given by (4.29).

Cone Tip Contribution

(U) The scattering amplitude for the cone tip is given by

$$S = - \frac{i}{4} \tan^2 \alpha\, e^{-2ika \csc \alpha} \quad . \qquad (4.45)$$

(U) Using this expression to calculate the time response, we get that

$$\bar{f}^{s}_{tip}(r, t) = \hat{x} \frac{Tc \tan^2 \alpha}{8 \pi r} \int_{0}^{\infty} \left\{ \frac{\sin (\omega + \omega_o)T/2}{(\omega + \omega_o) \frac{T}{2}} + \right.$$

$$\left. + \frac{\sin (\omega - \omega_o) T/2}{(\omega - \omega_o) \frac{T}{2}} \right\} \sin ka\, \tau_3 \frac{d\omega}{\omega} \qquad (4.46)$$

and

$$\tau_3 = \frac{r}{a} - 2 \csc \alpha - \frac{ct}{a} \qquad (4.47)$$

Low Frequency Range

(U) For $ka < 5$, there is not a closed form expression for the creeping wave component and even for $ka \geq 5$ the exact expressions for γ and S_c are so complicated that computations using them are not very easy. If ω_o is of sufficiently high frequency, perhaps we can then neglect the creeping wave contribution and extend formulas (4.39) and (4.35) to zero frequency.

4.6 Pulse Scattering from a Perfectly Conducting Flat Backed Cone.

(U) We consider backscatter from the flat backed cone as illustrated on the following page. For this case fairly accurate simple CW formulas are available over the entire frequency range. Hence it is reasonable to obtain the impulse response (response to a δ function incident pulse) directly which is here done in closed form. Superposition of impulse responses in the time domain can then be used to synthesize returns from actual pulse shapes.

(U) As in our previous work we assume an incident plane wave $\hat{x}\, E_o e^{i(kz - 2\pi\nu t)} dz$ and write the backscattered field

$$\vec{E}^s = \hat{x}\, E_o \frac{e^{i(kz-2\pi\nu t)}}{kz} S \quad . \tag{4.48}$$

We have already used the known CW answer by indicating that there is no depolarization and in fact S is given quite accurately for frequencies $\nu > \nu_c = c/(2\pi a)$ by the formula (Kleinman and Senior, 1963),

$$S \sim S_H^+ = C_1 \nu\, e^{iB_1\nu} + C_2 \nu^{1/2} e^{iB_2\nu} e^{-i\pi/4} \tag{4.49}$$

where

$$C_1 = \frac{-\pi a}{nc} \operatorname{cosec} \frac{2\pi}{n}$$

$$C_2 = C_1 (c/2a)^{1/2} \frac{1}{n\pi} \sin\frac{\pi}{n} \frac{\cos\frac{\pi}{n} - \cos\frac{3\pi}{n}}{(\cos\frac{\pi}{n} - \cos\frac{3\pi}{2n})^2}$$

$$B_1 = \frac{4\pi a}{c} \cot(\pi - \theta_o) = \frac{4\pi h}{c}$$

$$B_2 = \frac{4\pi}{c}(a + h) \quad , \qquad n = \frac{5}{2} - \frac{\theta_o}{\pi} \quad ,$$

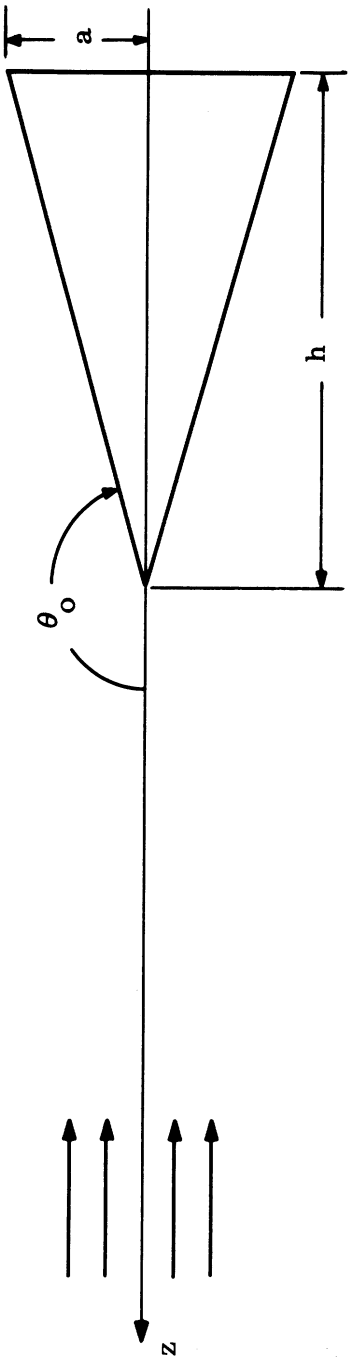

GEOMETRY FOR FLAT BACK CONE

are all real constants. The first term corresponds to radiation diffracted directly to the receiver from the edge of the base, the second term corresponds to diffracted radiation which has traveled across the base before a second diffraction returns it to the receiver.

(U) For $0 < \nu < \nu_c$ the Rayleigh formula gives good results*

$$S = S_R^+ = \nu^3 C_3$$

where

$$C_3 = (2\pi/c)^3 \frac{ha^2}{3} \left(1 + \frac{4a \exp\left[-h/(4a)\right]}{\pi h}\right) \quad . \tag{4.50}$$

(U) Define Fourier Transforms symmetrically

$$f(t) = \int_{-\infty}^{\infty} F(\nu)\, e^{-2\pi i \nu t} d\nu \quad \left(\equiv \frac{1}{2\pi} \int_{-\infty}^{\infty} F(\omega)\, e^{-i\omega t}\, d\omega \right) \tag{4.51}$$

$$F(\nu) = \int_{-\infty}^{\infty} f(t)\, e^{2\pi i \nu t}\, dt \quad . \tag{4.52}$$

Then an incident pulse field which strikes the tip at t = 0 is

$$\mathcal{E}^i(t, z) = \hat{x}\, E_o\, \delta\left(-\frac{z}{c} - t\right) \tag{4.53}$$

has Fourier transform

$$E^i(\omega, z) = x\, E_o\, e^{-i\frac{2\pi\nu}{c} z} \quad , \tag{4.53}$$

*The fact that formulas (4.49) and (4.50) together adequately cover all frequencies as far as $|S|^2$ is concerned is shown in the reference just cited where the formula for $|S|^2$ is given in Section 4.1. However, one must trace back the derivation of (4.50) to conclude that, in fact, S is real; $S = |S|$.

has Fourier transform

$$E^i(\omega, z) = \hat{x}\, E_o\, e^{-i\frac{2\pi\nu}{c} z} \quad , \tag{4.54}$$

(U) Hence the resulting backscattered field in this impulse excitation is

$$\vec{\mathcal{E}}^s(z/c - t) = \frac{\hat{x}\, cE_o}{2\pi z} \int_{-\infty}^{\infty} e^{i2\pi\nu\,(z/c - t)}\, \tilde{S}(\nu)\, d\nu \tag{4.55}$$

where $\tilde{S}(\nu) = S(\nu)/\nu$. Since $\vec{\mathcal{E}}^s(z/c - t)$ must be a real function $\tilde{S}(\nu) = S^*(\nu)$ and hence

$$\vec{\mathcal{E}}^s(z/c - t) = \frac{x\, cE_o}{\pi z}\, \mathrm{Re} \int_0^{\infty} e^{i2\pi\nu\,(z/c - t)}\, \tilde{S}(\nu)\, d\nu \quad . \tag{4.56}$$

(U) To approximate $\vec{\mathcal{E}}^s(z/c - t)$ we can replace $S(\nu)$ by the approximations valid in different ranges of ν, (4.49) and (4.50). Thus

$$\vec{\mathcal{E}}^s(z/c - t) \simeq \frac{\hat{x}\, cE_o}{2\pi\, z} \left[I_1 - I_2 + I_3 \right] \tag{4.57}$$

where

$$I_1 = 2\,\mathrm{Re} \int_0^{\infty} e^{i2\pi\nu\,(z/c - t)}\, \tilde{S}_H(\nu)\, d\nu$$

$$I_2 = 2\,\mathrm{Re} \int_0^{\nu_c} e^{i2\pi\nu\,(z/c - t)}\, \tilde{S}_H(\nu)\, d\nu$$

$$I_3 = 2\,\mathrm{Re} \int_0^{\nu_c} e^{i2\pi\nu(z/c - t)}\, \tilde{S}_R(\nu)\, d\nu \quad . \tag{4.58}$$

(U) We can evaluate these integrals after inserting (4.49) and (4.50) in the integrands as required.

$$I_2 = \frac{C_1}{\sqrt{|T_1|}} \sin\omega_c T_1 + \frac{C_2}{2\sqrt{T_2}} \left\{ C(2\sqrt{\nu_c |T_2|}) + S(2\sqrt{\nu |T_2|}) \right\} \qquad (4.59)$$

where C(x) and S(x) are the Fresnel integrals

$$C(x) = \int_0^x \cos(\pi/2\, t^2)\, dt, \quad S(x) = \int_0^x \sin(\pi/2\, t^2)\, dt ,$$

$$\omega_c = 2\pi \nu_c ,$$

$$T_1 = -t + (z + 2h)/c \quad \text{and} \quad T_2 = -t + (z + 2h + 2a)/c .$$

$$I_1 = C_1 \delta(T_1) + C_2/(2\sqrt{T_2}) \qquad (4.60)$$

Finally

$$I_3 = \frac{2C_3}{(2\pi |T_3|)^3} \left\{ 2\omega_c |T_3| \cos\omega_c |T_3|) + \right.$$

$$\left. + (\omega_c^2 |T_3|^2 - 2) \sin(\omega_c |T_3|) \right\} . \qquad (4.61)$$

(U) Causality requires that in (4.59) through (4.61) each response term is zero at a fixed z until t increases to make the T_i involved in that term equal to zero. To summarize

$$\vec{E}^s(z/c - t) = \hat{x} \frac{E_o c}{2\pi z} \left[(4.60) - (4.59) + (4.61) \right] . \qquad (4.62)$$

(U) For an arbitrary incident field $\mathcal{E}_a^i(-z/c - t)\,\hat{x}$ the response will be the convolution

$$\bar{\mathcal{E}}_a^s(z/c - t) = \int_0^\infty \mathcal{E}^s(z/c - y)\,\mathcal{E}_a^i(t - y)\,dy \quad . \tag{4.63}$$

(U) It is intended to investigate (4.62) for various incident pulses by using (4.63) for $\mathcal{E}^s$.

REFERENCES

Byrd, P.F. and M.D. Friedman (1954), Handbook of Elliptic Integrals for Engineers and Physicist, Springer-Verlag.

Caratheordory, C., (1958) Conformal Representation, Cambridge Tracts in Mathematical Physics 28, Cambridge.

Copson, E.T., (1950) An Introduction to the Theory of Functions of a Complex Variable, Oxford.

Crispin, J.W. Jr., R.F. Goodrich and K.M. Siegel (1959), "A Theoretical Method for the Calculation of the Radar Cross Sections of Aircraft and Missiles," The University of Michigan Radiation Laboratory Report No. 2591-1-H.

Davis, P.J. and P. Rabinowitz, (1967) Numerical Integration Blaisdell.

Fair, W.G. and Y.L. Luke, (1967) "Rational Approximations to the Incomplete Elliptic Integrals of the First and Second Kinds," Math. Comput. Vol. 21, pp. 418-422.

Fox, L., (1967) "Romberg Integration for a Class of Singular Integrands," Comput. J. 10, pp. 87-93.

Gautschi, W. (1967) Algorithm ... Gaussian Quadrature Formulas, Submitted for publication.

Goodrich, R.F., B.A. Harison, E.F. Knott, T.B.A. Senior, V.H. Weston and L.P. Zukowski (1967a) "Investigation of Re-entry Surface Fields - Final Report," The University of Michigan Radiation Laboratory Report No. 7741-4-T. SECRET.

Goodrich, R.F., B.A. Harrison, R.E. Kleinman, E.F. Knott, and V.H. Weston (1967b) "Investigation of Re-entry Vehicle Surface Fields - Second Quarterly Report (U)," The University of Michigan Radiation Laboratory Report No. 8525-2-Q. SECRET

Honl, H., A.W. Maue and K. Westpfahl, (1961) Theorie der Bengung, Handbuch der Physik, Springer-Verlag, 25, No. 1 pp. 218-544.

Keller, J.B. (1960), "Backscattering from a Finite Cone," IRE Trans. on G-AP AP-8, No. 2, March.

References (Cont'd)

Kleinman, R.E. and T.B.A. Senior (1963), "Diffraction and Scattering by Regular Bodies - II; The Cone," The University of Michigan Radiation Laboratory Report No. 3648-2-T. (See Section 4.3).

Kober, H., (1960) Dictionary of Conformal Representations, Dover.

Logan, N.A. (1959) "General Research in Diffraction Theory," Vol. II, Lookheed Missile and Space Division Report No. 288088.

Maliuzhinets, G.D. (1958), "Excitation, Reflections and Emission of Surface Waves from a Wedge with Given Face Impedances," Dokl. Akad. Nauk SSSR, 121, 436.

McNamee, J., (1964) "Error Bounds for the Evaluation of Integrals by the Euler-Maclaurin Formula and by Gauss-type Formulae," Math. Comput. 18, pp. 368-381.

National Bureau of Standards, (1964) Handbook of Mathematical Functions, Applied Mathematics Series, Vol. 55.

Oberhettinger, F. (1954), "Diffraction of Waves by a Wedge," Comm. on Pure and Applied Math. VIII, p. 551-563.

Senior, T.B.A. and E.F. Knott (1964) "Research on Resonant Region Radar Camouflage Techniques," The University of Michigan Radiation Laboratory Report No. 6677-2-T, SECRET.

Senior, T.B.A. (1965) "Analytical and Numerical Studies of the Backscattering Behavior of Spheres," The University of Michigan Radiation Laboratory Report No. 7080-1-T.

Senior, T.B.A. (1967) "Physical Optics applied to Cone-Sphere-Like Objects," The University of Michigan Radiation Laboratory Report No. 8525-2-T.

Siegel, K.M. (1960) "Far Field Scattering from Bodies of Revolution," Applied Research Journal, 7.

Soules, G.W. and K.M. Mitzner, (1966) "Pulses in Linear Acoustics," Applied Research Department, Nortronics, Newbury Park, CA. ARD66-60R.

References (Cont'd)

Stratton, J.A. (1941), Electromagnetic Theory, McGraw-Hill Book Co. Inc.

Stenger, F., (1966) "Bounds on the Error of Gauss-type Quadratures," Num. Math. 8, pp. 150-160.

Weiss, R.F. and S. Weinbaum (1966), "Hypersonic Boundary-Layer Separation and the Base Flow Problem," AIAA Journal, Vol. 4, No. 8, August.

DISTRIBUTION LIST

Aerospace Corporation
Attn: H.J. Katzman
Bldg. 537, Room 1007
P.O. Box 1308
San Bernardino, CA 92402 — Copies 1-10 (incl.)

Air Force Cambridge Research Laboratories
Attn: R. Mack CRDG
L.G. Hanscom Field
Bedford, MA 01730 — Copies 11, 12

Advanced Research Projects Agency
Attn: W. Van Zeeland
The Pentagon
Washington, D.C. 20301 — Copies 13, 14

Air University Library
Attn: AU
Maxwell AFB, AL 36112 — Copy 15

Air Force Avionics Laboratory
Attn: William F. Bahret - AVWE - 2
Wright-Patterson AFB, OH 45433 — Copy 16

Space and Missile Systems Organization
Attn: Capt. J. Wheatley, SMYSP
Norton AFB, CA 92409 — Copies 17, 18

Space and Missile Systems Organization
Attn: BSYLD
Norton AFB, CA 92409 — Copies 19, 20

Electronics Systems Division (AFSC)
Attn: Lt. Nyman ESSXS
L.G. Hanscom Field
Bedford, MA 01730 — Copy 21

SECRET

Security Classification

DOCUMENT CONTROL DATA - R & D

(Security classification of title, body of abstract and indexing annotation must be entered when the overall report is classified)

1. ORIGINATING ACTIVITY (Corporate author) The University of Michigan Radiation Laboratory, Dept. of Electrical Engineering, 201 Catherine Street, Ann Arbor, Michigan 48108	2a. REPORT SECURITY CLASSIFICATION SECRET 2b. GROUP 4

3. REPORT TITLE

Investigation of Re-Entry Vehicle Surface Fields (U)

4. DESCRIPTIVE NOTES (Type of report and inclusive dates)

Quarterly Report No. 3, 18 June - 18 September 1967

5. AUTHOR(S) (First name, middle initial, last name)

Goodrich, Raymond F., Harrison, Burton A., Knott, Eugene F., Senior, Thomas B.A., Smith, Thomas M., Weil, Herschel, Weston, Vaughan H. Bowman, John J.

6. REPORT DATE	7a. TOTAL NO. OF PAGES	7b. NO. OF REFS
October 1967	142	27

8a. CONTRACT OR GRANT NO. F 04694-67-C-0055 b. PROJECT NO. c. d.	9a. ORIGINATOR'S REPORT NUMBER(S) 8525-3-Q 9b. OTHER REPORT NO(S) (Any other numbers that may be assigned this report) SAMSO-TR-68-4

10. DISTRIBUTION STATEMENT In addition to security requirements which apply to this document and must be met, this document is subject to special export controls and each transmittal to foreign governments or nationals may be made only with prior approval of SAMSO, SMSD, Los Angeles, CA 90045

11. SUPPLEMENTARY NOTES Further distribution by holder made only with specific prior approval of SAMSO, SMSD, Air Force Station, Los Angeles, CA 90045.	12. SPONSORING MILITARY ACTIVITY Hq. Space and Missile Systems Organization Air Force Systems Command Norton Air Force Base, CA 92409

13. ABSTRACT

SECRET

This is the Third Quarterly Report on Contract F 04694-67-C-0055 and covers the period 18 June to 18 September 1967. The report discusses work in progress on Project SURF and on a related short pulse investigation. Project SURF is a continuing investigation of the radar cross section of metallic cone-sphere shaped re-entry bodies and the effect on radar cross section of absorber and ablative coatings, antenna and rocket nozzle perturbation, changing the shape of the rear spherical termination, and of the plasma re-entry environment. The objective of the short pulse study is the determination of methods of modifying the short pulse signature of cone-sphere shaped re-entry bodies and of decoys. SURF investigations make use of experimental measurements in surface field and backscatter ranges to aid in the analytical formulation of mathematical expressions for the computation of radar cross section. A computer program for determining the radar cross section of any rotationally symmetric metallic body is being developed.

DD FORM 1 NOV 65 1473

SECRET

14. KEY WORDS	LINK A		LINK B		LINK C	
	ROLE	WT	ROLE	WT	ROLE	WT
Radar Cross Sections						
Surface Field Measurements						
Cone-Sphere Re-entry Bodies						
Absorber Coatings						
Plasma Re-entry Environment						
Short Pulse Discrimination						